HELLENIC REPUBLIC

National and Kapodistrian University of Athens

EST. 1837

Thesis

Biological and Imaging biomarkers in Huntington's disease

Βιολογικοί και απεικονιστικοί βιοδείκτες στη νόσο Huntington

Marianthi Breza

2022

National and Kapodistrian University of Athens
School of Health Sciences, Medical School
1st Department of Neurology, Eginition Hospital
Director: Professor Leonidas Stefanis

Thesis submitted for doctoral degree (PhD)

Biological and imaging biomarkers in Huntington's Disease

Marianthi Breza

ΔΙΔΑΚΤΟΡΙΚΗ ΔΙΑΤΡΙΒΗ

Βιολογικοί και απεικονιστικοί βιοδείκτες στη νόσο Huntington

Μαριάνθη Μπρέζα

Athens, 2022

Thesis Committee

Supervisor

Assist. Prof. Georgios Koutsis
Assistant Professor of Neurology & Neurogenetics
Co-head. Neurogenetics Unit
1st Department of Neurology, Eginition Hospital
Medical School, National and Kapodistrian University of Athens

Members of the Supervisory Committee

Prof. Leonidas Stefanis
Professor of Neurology & Neurobiology. Director
1st Department of Neurology, Eginition Hospital
Medical School, National and Kapodistrian University of Athens
&
Affiliated Investigator
Director of Laboratory of Neurodegenerative Diseases
Biomedical Research Foundation
of the Academy of Athens

Assist. Prof. Georgia Karadima
Assistant Professor of Biology & Neurogenetics
Co-head, Neurogenetics Unit
1st Department of Neurology, Eginition Hospital
Medical School,
National and Kapodistrian University of Athens

Members of the Evaluating Committee

Dr. Costas Vekrellis, BRFAA, Biomedical Research Foundation Academy of Athens
Assist. Prof. Evangelia Emmanouilidou, Assistant Professor Biochemistry. National and Kapodistrian University of Athens, Department of Chemistry
Assoc. Prof. Ioannis Zalonis, Associate Professor of Psychology-Neuropsychology. Laboratory of clinical neuropsychology, 1st Department of Neurology, Eginition Hospital
Assist. Prof. Georgios Velonakis, Assistant Professor of Radiology, Medical School, National and Kapodistrian University of Athens

President of Faculty of Medicine

National and Kapodistrian University of Athens

Gerasimos D. Siasos
Professor of Cardiology

Timeline

March 2016: PhD thesis application. topic designation & appointment of advisory committee
2021: Thesis submission
2022: Thesis defense

Preface – Acknowledgements

First and foremost, I would like to thank the patients and their families. Without their involvement in Huntington's disease (HD) research none of this work would be possible. I hope that this thesis will contribute in the search for HD biomarkers, provide a better evaluation of upcoming HD treatments and that in the near future HD would be treatable.

To everyone at the Neurogenetics Unit and at Eginition Hospital: you have all helped me to get this thesis finished and was happy to be part of this team.
I would like to thank my academic supervisors Prof. Leonidas Stefanis and Assist.Prof. Georgia Karadima and especially my supervisor Assist. Prof. Georgios Koutsis for their guidance, advice and mentorship throughout my PhD. Of course, I have to mention Professor Marios Panas who introduced me to the field of Neurogenetics and the team's lab members Chrisoula Kartanou, Dr. Athina Kladi and Zoi Kontogeorgiou for their work in the lab and support.
Much of the work presented in this thesis has arisen from collaboration. Completing this work would have been impossible if not for the support provided by Dr. Costas Vekrellis and Dr. Evangelia Emmanouilidou, Emmanouela Leandrou and Dr. Anastasia Bougea who measured a-synuclein levels in HD and helped me advance my research. During my PhD, I had the opportunity to encounter many people that offered me valuable insights and discussions. I would also like to thank Dr. John Tzartos and Dr. Jens Kuhle in Basel for measuring NfL levels for free in our patients. Furthermore, I must express my gratitude to Georgina Angelopoulou, Dimitrios Kasselimis, Andreas Charidimou and Assoc. Prof Potagas for their great help with MRI analyses. Also, I am thankful to Prof. Marios Politis, Dr. Heather Wilson, Dr. Edoardo de Natale, Dr. Iro Boura, Dr. George Dervenoulas, Dr. Georgios Velonakis and Efstratios Karavasilis for providing an imaging protocol and helping both with MRI acquisition and analysis. Athanasia Liozidou performed neuropsychological testing in all participants and we worked together throughout almost all stages of this work and I am really thankful for her support and contribution to this study. I also want to thank my colleagues and friends George Vavougios and Nikos Papagiannakis for helping me with

the statistical and computational analysis. Many thanks to Professor Henry Houlden for contributing genetic data and being a source of constant support and mentorship. Finally, I cannot help but pay tribute to my family and friends for their endless support, love and encouragement. This thesis would not have been nearly as fascinating without your help. Thank you all!!

Marianthi Breza
Athens, May 2021

Abstract
Biological and imaging biomarkers in Huntington's Disease
by Marianthi Breza

Huntington's Disease (HD) is a devastating, neurodegenerative disease with no cure available to date. Several clinical trials have failed and robust biomarkers are needed towards better study design. In this thesis, clinical, cognitive, imaging and biofluid (serum NfL and alpha-synuclein) known and potential markers were analyzed using a tailored framework, to characterize patients with manifest HD as well as pre-manifest HD, in comparison to controls.

All biomarker data were compared between manifest and pre-manifest HD, as well as matched controls. Furthermore, data from clinical scales, such as the Unified Huntington Disease Rating Scale), neuropsychiatric scales, and an extensive neuropsychological battery were correlated to baseline neuroimaging findings (using whole-brain and region of interest analysis) and other biomarker data. Summarizing the most important findings, neuromelanin-MRI values, (a novel MRI sequence), were correlated in HD for the first time with finger-tapping, apathy scale and HD-QoL. In addition, a pilot study with measurements of serum a-synuclein levels in HD was conducted showing elevated levels in manifest HD patients.

As an adjunct, genetic data from a recent GWAS in collaboration with UCL were used in parallel with other available DNA & RNA open databases to run computational analyses, with

a view to provide further insight on the *SNCA* pathway and other specific pathways implicated in the pathophysiology of HD.

In conclusion, the present thesis adds to the ongoing quest for biomarkers in HD hoping to lead to a better understanding of the disease as well as the prodromal phase of the disease, where upcoming treatments could be more efficient.

Impact of this thesis

This thesis focused on the analysis of diverse, reliable, and robust potential biomarkers of disease progression in HD. Huntington's Disease (HD) is a fatal, neurodegenerative disease. Despite the knowledge since 1993 of the defect in the HTT gene resulting in mutant toxic Huntingtin protein (mHTT), there are still no approved disease-modifying therapies that could treat this disease. As HD progresses, quality of life of HD patients is severely impaired by motor, psychiatric symptoms, and cognitive impairment. By end-stage disease patients are incapacitated, needing institutional care.

To date, over 100 therapeutics have been used in clinical trials in HD but only two were approved as symptomatic treatment for HD. Although in September 2015, the first targeted huntingtin-lowering drug entered a phase 1b/2a trial showing promising results with dose-dependent mHTT reduction in CSF, this study was recently terminated as no clinical benefit was reported. The lack of biomarkers-measures sensitive enough to detect efficacy could be a reason for this failure of several treatments. Biomarkers can be used as tools both for diagnosis and for staging disease. Furthermore, biomarkers could predict and monitor clinical response to intervention. More specifically, biomarkers can aid in stratifying and monitoring premanifest

HD subjects for clinical trials determining the optimal timing for initiation of treatment. The combination of wet and dry biomarkers constitutes a powerful approach to tackle this challenging problem.

The Neurogenetics Unit at the 1st Department of Neurology, University of Athens Medical School, Eginition Hospital has acted as referral center for patients with presumed Huntington's disease since 1995 (Panas et al., 2011). It has been the only laboratory within the public health service offering molecular diagnostic testing for HD to patients from all over Greece. Over 600 HD patients have been diagnosed in the Neurogenetics Unit and about 80 HD patients and pre-HD carriers are systematically followed up every year. This investigation could help towards the participation of the Greek HD patients in future HD clinical trials and provide new directions for clinical research to improve prevention, diagnosis, prognosis, therapy development. and management of HD patients.

In this thesis, using a tailored framework, I analyzed clinical, cognitive, imaging and biofluid (serum NfL) known and potential markers for characterization of patients with manifest HD as well as pre-manifest HD. Neuromelanin-MRI values, a novel MRI sequence, were correlated in HD for the first time with finger-tapping, apathy scale and HD-QoL. In addition, a pilot study with measurements of serum a-synuclein levels in HD was conducted showing elevated levels in manifest HD patients.

This approach could be an added value and lead to a better understanding of the disease and the prodromal phase of the disease, where upcoming treatments can be more efficient. Lastly, given the rarity of HD and difficulties that arise from motor symptoms, I also addressed the limitations raised by small sample size of the cohorts analyzed in this thesis. I anticipate that

the neuromelanin MRI sequence will be included in the design of future clinical trials for HD as a promising imaging marker.

Overall, this work presents progress towards the quest for biomarkers in HD and could be a prelude to larger multicenter studies and research experiments in the future. This project was initially planned to include 80 HD patients in collaboration with King's College that would provide more power to our study as well as a follow-up study (1 year), however, due to COVID19 pandemic only a few patients were re-evaluated, and the recruitment was disrupted.This thesis has resulted in a publishable piece of work, and two soon to be submitted for publication at the time of submitting this thesis. The work has also been presented at several conferences via platform talks and poster presentations.

PhD Thesis in an overview

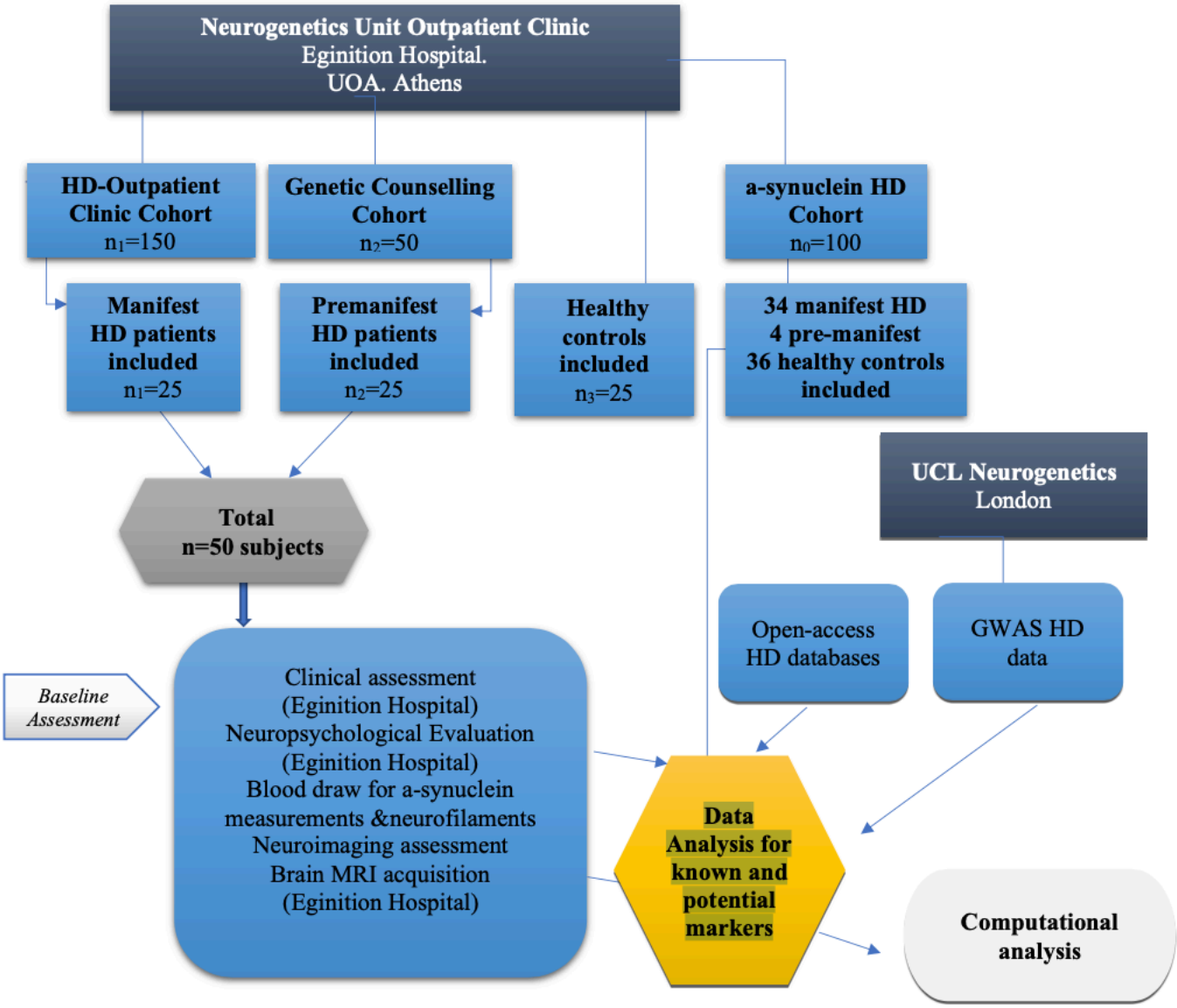

Hippocrates Oath – Όρκος του Ιπποκράτη

Ὄμνυμι Ἀπόλλωνα ἰητρὸν. καὶ Ἀσκληπιὸν. καὶ Ὑγείαν. καὶ Πανάκειαν. καὶ θεοὺς πάντας τε καὶ πάσας. ἵστορας ποιεύμενος. ἐπιτελέα ποιήσειν κατὰ δύναμιν καὶ κρίσιν ἐμὴν ὅρκον τόνδε καὶ ξυγγραφὴν τήνδε.

Ἡγήσασθαι μὲν τὸν διδάξαντά με τὴν τέχνην ταύτην ἴσα γενέτῃσιν ἐμοῖσι. καὶ βίου κοινώσασθαι. καὶ χρεῶν χρηίζοντι μετάδοσιν ποιήσασθαι. καὶ γένος τὸ ἐξ ωὐτέου ἀδελφοῖς ἴσον ἐπικρινέειν ἄῤῥεσι. καὶ διδάξειν τὴν τέχνην ταύτην. ἢν χρηίζωσι μανθάνειν. ἄνευ μισθοῦ καὶ ξυγγραφῆς. παραγγελίης τε καὶ ἀκροήσιος καὶ τῆς λοιπῆς ἁπάσης μαθήσιος μετάδοσιν ποιήσασθαι υἱοῖσί τε ἐμοῖσι. καὶ τοῖσι τοῦ ἐμὲ διδάξαντος. καὶ μαθηταῖσι συγγεγραμμένοισί τε καὶ ὡρκισμένοις νόμῳ ἰητρικῷ. ἄλλῳ δὲ οὐδενί.

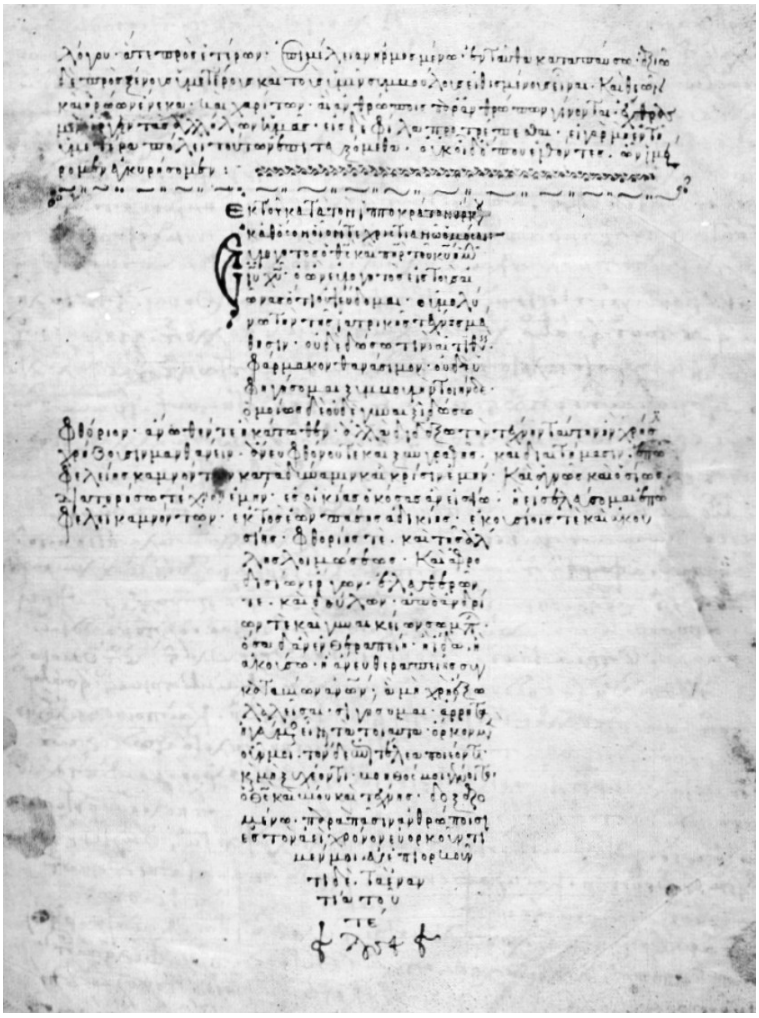

Διαιτήμασί τε χρήσομαι ἐπ' ὠφελείῃ καμνόντων κατὰ δύναμιν καὶ κρίσιν ἐμὴν. ἐπὶ δηλήσει δὲ καὶ ἀδικίῃ εἴρξειν.

Οὐ δώσω δὲ οὐδὲ φάρμακον οὐδενὶ αἰτηθεὶς θανάσιμον. οὐδὲ ὑφηγήσομαι ξυμβουλίην τοιήνδε. Ὁμοίως δὲ οὐδὲ γυναικὶ πεσσὸν φθόριον δώσω. Ἁγνῶς δὲ καὶ ὁσίως διατηρήσω βίον τὸν ἐμὸν καὶ τέχνην τὴν ἐμήν.

Οὐ τεμέω δὲ οὐδὲ μὴν λιθιῶντας. ἐκχωρήσω δὲ ἐργάτῃσιν ἀνδράσι πρήξιος τῆσδε.

Ἐς οἰκίας δὲ ὁκόσας ἂν ἐσίω. ἐσελεύσομαι ἐπ' ὠφελείῃ καμνόντων. ἐκτὸς ἐὼν πάσης ἀδικίης ἑκουσίης καὶ φθορίης. τῆς τε ἄλλης καὶ ἀφροδισίων ἔργων ἐπί τε γυναικείων σωμάτων καὶ ἀνδρῴων. ἐλευθέρων τε καὶ δούλων.

Ἃ δ' ἂν ἐν θεραπείῃ ἢ ἴδω. ἢ ἀκούσω. ἢ καὶ ἄνευ θεραπηίης κατὰ βίον ἀνθρώπων. ἃ μὴ χρή ποτε ἐκλαλέεσθαι ἔξω. σιγήσομαι. ἄῤῥητα ἡγεύμενος εἶναι τὰ τοιαῦτα.

Ὅρκον μὲν οὖν μοι τόνδε ἐπιτελέα ποιέοντι. καὶ μὴ ξυγχέοντι. εἴη ἐπαύρασθαι καὶ βίου καὶ τέχνης δοξαζομένῳ παρὰ πᾶσιν ἀνθρώποις ἐς τὸν αἰεὶ χρόνον. παραβαίνοντι δὲ καὶ ἐπιορκοῦντι. τἀναντία τουτέων.

CV

Table of Contents

Glossary - Abbreviations

3T 3 Tesla

HTT huntingtin protein

mHTT Mutant huntingtin

HD Huntington's disease

CSF cerebrospinal fluid

CAG Cytosine-Adenosine-Guanine

DBS Disease Burden Scores

MRI Magnetic resonance imaging

TMS Total Motor Score

UHDRS Unified Huntington's Disease Rating Scale

VBM Voxel-Based Morphometry

PGD Preimplantation genetic diagnosis

MoCA Montreal Cognitive Assessment

PolyQ Polyglutamine

cUHDRS composite Unified Huntington's Disease Rating Scale

WM White matter

WAIS Wechsler Adult Intelligence Scale

PET positron emission tomography

GLM generalized linear model

FLAIR Fluid Attenuated Inversion Recovery

DTI Diffusion Tensor Imaging

PVE Partial volume estimates

QC Quality control

ROI Region of interest

ANTs Advanced Normalization Tools

fMRI Functional Magnetic Resonance Imaging of the Brain

MNI Montreal Neurological Institute

MPRAGE Magnetization prepared rapid gradient echo

NfL Neurofilament light protein

rs-fMRI Resting state fMRI

SD Standard deviation

SDMT Symbol digit modality test

sMRI Structural MRI

TIV Total intracranial volume

TFC Total Functional Capacity

VBM voxel-based morphometry

AES apathy evaluation scale

ASL Arterial Spin Labeling

LC Locus Coeruleus

SN Substantia Nigra

To all patients……

suffering from rare diseases……

1. Introduction

1.1 Background

Huntington's disease (HD) (*MIM#143100)* is an autosomal dominant inherited neurodegenerative disorder. This fatal disease is caused by a CAG repeat expansion in the *huntingtin* gene (HTT) (chromosome 4) encoding the huntingtin protein (Htt). HD is the most common of the nine known triplet repeat disorders (polyQ), clinically characterized by progressive motor dysfunction (movement disorders, especially chorea), cognitive decline, and psychiatric manifestations that will eventually lead to death, typically 15-20 years following symptomatic onset (Bates et al., 2015).

Prevalence of HD

HD is a rare disease with a worldwide prevalence of ~12 per 100.000 individuals in European populations (Pringsheim et al., 2012). Although rare diseases are defined as of low prevalence, the total number of affected cases is high. In Greece, around 40 new cases are diagnosed each year and approximately 600 Greeks suffer at any time from the disease. The prevalence differs by more than tenfold across geographical locations. The highest prevalence in the world was reported in Venezuela (700 cases/100.000). A higher prevalence is described in Europe, Australia and North America, and a lower prevalence in Asia. *HTT* gene haplotypes and different diagnostic approaches and criteria could be responsible for this variation.

Onset of the disease is in the adult life span and individuals may have expanded CAG repeats without manifesting disease. An incomplete penetrance is reported at the lower cut-off of the CAG repeats (36-39 CAG repeats). Consequently, expanded repeats' frequency might be higher in the general population than previously established. (Reinhard et al. 2021, Panas et al., 2011).

Prognosis

HD is a devastating neurodegenerative disease with no cure available. Disease duration is usually between 15 to 20 years. CAG repeats except from predicting age of clinical onset have been found to also predict the age of death. A larger CAG repeat expansion size has been associated with a higher rate of motor, cognitive, and functional measures deterioration. Progression of behavioral manifestations however, was not related to CAG expansion. Homozygotes for fully penetrant HD have been rarely reported and presented similar age of onset with heterozygotes but a higher rate of disease progression. HD patients are led to complete dependency in everyday activities, full-time care and finally, death. Pneumonia has been reported as the most frequent cause of death, followed by suicide (Bates et al. 2015, Roos. 2010).

1.2 Pathophysiology

Although the mutation underlying HD has been known since 1993, the exact pathomechanism remains to be elucidated. The precise mechanism of neurodegeneration in HD is believed to involve Htt aggregation. The fact that the normal function of HTT protein also remains to be discovered, complicates understanding of the underlying mechanism. HTT includes a polyglutamine tract encoded by uninterrupted CAG trinucleotide repeats in the first exon of *HTT*. HD patients carry expansions of 36 or more CAG repeats, while wild-type alleles are up to 26 CAG repeats. It is assumed that both the gain-of-function of the mutant huntingtin (mutHTT) and the loss of function of the wild-type HTT protein contribute to HD pathology. The toxicity of mutant HTT (mHTT) is thought to be cell-type dependent (Bates et al., 2015, Roos 2010).

Huntingtin protein (HTT)

As previously stated, unravelling the function of normal huntingtin protein as well as mutant HTT (mHTT) has been a major focus of HD research. Humans have the longest polyglutamine tract that increased in length throughout vertebrate evolution. HTT is known to be involved in development of the central nervous system (neural tube formation, neuroblast migration), axonal transport, function of synapses and survival of cells and interacts with DNA in many genes. HTT knockout mice did not survive before birth and died after nervous system formation (Tabrizi et al., 2020).

Mutant HTT (mHTT)

The mHTT protein is a large, intracellular protein that tends to aggregate. mHTT is produced from CAG repeat expansion and is involved in many cellular functions. Although mHTT is known to be toxic and leads to cell death, identifying primary or secondary pathogenic processes remains challenging. It is known that the length of the polyglutamine tract affects the post-translational modification of HTT (Pennuto et al., 2009). Post-translational modifications of HTT affect subcellular distribution, stability, cleavage, and function of the protein. mHTT causes transcriptional dysregulation both in CNS and in the peripheral tissues, resulting in immune response upregulation and mRNA processing upregulation, followed by downregulation of synaptic function and metabolic processes (Tabrizi et al., 2020). The anatomical distribution of transcriptional disruption correlates with areas of cell death being most marked in the caudate nucleus. In the peripheral tissues (blood, muscle) of HD patients, dysregulated gene sets overlap with dysregulated genes in the caudate (Hensman Moss et al., 2017). Striatal medium spiny neurons are known as the most vulnerable to mHTT. However, neuronal death and dysfunction also occurs in the cerebral cortex.

mHTT CSF concentration is very low, thus difficult to quantify. Several studies report approaches to reduce expression of mHTT and CSF quantification has been extremely challenging. HTT and therefore mHTT is ubiquitously expressed and it is difficult to distinguish between CNS-derived mHTT and peripheral mHTT (Tabrizi et al., 2020).

Pathomechanism

The exact pathomechanism remains to be elucidated. mHTT is folded abnormally, producing soluble monomers of HTT protein which combine and form oligomers. Consequently, these oligomers act as seeds and form mHTT fibrils and large inclusions in both the cytoplasm and nucleus. In the past, large mHTT inclusions were thought as pathogenic but recent studies propose N-terminal mHTT oligomers as toxic and that in contrast large mHTT inclusions could even be protective (Tabrizi et al., 2020). A study showed that mHTT spread is distinct from 'prion-like'. mHTT spread was demonstrated between neurons via functional synapses in induced pluripotent stem cell (iPSC)-derived HD neurons in a wild-type mouse corticostriatal brain slice from HD mouse cortical neurons and following injection of an mHTT fragment into wild-type mouse cortex (Pecho-Vrieseling et al., 2014). Evidence for cell-to-cell spread of mHTT in humans is limited. Post-mortem examination of the graft in individuals who received fetal striatal transplants showed inclusions in the extracellular matrix. mHTT was suggested to be released by neurons, although no inclusions were found within grafted cells (Srinageshwar et al., 2020).

Regarding protein degradation, two main systems are thought to be implicated in HD pathogenesis: ubiquitin–proteasome system and autophagy. Ubiquitin–proteasome system

clears proteins that are damaged and autophagy degrades protein complexes and damaged organelles. Evidence from studies suggests that ubiquitin-proteasome and autophagy systems are compromised in HD, and autophagy induction increased mHTT clearance in animal HD models improving phenotype (Martin et al., 2015, Tabrizi et al., 2020).

Inflammation & immune system

Inflammation and immune system have been implicated in several neurodegenerative diseases, including Alzheimer's disease, Parkinson's disease, amyotrophic lateral sclerosis (ALS) and HD. However, if this inflammation is a primary mechanism or a secondary response to other pathologies remains to be seen. Immune activation has been reported in peripheral blood of HD patients, with higher levels of pro-inflammatory cytokines and other molecules (Tabrizi et al., 2020).

Overall, there are multiple theories proposed in the pathogenesis of HD, presumably occurring in parallel, including neuronal aggregates (intracytoplasmic/intranuclear inclusions with mHTT) in proteolytic HD pathway, a possible impairment of the ubiquitin-proteosome pathway, transcriptional dysregulation, excitotoxicity (increased glutamate and glutamate agonist release) mitochondrial dysfunction and altered energy metabolism and changes in axonal transport and synaptic dysfunction. Recent studies have suggested the co-occurrence of mixed proteinopathies, particularly in the late-stage of neurodegenerative diseases (St-Amour et al., 2018).

1.3 Neuropathology

The primary structures affected in HD neurodegeneration are the putamen, caudate and the cerebral cortex. Caudate volume was reduced by 53%. and putamen by 46% in a study including end-stage HD patients compared to controls (Guo et al., 2012). Atrophy of the cortex (cortical volume reduced by 23%) was noted and only the temporal lobes were relatively spared. Within the cortex, the occipital lobe showed the greatest difference, followed by frontal and parietal regions. CAG repeat length and motor impairment correlated with cortex atrophy but not with atrophy of the subcortical regions. More severe psychiatric symptoms correlated with cingulate cortex atrophy (Thu et al., 2010).

Staging HD neuropathology into five grades (0-4) has been established back in 1985 with striatal atrophy and selective vulnerability of medium spiny neurons as the hallmarks of the earliest signs of HD neuropathology (Deng et al., 2004). Particularly, enkephalin-containing medium spiny neurons in the basal ganglia in the indirect pathway are the most susceptible. In addition, loss of substance-P containing medium spiny neurons in the direct pathway results in akinetic and dystonic manifestations. mHTT aggregates/inclusions are also found within the cytoplasm, nucleus and dystrophic (Burgess et al., 2020; Davies et al., 1997; DiFiglia et al., 1997; G. M. Halliday, D. A. McRitchie, V. Macdonald, K. L. Double, R. J. Trent, 1998).

Of note, evidence for neuroinflammation and reactive gliosis has been also identified in neuropathological studies (increased astrocytes, activated microglia and oligodendrocytes). starting initially within the striatum. More specifically, reactive microglia have been found within the neostriatum close to medium spiny neurons (Simmons et al., 2007). This pattern appears to be unique and has not been observed in other neurodegenerative diseases. In

addition, evidence exists for increase of complement pathway components within HD striatal neurons, myelin and astrocytes in comparison to controls, components which are thought to originate from reactive microglia (Tabrizi et al., 2020). A biochemical change occurring during astrocytosis and microglial activation is increased binding of a peripheral type benzodiazepine binding sites (PTBBS) ligand. Inflammatory gliosis has also been found within the putamen and frontal cortex in HD brain tissue (Bates et al., 2015; J.C. Hedreen, 1995; Singhrao et al., 1999)

Neuropathology progression theories in HD

Several theories have been proposed for progression of neural pathology in HD. Most theories are related to basal ganglia. The basal ganglia include the striatum (caudate and putamen), substantia nigra, the subthalamic nucleus and the globus pallidus. It is now well-established that basal ganglia affect not only motor but also cognitive and emotional processing, through three main circuits the motor, associative or cognitive and limbic or emotional circuits. These three networks of the basal ganglia interact with a number of cortical regions (Figure 1) (Jahanshahi et al., 2015).

A theory proposed to disrupt these circuits is the hypothesis of a prion-like disease progression. Pathology is thought to spread from cell-to-cell. Brain regions that are close to the "epicentre" of disease or nearby will degenerate prior to distant regions. However, this theory has not been confirmed. Another hypothesis is that atrophy progression in HD could be related to altered brain connectivity occurring through a mechanism of transneuronal degeneration and not prion-like spread. Cortico-striatal regions were more affected in those with HD, with reduced connectivity between striatal regions and both frontal and parietal/occipital

regions. (Jahanshahi et al., 2015; McColgan et al., 2018).

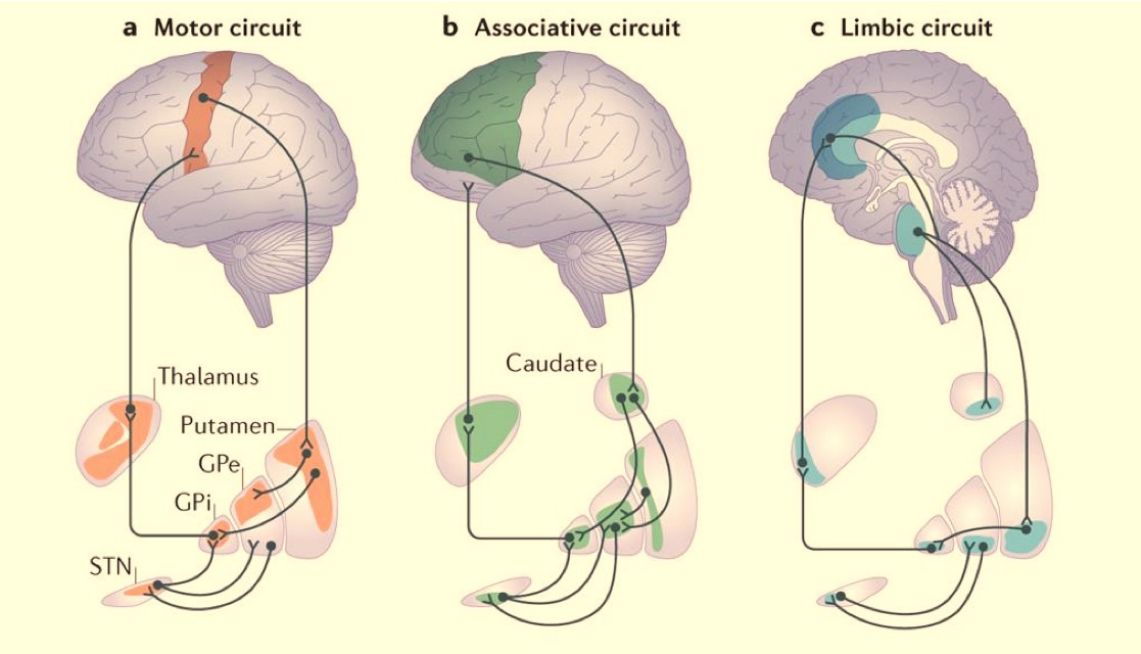

Figure 1. Three circuits models connecting basal ganglia to the cortex (Jahanshahi et al., 2015).

1.4 Clinical characteristics

HD is typically characterized by a triad of psychiatric, movement and cognitive impairment. A wide spectrum of phenotypic presentations has been described in HD ranging from the akinetic form of Westphal (juvenile HD) to apathy and suicidal behavior, while signs and symptoms could change during disease progression. Symptoms usually develop between 35-45 years of age. However, onset of HD disease has been described from 2 to 87 years. The disease gradually progresses to death usually 18 years from motor onset with an exception of late-onset HD, which may progress more slowly (Ross et al.,2014).

Motor features

Chorea and dystonia are the main motor symptoms of HD, present in about 90% of symptomatic patients. Gait impairment is noted, attributed to chorea, dystonia, and also to impairment in motor control and postural reflexes, making patients prone to falling. Motor impersistence is described. Hypophonia, dysarthria and dysphagia, cause significant morbidity. Eye movement abnormalities (impairment of both vertical. horizontal saccades and initiation deficits) occur early. As the disease progresses, pursuit is impaired with slower velocity, saccadic instructions and gaze impersistence. Motor features of HD are assessed using the UHDRS TMS, with ratings for items that include eye movements, speech, chorea, dystonia, rapid alternating movements, bradykinesia and gait (Bates et al., 2015; Wild & Tabrizi, 2017).

Psychiatric features

Psychiatric disturbances are thought to precede motor disease onset with symptoms even 10 years before onset. Psychiatric manifestations such as depression, anxiety and apathy are common in HD. Apathy is reported in symptomatic HD (55.8%), as well as prior to motor onset. Psychotic features are rarer, although additional factors may predispose to schizophrenia-like symptoms. Irritability is usually described (up to 65.4%) and also aggressiveness. Obsessions and compulsions can also be features of the disease (Lovestone et al., 1996; Reedeker et al., 2011) .

Cognitive features

Although motor manifestations are more prominent, cognitive deficits are also apparent in HD, constituting one of the main features of the disease. Several cognitive domains are

affected, mainly in the later stages of HD but also in premanifest HD carriers, such as processing speed, executive function and multitasking. Studies of cognitive dysfunction in premanifest stages of HD presented controversial results (Papoutsi et al., 2014).

As described in psychiatric manifestations, cognitive impairment often precedes motor onset. Subtle cognitive deficits could be detectable more than a decade prior to predicted motor onset, deficits which gradually evolve as motor onsets approaches (Tabrizi et al., 2012). Severity of cognitive impairment in HD varies and worsens with disease progression. Cognitive deficits are reported mainly in executive functioning, but also attention, memory. psychomotor speed, verbal fluency and visuospatial functioning (Paulsen et al., 2013; Snowden et al., 2002).

Many studies in manifest HD report memory impairment in both early and later stages of HD. Of the memory subtypes (short term, long term, working memory), working memory was the most common and consistent finding of memory impairment in HD, even in premanifest HD subjects (Dumas et al. 2013, (Tabrizi et al., 2009).

Symbol Digit Modalities Test (SDMT) and finger tapping have been studied as measures of psychomotor speed and found to be impaired in both premanifest HD and manifest HD. SDMT also had the biggest effect size for measuring change in performance over 24 months in early HD patients compared with controls, and a strong association with TFC/TMS (Larsen et al., 2015; Tabrizi et al., 2012; Vaportzis et al., 2015). In early manifest patients, a correlation between basal-ganglia cortical connectivity and higher results on the SDMT and Stroop word reading test has recently been shown, implying that altered structural connectivity directly leads to clinical phenotype in HD. Stroop interference task was also used to examine fronto-striatal circuitry in premanifest HD. Response times were longer in

premanifest HD participants than in controls, which was linked to the ACC–basal ganglia networks (Larsen et al., 2015; Tabrizi et al., 2012; Vaportzis et al., 2015).

Emotion recognition is another area showing dysfunction in both early HD and premanifest HD. Recognition of negative feelings is mainly affected, and has been shown to be seriously impaired in premanifest HD. Executive function (planning, decision making. and monitoring cognitive processes) which is considered to be regulated by the prefrontal cortex was also found impaired in HD. In problem solving, patients in the early and late stages of HD, as well as premanifest HD had deficits when compared to controls (Hart et al., 2013; Larsen et al., 2015; Tabrizi et al., 2012).

In premanifest HD, working memory and visuomotor performance were usually affected in those closer to predicted disease onset. Regarding HD carriers far from the predicted disease onset or those with less pathology, results vary in different studies and cognitive decline could be difficult to observe. No differences were reported in cognition between premanifest HD and healthy controls over 24 months in a study including large battery of cognitive tests However, the failure to identify cognitive deficits in HD carriers temporally far from predicted disease onset, does not mean that a decline has not already began (Harrington et al., 2012; Tabrizi et al., 2012).

1.5 Diagnosis - Diagnostic Genetics

HD is a monogenic disorder, inherited in an autosomal dominant manner. The expansion of the trinucleotide CAG repeat within exon 1 of the huntingtin (HTT) gene on the short arm of chromosome 4 at 4p16.3 causing the disease was discovered in 1993. The expansion is

translated into a polyglutamine stretch in the mutant Huntingtin protein (mHTT). (Hoogeveen et al., 1993).

The gold standard for diagnosis is targeted genetic testing of the CAG repeat size. A cut-off of 26 or fewer repeats is normal, and does not lead to HD. Allele size of 27-35 is rare and has also not been associated with an HD phenotype. Carriers of 27-35 repeats are at risk of transmitting a disease causing mutation to their offspring (Hendricks et al., 2009). This is due to a phenomenon known as anticipation, in which the CAG repeat length tends to increase from one generation to the next. because of meiotic instability of the trinucleotide repeat. Furthermore, except for the meiotic instability that increases the inherited CAG repeat length. somatic instability is described resulting in extremely large CAGs in affected HD brain regions from HD patients. This may be a driving mechanism of disease progression but currently cannot be assessed in vivo. However, taking into consideration the instability of the CAG repeat, the intermediate allele category may be at risk of having offspring with an expanded allele in the range that causes disease. Reduced penetrance HD-causing alleles are alleles with a size of 36-39 repeats, in which case carriers may or may not manifest HD symptoms within an average lifespan. Carriers of allele sizes of 40 or more repeats are expected to manifest the disease, with a penetrance increasing up to 100% by 40 repeats given an average life (McDonnell et al., 2021).

Extreme phenotypes of HD

Juvenile-onset HD or Westphal-akinetic variant & Late-onset HD

Although up to 121 CAG repeats have been reported, most HD carriers of the expansion have 40-44 repeats. HD mutation carriers with larger CAG repeats (usually >60), can manifest

symptoms before the age of 21, which is known as Juvenile onset HD or Westphal-akinetic variant (Fusilli et al., 2018).

Late-onset Huntington's disease (LoHD) is defined as HD with an onset after 50 years but in more recent studies as onset after 60 years (Chaganti et al., 2017). About 4.4–11.5% of individuals with HD have an onset age of over 60. Presentation and prognosis of LoHD varies. Diagnosis of LoHD can be missed in sporadic cases due to the low *a priori* likelihood with substantial implications (Koutsis et al., 2014).

Repeat count	Classification	Disease status	Risk to offspring
<26	Normal	Will not be affected	None
27–35	Intermediate	Will not be affected*	Elevated but <<50%
36–39	Reduced Penetrance	May or may not be affected	50%
40+	Full Penetrance	Will be affected	50%

Walker, 2007

Table 1 *Classification of the trinucleotide repeat. and resulting disease status. depends on the number of CAG repeats.*

**Recent observations suggested that older patients with intermediate alleles may develop some mild choreatic symptoms and a slightly faster cognitive decline (Cubo et al. 2016, MDS online teaching course available https://www.movementdisorders.org/Courses/Huntingtons-Disease-Genetics-and-Pathophysiology1.html).*

Instability of the CAG repeat length

Expansion and contraction of the CAG repeat size has been observed with the CAG repeat number varying from generation to generation. It is well known that the CAG repeat tends to expand, particularly in paternal transmission (Sun et al., 2016). This tendency of the CAG repeats to expand is described as anticipation, a phenomenon reported in HD as well as in other neurodegenerative diseases such as SCAs 1,2, 3, 6, 7 and DRPLA. The CAG repeat expansion in HD is also prone to somatic mosaicism, which is expansion-biased and age-dependent. A tissue-specific somatic repeat instability has been also described. Somatic instability was found especially high in the striatum and cortex of HD cases but it was also detected in the liver, and it was absent in the cerebellum (Monckton, 2021; Tomé et al., 2013).

Clinical diagnosis

Motor symptoms (mainly chorea) have been characterized historically as the main clinical feature of HD patients used for a clinical diagnosis, and present in most cases. Clinical diagnosis of HD was defined by the Huntington Study Group as manifestation of unequivocal motor abnormalities that cannot be otherwise explained (Huntington Study Group, 1996). This led to several problems regarding the estimation of age of onset, as it is now well-established that many HD mutation carriers often present with cognitive, behavioural and psychiatric changes several years before onset of motor symptoms. We should note that in this thesis, HD mutation carriers with a clinical diagnosis (motor onset, UHDRS >=4) were categorized as manifest HD and those without sufficient motor signs and symptoms to have a clinical diagnosis were included in the premanifest HD cohort (PreHD) (Huntington Study Group, 1996).

Prenatal diagnosis and genetic counselling

In cases of molecularly confirmed family history of HD, a prenatal diagnosis with DNA testing can be advised. Between the 10^{th}- 12^{th} week of pregnancy chorionic villi sampling is performed, whereas amniocentesis between the 15th to 17th week, where DNA-testing can be carried out. Preimplantation diagnosis is also advised and is available in several countries. In preimplantation diagnosis, a cell from the embryo (eight-cell stage) is used for genetic testing. Only embryos without the expanded CAG repeat are implanted in the endometrium and allowed to develop (Stern, 2014).

1.6 Disease onset

The onset of symptoms is inversely associated with CAG repeat expansion size, usually occurring at the age of mid-40s. However, subclinical changes and pathological processes are thought to precede the initiation of symptoms by several years. Longer repeats tend to cause an earlier onset of disease (Bates et al., 2015).

Disease onset is defined as the point when a person who carries a CAG- expanded HTT allele develops "the unequivocal presence of an otherwise unexplained extrapyramidal movement disorder" (motor symptoms such as chorea, bradykinesia, rigidity). However, the transition from premanifest to manifest HD does not have a clear threshold, making it more challenging for registries, clinical trials, physicians, and investigators to categorize these patients. For example, slower saccades, delayed initiation of saccades, irregular finger tapping, psychiatric symptoms and cognitive changes have been described before motor onset. There may be more subtle features to these prodromal phases of HD that have not been observed and investigated yet (Bates et al., 2015; Tabrizi et al., 2011, 2009a).

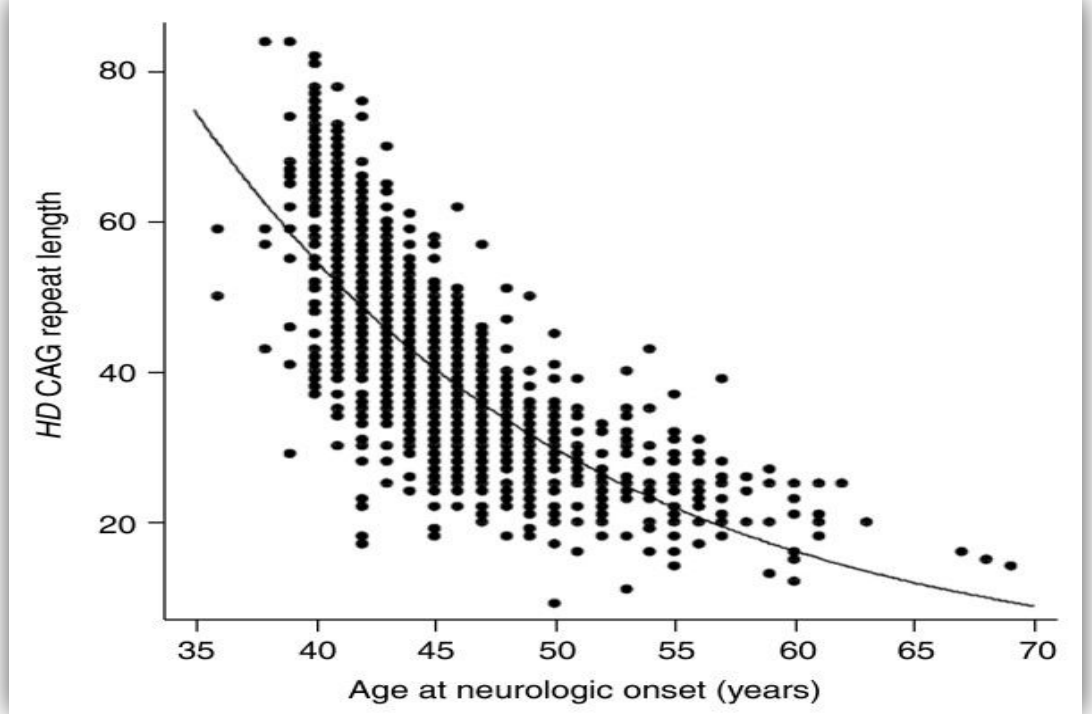

Figure 2: *Relationship Between CAG Repeat Length & Age of Onset in Huntington's Disease Patients* (Gusella & MacDonald, 2009).

Despite a strong relationship with CAG repeat length in peripheral blood leukocytes, a large variability in age of onset of motor symptoms is reported. Between 40-45 CAGs, even 20-40 years differences in the age of onset of individuals with the same CAG length are described. CAG repeat length accounts for about 67% of age of onset variation. Other factors such as environmental and genetic modifiers that influence and modify the HD phenotype have been suggested (Gusella & MacDonald, 2009; The U.S.–Venezuela Collaborative Research Project* and Nancy S. Wexler, 2004).

Disease burden score

Several approaches have been used to estimate the expected burden of pathology, using age and CAG repeat number. The most known score is the "disease burden score", DBS= age x [CAG-35.5]. However, a study of a small number of neuropathological samples didn't support the use of this score. A parametric survival model has also been developed by Langbehn and colleagues predicting motor onset probability at different ages based on a large cohort of manifest and premanifest HD patients (Langbehn et al., 2004); Sanchez-Pernaute et al.. 1999 ;Penney et al., 1997).

1.7 Genetics

Genetic modifiers offer the potential of new drug targets that could be uncovered directly in humans using modern genetics. The first genome-wide association study in HD revealed several hits from genes within DNA repair and handling pathways (Genetic Modifiers of Huntington's Disease (GeM-HD) Consortium*, 2015). By far the most important disease modifying genetic factor in HD and other triplet repeat disorders is the size of the CAG-expansion in the abnormal allele, as detected in DNA from peripheral blood leukocytes. A strong inverse correlation is present, with a higher number of repeats leading to earlier disease onset. However, CAG-repeat size does not account for more than ~60% of variability in onset. Cells in the basal ganglia and cerebral cortex seem to be particularly vulnerable to substantial increases in CAG-repeat size with mitosis. Somatic mosaicism is significantly influenced by genes implicated in DNA repair pathways (Bettencourt et al., 2016).

Recent GWAS studies suggest that specific SNPs in DNA repair genes can act as genetic modifiers of age of onset in HD patients. This has been recently replicated in a Greek cohort of 350 HD patients (Bettencourt et al., 2016). These SNPs could plausibly influence HD disease

progression and this has been recently verified in the TRACK-HD cohort and replicated in the REGISTRY cohort. However, possible effects of these polymorphisms on expression and RNA data-signatures of HD have not been fully investigated (Hensman Moss et al., 2017) Bettencourt et al. 2016, Genetic Modifiers of Huntington's Disease (GeM-HD) Consortium*, 2015; Lee et al., 2012).

1.8 Therapeutics & Management

Over the last decades, more than 100 clinical trials have been conducted in HD with almost no beneficial effect on HD. At present, there is no approved disease-modifying therapy for HD and much remains to be clarified regarding the mechanisms underlying the progression of neurodegeneration. Current treatment of HD is symptomatic. Tetrabenazine and deutetrabenazine are the only FDA- approved agents for symptomatic treatment of HD as they have been demonstrated to reduce chorea. Neuroleptics are also used off-label for chorea as well as psychotic symptoms. SSRI/SNRIs and benzodiazepines are often prescribed for depression, anxiety, and agitation (Bashir & Jankovic, 2018). More than 30 clinical trials are ongoing for HD, as registered on clinicaltrials.gov.

RNA-based Therapies

Therapies aimed at targeting huntingtin and lowering its expression have shown promising results. An antisense oligonucleotide (ASO) was the first huntingtin-lowering therapeutic that entered human trials in September 2015. It is understood that therapeutic intervention should be attempted at the earliest possible disease stages to be maximally effective. Although initially promising results have been reported from a phase I/II gene-silencing study in December 2017 (Ionis-HTTRx trial) with dose-dependent mHTT reduction in CSF, this study was recently

terminated as no clinical benefit was reported (Wiggins & Feigin, 2021). Likewise, a phase Ib/IIa randomized, multicenter, double-blind, and placebo-controlled clinical trial for both WVE-120101 and WVE-120102, has failed to show clinical benefit (NCT03225833-PRECISION-HD1. NCT03225846 -PRECISION-HD2) (Wiggins & Feigin, 2021).

Small-Molecule Modulators of RNA Delivery

Small molecules that downregulate HTT protein levels have been identified from stem cells of HD patients. Ongoing studies in preclinical phase have shown promising results in reducing brain HTT levels in mice. Recently, branaplam (also known as LMI070) which was administered to patients with SMA, has been granted an Orphan Drug Designation for HD, with plans to begin a Phase IIb trial in HD patients in 2021, after identifying a reduction in HTT mRNA (Wiggins & Feigin, 2021).

DNA-based Therapies

DNA-based therapies (zinc finger nucleases (ZFNs), transcription activator-like effector nucleases (TALENs), and CRISPR/Cas9 system) are in preclinical phases. Zinc finger proteins (ZFPs) are DNA-binding elements that bind directly to the mutant HD gene allele, blocking transcription of the mutant huntingtin gene. All three methods resulted in the reduction of mHTT expression in mouse models (Pan & Feigin, 2021; Tabrizi et al., 2020).

Therapies Targeted at Aberrant Downstream Pathways

Post-synaptic proteins have been implicated in the aberrant downstream signaling post-synaptic activation of pro-death pathway signaling at the cortico-striatal synapse, such as extrasynaptic NMDA receptors (GluN2B), sigma 1 receptors (SIG1R), post-synaptic density protein 95 (PSD95) and phosphodiesterase 10A (PDE10A) (Niccolini et al., 2015). Pridopidine

is a small molecule with high affinity for SIG1R. Preclinical studies of pridopidine normalized cellular membrane calcium levels, improving motor and psychiatric phenotypes in mouse models and increased BDNF levels, improving survival (Shannon, 2016). However, Phase II and III clinical trials (HART, MermaiHD) and a follow-up phase II clinical trial (PRIDE-HD) didn't show any clear clinical benefit (Pan & Feigin, 2021). Semaphorin 4D is a transmembrane signaling molecule that promotes B cell and dendritic cell activation. In addition, SEMA4D promotes glial cell inflammatory transformation in neurodegenerative diseases like HD. Reduction of neuroinflammation and prevention of autoimmune encephalomyelitis was shown in preclinical studies with a blocking monoclonal antibody to SEMA4D (pepinimab) in rodents (Pan & Feigin, 2021).

Clinical rating scales in HD clinical trials

Clinical rating scales have been used as primary end points in clinical trials and other studies of HD. However, they lack sensitivity when changes are needed to be measured longitudinally over years. A lack of proper biomarkers to accurately measure changes contributes to a lack of disease-modifying therapies for HD. Clinical scales are subject to human error and inter-/intra-rater variability. In addition, clinical scales are not properly designed to fit every patient,

particularly premanifest HD mutation carriers, which is the most important and promising group likely to benefit more from disease modifying therapy (Winder et al., 2018).

There is, therefore, a pressing need for the identification from the earliest disease stages of reliable and robust biomarkers of HD progression, which are crucial for the further development and evaluation of such potential disease-modifying treatments. The availability of genetic testing and the full penetrance of HTT mutation in people with more than 40 CAG expansions provide a unique window of opportunity to examine the pattern of signs, symptoms and neurobiological changes as they emerge and study the clinical course of HD before the development of overt symptoms. Consequently, there is an urgent need to identify biomarkers that are able to monitor disease progression and assess the development and efficacy of novel disease modifying drugs. The identification of easily obtainable, reliable, and robust biomarkers of HD progression is crucial for future clinical trials.

1.9 Quest for biomarkers in HD

Biofluid and imaging biomarkers are expected to revolutionize the therapeutics field, particularly in combination with clinical measures, offering reliability, reproducibility. accuracy and quantification of pathobiological processes pathobiological processes, hopefully at a low cost. Furthermore, they are expected to empower clinical trials and provide useful hypotheses for new drug development and insights into the pathomechanism of disease. Biofluid biomarkers could provide molecular quantification of biological processes, whereas imaging biomarkers could provide quantification of changes in the brain at a structural level. When combined they could provide information for a more comprehensive evaluation of disease stage and progression useful for clinical trials (Zeun et al., 2019a).

Biomarker definition

A biomarker is defined as an entity that can be quantified providing an indication of disease-related processes, natural variation, or in the context of interventional studies, treatment response and efficacy. Biomarkers are expected to serve as mediators for a more accurate diagnosis, prognosis and treatment. They should be used for detecting early disease, widening thus the window to begin treatment promptly. Regarding clinical trials. biomarkers could stratify patients more accurately and in case of a disease modifying therapy could measure efficacy (FDA-NIH Biomarker Working Group, 2016).

Several biomarker subtypes are described, as categorized by the FDA/NIH developed Biomarker, EndpointS and other Tools (BEST). Diagnostic biomarkers, monitoring, pharmacodynamic or response, predictive, prognostic, safety, susceptibility/risk and surrogate biomarkers are some applications-subtypes of biomarkers. Each subtype has specific criteria but a single biomarker could be used in multiple applications and consequently belong to many subtypes simultaneously (FDA-NIH Biomarker Working Group, 2016).

The ideal biomarker is easily accessible, easy to obtain (how invasive the technique to access) and measure, and could be used as a surrogate endpoint for clinical trials or to aid clinical decision making. Quantification should be reliable and behind every robust biomarker, a strong biological reasoning exists representing a physiological mechanism. To obtain a regulatory approval for a candidate biomarker an extensive and formal validation process is needed to ensure that it meets all criteria for measurability, accuracy, specificity and reproducibility. Guidelines are provided by regulatory authorities but no candidate biomarker has succeeded yet for HD. Finally, an ideal biomarker should be appropriate to use across all disease models and it could be used as a translational biomarker in preclinical

development of therapies (Tabrizi et al., 2020, FDA-NIH Biomarker Working Group, 2016, EMA, 2008).

Biofluids

Biofluids are biological fluids that are secreted, excreted or obtained using methods such as blood draw or lumbar puncture. Commonly used biofluids are blood, urine, cerebrospinal fluid (CSF), saliva or sweat. Several biological molecules can be quantified in biofluids including proteins, RNA and DNA. There are many benefits of using biofluids for biomarkers. Highly specific and robust assays can be developed to produce consistent and objective measurements. Biofluids can also be stored in biobanks for long periods and be re-evaluated in the future with more sensitive techniques. Biomarkers such as CSF, plasma NfL. and CSF mHTT have been used in the HTT-lowering therapies trials and are included in ongoing and planned trials. These markers seem to be promising, useful and informative (Tabrizi et al. ,2020).

1.9.1 Neuronal damage biomarkers

Biofluid biomarkers that measure neuronal damage accurately could be a rapid, less expensive,and more specific measure of disease progression or therapeutic efficacy. The best candidates for biochemical biomarkers of neuronal damage in HD were first studied in other neurodegenerative diseases. Most notable markers of neuronal damage, and analyzed in this thesis are neurofilament light protein (NfL) levels. Dying neurons in neurodegenerative diseases are known to release proteins that can be quantified in CSF. Tau protein and NfL (light subunit of neurofilament triple protein, a component of the neuronal cytoskeleton) are well-established as markers of neuronal death in HD and other neurodegenerative diseases. Tau and NfL have been investigated in many HD cohorts (Niemelä et al., 2017).

S100B

S100B in serum was the first molecule of neuronal damage in HD that was measured by Stoy and colleagues in 2005. Commercially available ELISA assays were used for quantification. S100B is a known marker of acute brain injury, and it is thought to be released by astrocytes inresponse to damage. However. no difference was detected between HD patients and healthy controls (Zeun et al., 2019a).

Tau protein

Tau is secreted from neurons into CSF. Tau is an axonal protein, promoting microtubule stability and assembly. Total tau levels increase in response to acute brain injury indicating non-specific neuronal damage. Abnormally phosphorylated tau inclusions were identified in HD brain, suggesting that tau may contribute to pathogenesis. Abnormal tau phosphorylation and truncation may also promote neuronal damage by causing disassembly of microtubules and impaired axonal transport (Masnata & Cicchetti, 2017).

Tau studies in HD have shown inconsistent results. CSF levels of tau were found significantly elevated in HD. However, due to overlap. tau could not provide distinction between presymptomatic and symptomatic groups and showed no correlations with clinical measures. No group differences in CSF tau were observed in another study. In contrast, Rodrigues et al. found higher CSF tau in HD mutation carriers and several UHDRS components were significantly associated with tau. Phosphorylated tau was reported to be lower in premanifest HD but there was no significant difference after adjusting for age (Constantinescu et al., 2009, 2011, Mandelkow 2012, Vinther-Jensen et al.,2016. Rodrigues et al., 2016a. Zetterberg 2017. Niemelä, Burman et al. 2018).

mHTT

mHTT is known to be released from dying-damaged neurons. Quantification of mHTT in CSF samples can be reliably measured with ultrasensitive immunoassays. mHTT measurements have been also used in clinical trials. mHTT in HD CSF correlates with disease stage and severity. The first quantification of soluble mHTT was in 2009 in human whole blood. A study a few years later revealed significant differences between manifest HD and premanifest, but also across different stages of disease. Disease burden score and several neuroimaging markers like caudate atrophy and ventricular expansion were significantly correlated with mHTT. mHTT in peripheral blood did not correlate with disease burden score or with Unified Huntington's Disease Rating Scale (UHDRS) Total Motor Score (TMS) and showed no difference in premanifest and healthy controls (Byrne & Wild, 2016). In 2015, Wild and colleagues developed a novel femtomolar-sensitive immunoassay and quantified mHTT in CSF. mHTT CSF level was correlated with onset probability in premanifest and with disease severity (UHDRS Total Motors Score (TMS), symbol-digit modality test, Stroop colour naming test, Stroop word reading test, Stroop interference test) in manifest HD. Furthermore, an association was shown between mHTT, neurofilament light chain (NfL) and total tau. (Byrne & Wild, 2016).

Overall, quantifying mHTT has been challenging since it is present in low concentrations in biofluids and is ubuiquitously produced. It is difficult to distinguish between CNS-derived mHTT and periphery-derived mHTT. However, currently CSF mHTT. has been used to interpret the effects of HTT-lowering therapies and is included in ongoing and planned clinical trials. Longitudinal studies and more clinical trials are needed for CSF mHTT to be validated as a pharmacodynamic marker of HTT lowering (Zeun et al., 2019b).

Neurofilament light chain (NfL)

Another group of molecules associated with axonal injury and neurodegeneration are the neurofilament proteins of the axonal cytoskeleton. Neurofilament light chain (NFL) is a 70 kDa protein with highly specific expression in central and peripheral nerves, belonging to class IV intermediate filament family. Its normal roles are axonal stability and radial growth. NfL are present in axons and synapses and it is speculated that they are released from synapses into CSF. NfL monomers assemble into dimers, tetramers and then cylindrical filaments that elongate by end-to-end annealing. NfL protein is released by neuronal damage. Three isoforms exist: the heavy, the medium and the light chain (Khalil et al., 2018). Studies suggest that some of the earliest detectable changes occurring in HD are elevated concentrations of NfL and mHTT, followed by changes in imaging markers (e.g caudate atrophy) motor scores and cognitive measures. In 2007, Wild and colleagues measured neurofilament heavy chain using an in-house ELISA assay. No difference was found between premanifest HD and healthy controls or between pre-manifest and manifest HD (Tabrizi et al., 2020). Constantinescu and colleagues using an in-house ELISA assay detected and measured the light chain isoform in the CSF of HD patients in 2009. NfL was found to be significantly elevated and a positive correlation between the UHDRS Total Functional Capacity (TFC) and neurofilament light chain (NfL) was reported (Constantinescu et al., 2009). Currently, several studies have reported higher CSF NfL concentrations in HD than in healthy controls. Furthermore, NfL levels increased with disease progression and predicted progression rate in HD (C. A. Ross et al., 2014). NfL is known to originate in the CSF. Consequently, CSF and plasma NfL levels are strongly correlated. In a mouse model of HD, CSF NfL correlated with brain atrophy and disease severity in mouse models.

CSF NfL increases with age and is found elevated in many neurological disorders in acute or progressive neuronal injury, such as traumatic brain injury, prion disease, neuroinflammatory

conditions such as multiple sclerosis and neurodegenerative conditions such as Huntington's disease, amyotrophic lateral sclerosis, FTD and AD (Zeun et al.. 2019b. Wild et al. 2007).

Although CSF NfL was more strongly associated with brain volume than plasma NfL, plasma NfL was a better predictor of progression rate than CSF NfL. Plasma NfL levels were elevated in manifest HD compared to controls and increased with disease severity, predicting degree of brain atrophy. In premanifest HD, plasma NfL levels predicted clinical onset within the next 3 years and disease progression (Zeun et al., 2019a). In 2015, a single molecule assay (SIMOA) technology was used for the first time for quantification of NfL in blood. Plasma levels of NfL were found increased at every disease stage when compared to controls, even in the early premanifest group with significant differences even between early and late premanifest and were associated with CAG repeat length. Higher CAG repeat counts were associated with earlier and higher increases in plasma Nf. Baseline plasma NfL predicted subsequent disease onset within three years in premanifest mutation carriers, as well as change in measures of cognitive and functional ability and brain atrophy and it was the first time a biofluid marker has shown such predictive value (Zeun et al., 2019a). To conclude, NfL appears to be a robust biomarker of HD disease progression and neuronal damage and has been shown to be higher in the plasma and CSF of HD patients in several different cohorts (Zeun et al.,2019b, Niemelä et al., 2017, Vinther-Jensen et al.,2016, Wild et al., 2015, Waldö et al.,2013, Constantinescu et al.,2009).

1.9.2 Inflammatory markers

Neuroinflammation has been implicated in HD in several studies. Over-activation of microglia, and abnormalities of the innate immune system have been described in HD

patients. mHTT is present in leukocytes and microglia and has the potential to derange the immune system. The immune system could be used as a source of biomarkers of HD as well as of markers of therapeutics targeting the immune system. However, such biomarkers are limited by infections and other immune derangements unrelated to HD ((Björkqvist et al., 2008), Dalrymple et al., 2007).

YKL-40

YKL-40 (member of the glycosyl hydrolase family 18, also known as Chitinase-3-like protein 1, CHI3L1) was suggested as a marker of microglial activation. It was investigated in HD after elevation in other neuroinflammatory diseases was described. YKL-40 plasma increased with age in healthy controls but did not reach statistical significance when corrected for age (Zeun et al., 2019a). In later studies, age-adjusted YKL-40 was elevated in HD mutation carriers and was associated with motor and functional decline. CSF levels of the microglia-derived inflammatory mediator YKL40, the immune cell-derived enzyme chitotriosidase and the pro-inflammatory cytokine IL-6 were higher in HD patients compared to healthy controls in another study. CSF levels of YKL40 also increased with disease progression (Rodrigues et al.. 2016b, Vinther-Jensen et al.. 2014, Aronson et al.. 1997).

Clusterin

Clusterin (also known as Apolipoprotein J) is a chaperone glycoprotein. Clusterin has shown promising results as a biomarker of neurodegeneration and a genetic modifier of Alzheimer's disease with unknown mechanism (Silajdžić et al., 2013). It was found to be increased in HD plasma and CSF using ELISA techniques in one study. However, another study using ELISA

in serum did not confirm these results. Further studies are needed to understand this candidate biomarker (Silajdžić et al., 2013).

IL-6 and IL-8

IL-6 and IL-8 were found elevated in blood plasma. More specifically, elevation of the pro-inflammatory cytokine interleukin-6 (IL-6) is the earliest reported marker of immune activation in HD. However, recently, IL-6 deficiency was found to exacerbate the effects of mutant huntingtin in model mice through dysregulation of genes related to HD pathobiology in striatal neurons, suggesting that modulation of IL-6 promotes proper regulation of genes associated with synaptic function and maybe promising as an HD therapeutic target. (Wertz et al. 2020, Zeun et al., 2019a, Huang et al., 2011, Björkqvist et al., 2008).

1.9.3 Kynurenine pathway metabolites as HD markers

Before the identification of *HTT* as the cause of HD, quinolinic acid (QA) lesioned mice were used to study HD as an experimental model. QA is a key component of the kynurenine pathway (KP), which encompasses the oxidative metabolism of tryptophan. QA is toxic for medium spiny neurons. QA and kynurenic acid (KA) have been found altered in HD CSF. However, CSF KP metabolites were studied before the discovery of the HD causative gene. In 2005, Stoy and colleagues quantified six components of the kynurenine pathway in the blood of HD and healthy controls (tryptophan, kynurenine, KA. 3-hydroxykynurenine, 3-hydroxyanthranilic acid (3HAA) and xanthurenic acid). The kynurenine:tryptophan and KA:kynurenine ratios were found elevated in HD patients (Stoy et al., 2005). Levels of the redox-active 3HAA were decreased in HD patients compared to healthy controls. A greater

conversion of tryptophan to kynurenine was suggested in HD patients. KP metabolites in blood seem to not have equal ability to cross the blood-brain barrier (e.g tryptophan and kynurenine pass easily in contrast to other components such as 3HAA, KA). This questions whether blood is a relevant medium to measure disease markers of HD-related neuropathology. Blood also may be too dynamic for measuring metabolic markers to give a meaningful indication about HD disease processes (Zeun et al., 2019a, Heyes et al., 1992).

1.9.4. Transglutaminase activity

Transglutaminases are enzymes involved in reactions between glutaminyl- and lysyl-containing molecules or polyamines. It has been showed *in vitro* that expanded polyglutamine strengthens transglutaminase activity. This proposed that transglutaminases may be involved in the regulation of mHTT aggregation. Moreover, treatment of HD transgenic mice with cystamine (an inhibitor of transglutaminase) alleviated HD symptoms. Several markers for transglutaminase activity have been investigated in the CSF of HD patients such as Nε-(γ-l-Glutamyl)-l-lysine (GGEL), γ-Glutamylspermidine, γ-Glutamylputrescine and bis-γ-Glutamylputrescine. All the markers were found elevated in HD patients. However, a randomized. placebo-controlled, phase 2/3 clinicaltrial of cysteamine (CYST-HD) in HD patients did not show any clinical benefit (Kumar et al., 2015).

1.9.5. Neurotransmitters

Based on the loss of GABAergic medium spiny neurons that was described in HD, studies of the GABAergic system have emerged. Several studies were performed with inconsistent results showing lower concentrations of GABA and increase in homocarnosine (a dipeptide containing GABA), in HD when compared to controls. Results from a randomized, double-blinded trial in patients using isoniazid and γ-acetylenic GABA were disappointing with contradictory findings (Garret et al., 2018). Dopamine metabolites were also investigated as promising biofluid biomarkers. However, CSF levels of dopamine and its metabolites showed inconsistent results. Homovanillic acid (HVA) and other dopamine metabolites, were shown to decrease in some studies, whereas no difference was reported in others (Silajdzi´ et al. ,2018).

1.9.6. Transcriptomic and proteomic approaches

It is well-established that HD causes transcriptional dysfunction, possibly due to mHTT and DNA interactions. Transcriptional differences in blood in a panel of 12 genes were found in one study, between controls and HD carriers (Runne et al., 2007). However, these results could not be validated in other studies. Larger populations are needed to be included in studies, using more recent methods for promising transcriptomic biomarkers to be discovered. Similarly, proteomic studies in CSF, blood and urine have failed to discover new promising biomarkers, with the exception of immune dysfunction as we previously described (Miller et al. 2016, Runne et al.2007).

1.9.7. Oxidative stress

Oxidative stress has been implicated in many neurodegenerative diseases. F2-isoprostanes and 8- Hydroxy-2-deoxyguanosine (8OH2'dG) have been investigated in HD as markers of oxidative stress. F2-isoprostanes, a marker for lipid peroxidation, was found elevated in HD

CSF, as previously described in AD (Miller et al., 2014). However, these findings were not replicated in another study. Several randomized clinical trials were performed investigating antioxidants, such as ethyl- EPA, creatine, and coenzyme Q10 with disappointing results (Zeun et al., 2019a).

1.9.8 Neuroendocrine and metabolic markers

Over 50 neuroendocrine and metabolic molecules have been investigated in HD. BDNF (brain derived neurotrophic factor), a peptide related to the survival of striatal neurons, was found decreased in the blood of HD expansion carriers (Ciammola et al., 2007). However, this was not validated in other studies. To date, no study has measured BDNF in CSF. Melatonin is a hormone secreted by the pineal gland. Its role is in the sleep-wake cycle, which is known to be dysregulated in HD. No differences were shown in two studies in plasma melatonin in HD patients. A larger study showed a decrease in hormone concentration with disease progression, even in premanifest HD (Wang et al., 2014).

1.10 Huntington's disease & α-synuclein

As previously stated, the exact pathomechanism underlying HD remains to be elucidated. Increased α-synuclein aggregation has been reported in human post-mortem putamen samples from HD patients. A cross-talk between Htt aggregation and α-synuclein has been speculated, suggesting a modifying effect of α-synuclein on Htt aggregation, even though the mechanism underlying such a potential interaction is still obscure. There is interest, therefore, in investigating the role of α-synuclein in HD. (Jimenez-Sanchez et al.. 2017, St-Amour et al., 2018).

In neurological disorders that do not exhibit α-synuclein pathology, peripheral α-synuclein hasbeen put forward as a potential marker of neurodegeneration. In the context of Parkinson's disease (PD), the detection of pathological α-synuclein in the periphery has been evaluated based on the proposition that the disease could involve the autonomic nervous system years before spreading to the central nervous system (Klingelhoefer & Reichmann, 2015).

Even though the role of serum and plasma a-synuclein as a potential biomarker in neurodegenerative synucleinopathies has been extensively investigated in recent years, findings remain controversial. Interestingly, several studies, including a recent meta-analysis of plasma a-synuclein in PD, have demonstrated elevated levels compared to controls. In contrast, declining levels of plasma α-synuclein have been observed with normal ageing (Lin et al., 2017). To the best of our knowledge, no reports of serum α-synuclein levels in patients with HD have been published to date. Given that behind every biomarker exists a biological reasoning representing a physiological mechanism and the fact that increased α-synuclein aggregation has been reported in human HD post-mortem putamen samples, we presently sought to investigate serum α-synuclein levels in patients with HD, using ELISA and compare them to controls (Stefanis et al. 2012, Bougea et al., 2019, Lin et al., 2017, Duran 2010) .

1.10 Neuroimaging markers

Neurodegenerative diseases including Huntington's disease (HD) are now recognized to start years before symptoms appear. Neuroimaging has become a standard practice in diagnosis of neurodegenerative diseases. The use of diverse magnetic resonance imaging (MRI)

techniques (modalities) and the introduction in the field of an increasing array of PET ligands have provided a breakthrough in traditional imaging. Neurodegenerative diseases can be identified, and progression can be measured by a plethora of objective imaging markers. This is crucial not only in the everyday clinical setting but also for monitoring patients in clinical trials, to assess efficacy of the treatment under investigation. (Ross et al., 2014).

Neuroimaging (mainly MRI) has been widely used in the diagnostic work up of HD patients. The main finding is atrophy of the head of the caudate nucleus, however atrophy of the putamen and mild atrophy of the globus pallidus may be depicted. Compensatory enlargement of the frontal horns of the lateral ventricles is also noticed. Consequently, both the distance between the medial edge of the caudate nuclei (intercaudate distance), and the ratio of the intercaudate distance to the inner tables of the scull increase, while the ratio of the distance between the lateral margins of the lateral ventricles to the intercaudate distance is low(Aylward et al., 1991, Ho et al., 1995). On T2 weighted images high signal intensity may be noticed in the caudate nuclei and the putamina in juvenile HD (Schapiro et al., 2004). However, striatum may also appear T2 hypointense due to iron deposition (Chen et al., 2019). Striatum hypointensity may be more evident on Susceptibility weighted imaging (SWI). Low signal intensity on SWI may sometimes appear in the red nucleus and in the substantia nigra (Macerollo et al., 2014).

Low FDG uptake in PET in basal ganglia precedes detectable atrophy, and it may be accompanied by frontal lobe hypometabolism (Ahmad et al., 2014). Perfusion defects in

basal ganglia and frontal lobes may be seen in Single Photon Emission Computed Tomography (SPECT) (Harris et al., 2015).

By investigating a diverse set of multi-modal neuroimaging approaches it may be possible to track the trajectory of different tissue properties in a more meaningful way. This could yield an appropriate set of biomarkers not only for HD characterization, but also for therapeutic intervention studies.

Imaging Biomarkers & Huntington's disease

A number of different imaging modalities are now being used, including structural MRI, diffusion tensor imaging, functional MRI and PET. Numerous image processing techniques and methods chosen can have a significant impact on output metrics being considered as biomarkers. Before such measures can be effectively utilized as a biomarker, rigorous validation of the acquisition and analysis technique is required and has been lacking in many imaging studies to date. Three modalities are the most commonly used in neuroimaging research, structural, diffusion and functional imaging (Wilson et al. 2018).

Two large international collaborative studies (Track-HD, Predict-HD) showed that disease-related atrophy of the striatum and white matter is present many years prior to the expected symptom onset. Atrophy changes are observed through the different stages of the disease, including premanifest HD cases. The studies concluded that it is possible to measure neurodegeneration via yearly assessments of striatal, cortical and white-matter volumes (Paulsen et al., 2014). Tabrizi et al. 2011).

TRACK-HD was a longitudinal study focusing on the identification of sensitive and reliable biomarkers of HD progression utilizing annual assessments involving MRI brain imaging and clinical measures in premanifest and early manifest HD. MRI measures showed significantly increased total brain atrophy rates in both premanifest and early manifest HD at 12 months. Caudate and putamen volume was reduced by 1.4 to 4.5% compared to baseline levels in both premanifest and manifest patients. White-matter changes were also observed around the striatum and within the corpus callosum (Claassen et al. 2017, Tabrizi et al. 2012).

MRI data acquisition

MRI scanning alters the state of hydrogen atoms in the body using radiofrequency and magnet pulses. The energy created by these changes via the manipulation of atoms within the body in state can be measured. An output of the latter produces an MRI image. Then, varying MRI acquisitions can be used to capture different characteristics and functions of the brain (Currie et al., 2013).

1.10. Structural imaging markers

Structural MRI

Structural MRI has been extensively used in HD research since it provides the ability to investigate the brain anatomy and quantify whole-brain and regional atrophy. Macroscopic effects of HD neuropathology on brain structure could be visualized in vivo via structural MRI. Structural MRI use is limited for clinical diagnosis, as genetic testing is available in HD. However, it could provide information for disease progression. Given that many upcoming novel therapies in HD have shown promising results, structural imaging markers

are needed to assess efficacy. Currently, structural neuroimaging measures are used as markers for outcome measures in HD clinical trials.

The most studied imaging acquisition in HD is a structural volumetric MRI scan. T1-weighted image is used for the contrast between grey and white matter it provides. The contrast helps to accurately delineate structures of interest. A number of different brain regions have potential as biomarkers of disease progression in HD. As previously described, it is well-established that prior to clinical diagnosis, which is defined as motor onset, there may be subtle impairment in the motor, cognitive, neuropsychiatric domains as well as brain structural changes. Even from the very earliest stages changes are reported several years before (Tabrizi et al. 2009. (Paulsen et al., 2014)Paulsen et al.2008).

sMRI is used to estimate different brain regions characteristics such as volume, surface area, cross-sectionally or longitudinally. sMRI measures can be easily replicated across multiple study sites and are known to exhibit the greatest effect sizes in longitudinal change. Three main measures have been used when analyzing analyzing MRI data: regional volumetric, voxel-based morphometry (VBM) and cortical thickness (CT) analyses (Georgiou-Karistianis et al., 2013; Hobbs et al., 2013)

Analysis of sMRI data

Two main approaches have been used for sMRI data processing. 1.Exploratory whole-brain analysis and 2. Hypothesis-driven region of interest (ROI) analysis. Both methods offer complementary information, and within these broad techniques there are a multitude of different measurements that can be performed.

Exploratory Whole-Brain Analysis Approach

A more exploratory, whole-brain analysis approach could be used to study volumetric differences in HD. Widespread atrophy is reported in HD in regions beyond the striatum and throughout the cortex. Voxel-based morphometry (VBM) has revealed many widespread volumetric differences including the cingulate, pre-central and pre-frontal cortices, occipital, parietal, and temporal cortices in manifest HD (Tabrizi et al. 2011. 2009, Hobbs et al.2010).

WM atrophy has been shown to predict onset in the premanifest stage. In premanifest HD, a pronounced loss of WM is reported localized to the frontal lobe, the striatum, and posterior-frontal regions. In early HD, volume loss seems to affect all lobes with a widespread atrophy. In manifest HD, significant WM atrophy was identified compared to healthy controls across all disease stages. WM atrophy has also been associated with a longer CAG length and cognitive and motor decline (Scahill et al. 2013, Paulsen et al.2010, Tabrizi 2009, 2012).

However, whole-brain analysis studies have not shown consistency in findings in premanifest stages. A few studies with small sample size did not report any differences in WM atrophy when compared to controls. This may be attributed to a small sample size, but also to the unique characteristics of each premanifest HD group (far from or close to estimated motor onset). WM atrophy has been shown to be sensitive both in premanifest and manifest HD progression and strongly correlated with UHDRS TFC, motor skills, and estimated time to disease onset (Scahill et al.. 2013. Tabrizi et al. 2012. Paulsen et al.. 2010.Hobbs et al.. 2010).

Hypothesis-driven region of interest (ROI) analysis

Hypothesis-driven ROI analysis studies allow for the analysis of well-known affected structures based on a priori hypotheses, whereas whole-brain studies enable a more

exploratory analysis without the need for a priori assumptions to be made. Several HD studies using ROI analysis have focused mainly on the most known affected structures, the caudate nucleus and putamen, showing pronounced volume loss of these regions in both premanifest and manifest HD cases when compared with healthy controls (Aylward et al. 1996, Paulsen et al. 2006b, Rosas et al. 2001, Tabrizi et al. 2009, Wolf et al. 2013).

The gold-standard ROI analysis technique is manual segmentation from an expert that traces by hand the outline of a structure on every MR image. This method is time-consuming, subject to inter- and intra-rater variability. Automated techniques have been developed allowing for large numbers of MRIs to be analyzed by several raters for clinical trials. Poorly defined boundaries in anatomical structures, as for example in WM analyses could affect accuracy and results both in manual and automated methods.

Caudate and putamen

Atrophy of the basal ganglia structures, particularly the striatum, is well established in manifest HD. Caudate volume is the most sensitive biomarker of disease progression during the premanifest HD and manifest HD stages. Atrophy of the caudate and putamen has been observed in several studies from 15-20 years prior to predicted disease onset. Volume of these structures has been found to correlate specifically with HD motor impairment. Several studies showed accelerated rates of atrophy in the caudate compared to the putamen. However, the TRACK- HD study reported accelerated rates of atrophy in the putamen compared to the caudate. This could be attributed to the fact that the caudate is easier to delineate than putamen. This atrophy generally increases through the different stages of the disease correlating with disease severity. By the time of symptom onset, striatal volumes have already been reduced to approximately 50% of their volume. An annual rate of change

has been estimated between different studies of up to 4% per year in the caudate and 3% per year in putamen, increasing in manifest disease. (Georgiou-Karistianis et al. 2013, Tabrizi, Scahill et al. 2013, (Aylward et al., 2011).

There is also inconsistency on whether the rate of change in striatal atrophy varies with disease stage. Step-wise accelerated rates of change from the earliest premanifest stage through to early-stage disease with a slow-down of the rate after symptoms onset have been reported in TRACK-HD. However, in the PREDICT-HD study rates did not accelerate across their premanifest cohort, but differences in methodology could be the reason (Tabrizi et al., 2012). Tabrizi, Scahill et al. 2011, Aylward, Nopoulos et al. 2011).

Atrophy rates and baseline striatal volume predicted conversion to manifest HD in TRACK-HD, PREDICT-HD studies. Striatal atrophy was significantly correlated with UHDRS total motor score (TMS), paced finger tapping and tongue force. Caudate volume loss was found to be associated with deficits in emotion recognition, verbal learning and working memory. Putaminal atrophy was associated with executive dysfunction and emotion recognition (Tabrizi, Reilmann et al. 2012, Tabrizi, Scahill et al. 2011, Aylward, Nopoulos et al. 2011). Volume changes in the nucleus accumbens, pallidum and thalamus have been described from the premanifest stage. In addition, thalamic atrophy has been observed in premanifest and manifest HD in longitudinal studies. Thalamic atrophy correlated inversely to CAG length. A correlation between thalamic volume TMS and cognitive dysfunction has also been reported (Aylward, Nopoulos et al. 2011, Hobbs, van den Bogaard, Dumas et al. 2011).

No differences were identified in non-striatal subcortical structures such as the globus pallidus and nucleus accumbens in any of these structures in one study. Furthermore, regions such as

the cingulate, thalamus, and hippocampus showed significantly lower volumes compared with controls. However, findings were inconsistent regarding the amygdala. Smaller structures do not have well-defined in terms of anatomic boundaries, consequently measurements vary (Hobbs et al.. 2011; Aylward et al., 2011a; Tabrizi et al.. 2011; Henley et al.. 2009; Rosas et al., 2003).

Cortical structures

Cortical involvement has been mainly described after conversion to manifest disease. For cortical volumes semi-automated and automated segmentation techniques (e.g.Statistical Parametric Mapping (https://www.fil.ion.ucl.ac.uk/spm/), Freesurfer (https://surfer.nmr.mgh.harvard.edu/), FSL are used. Cortical thickness reductions have been identified both in premanifest and manifest HD. Cortical thinning changes are less sensitive over time in manifest HD than other structural measures such as striatal areas. Longitudinal and cross-sectional studies showed reduced whole brain and grey matter volume in HD manifest and premanifest carriers, accompanied by an associated increase in CSF spaces (Tabrizi et al., 2013).Grey mater (GM) degeneration in premanifest HD is well documented, both regional volume loss as well as cortical thinning. Total grey matter volumes were significantly correlated to decline in TFC in early HD. However, age and CAG repeat length predicted changes in premanifest HD longitudinally in all imaging measures except grey matter. (Tabrizi, Scahill et al. 2013).

Currently, WM degeneration in HD is an established hallmark of the disease, identified also in premanifest HD gene-carriers. A few studies have investigated whole-WM as an ROI to measure atrophy. Cerebral WM volume has been found to be significantly lower in premanifest HD and early HD in comparison to healthy controls particularly in the frontal

lobe area. Limitations of ROI WM studies are that global volumes of WM are compared, therefore it is difficult to identify atrophy in specific regions of the cerebral WM. Whole-brain mapping techniques may provide more information. WM atrophy correlated with motor and cognitive function and TFC. Findings for WM volume were inconsistent for prediction of clinical conversion of the disease in two large studies. However, it seems that white matter atrophy may be able to track disease progression from early premanifest stages of the disease (Hobbs et al. 2015, Tabrizi et al. 2013, 2009, Aylward et al. 2011, Paulsen et al.2010, Rosas et al. 2008).

Previous studies highlighted that striatal and WM loss occurs earlier in the disease prior to onset of symptoms. A greater rate of grey matter loss has been described after clinical conversion. Furthermore, measuring structure of the cortex is more complex, a fact that causes variability in measures, reducing sensitivity of global atrophy (Tabrizi, Reilmann et al. 2012, Paulsen, Nopoulos et al. 2010).

Longitudinal studies performed earlier were not sensitive enough to detect longitudinal changes in white matter but recently significantly elevated rates of white-matter atrophy were found even in premanifest HD when compared with controls in studies with larger cohorts. TRACK-HD and PREDICT-HD showed white matter atrophy even in early premanifest HD stages, as well as progressive atrophy in manifest HD with the most prominent changes in the areas of the striatum and corpus callosum. Axonal damage and/or demyelination has been speculated to occur, even in advance of widespread volume loss (Tabrizi, Scahill et al. 2011, Hobbs et al. 2013). FreeSurfer-measured cortical thickness identified cross-sectional reductions and gyral enlargement in premanifest HD. Neurodevelopmental abnormalities were speculated to cause gyral enlargement. A recent study showed that cortical thinning was less sensitive to changes

over time than other structural markers when studied longitudinally in manifest HD (Hobbs et al. 2015, Tabrizi, Scahill et al. 2013,2009, Nopoulos et al. 2007, Fischl et al. 2000).

CAG repeat length & imaging markers

It is well-established that CAG repeat length influences age of HD onset and it has been proposed that it may change rates of structural markers. Several studies have found structural measures such as the striatum and mainly the caudate to correlate with CAG repeat length, after controlling for age (Langbehn et al.2010, Henley et al. 2009).

1.11 Neuromelanin sequence

Dopaminergic neurons of the SN, particularly in the SN *pars compacta,* contain neuromelanin (NM). NM is a highly paramagnetic dark pigment that is believed to form by oxidative polymerization of dopamine or noradrenaline. NM has been proposed as neuroprotective in brain oxidative damage by free radicals and ferric iron, but also has been linked to neurodegeneration through disruption of iron homeostasis. Dysregulation of the nigrostriatal pathway and the possible disruption of iron homeostasis in HD resulting in striatal volume loss, may be associated with SN degeneration and NM depletion.

A few studies have investigated the nigrostriatal pathway in HD. Recently, specifically designed T1-weighted MRI sequences (NM-MRI) been developed to detect *in vivo* SN NM signal changes. To date, only one study has been published using NM-MRI, (Leitao et al. 2020), showing loss of NM in this region, supporting the implication of dopaminergic neuronal changes in HD pathology. NM-MRI has been investigated in other

neurodegenerative diseases like PD and results indicate that it could a promising biomarker but further studies in larger cohorts are needed (Leitao et al. 2020).

1.12 Aims of this Thesis

The purpose of this study was to analyze a set of clinical, imaging and biofluid (serum NfL and alpha-synuclein) biomarkers, both known and potential, for characterization of patients with manifest HD as well as pre-manifest HD expansion carriers. All biomarker data were compared between manifest and pre-manifest HD, as well as matched controls. The role of serum a-synuclein was specifically investigated as a novel potential marker, in an attempt to provide insights into the HD pathophysiology, taking into consideration the known interplay of a-synuclein with mHtt.

As an adjunct, genetic data from a recent GWAS were used in parallel with other available DNA & RNA-expression open databases to run computational analyses with a view to providing further insight on the *SNCA* pathway and other specific pathways implicated in the pathophysiology of HD. Appropriate matched healthy controls were used for all parts of this thesis. Cross-sectional comparisons and correlations of neurological, neuropsychiatric and cognitive findings with neuroimaging data were explored.

The identification of diverse, reliable and robust biomarkers of disease progression in HD is crucial for the adequate evaluation of potential future disease-modifying therapies. The combination of wet and dry biomarkers constitutes a powerful approach to tackle this challenging problem. The work in this thesis aims to add to this progress through an investigation of novel structural imaging techniques, such as NM-MRI, as well as novel biofluid markers like a-synuclein in premanifest and manifest HD.

2. Methods

Study Design

This is a prospective, longitudinal study. All participants gave informed written consent prior to study participation. All study procedures were approved by Eginition institutional review board. Patients for each study cohort were selected from an initial pool of manifest HD patients and premanifest HD expansion carriers clinically assessed and registered in a database during the last two years before the onset of this study (80 manifest HD, 20 premanifest HD). After detailed clinical phenotyping and consideration of what clinical data was pertinent to this study, clinical notes were interrogated and data inputted into properly designed databases. Important information such as time of disease onset, was cross checked over multiple source documents within the notes to ensure that the most accurate data was obtained. Of these selected HD cases, 14 manifest HD and 11 pre-manifest HD expansion carriers were included in this study. Basic demographic and clinical details of the initial HD pool are described in the following table (Table 2). All data and NfLs were measured at baseline.

Variable	**HD patients**	**Premanifest HD carriers**
N (Total=100)	N_1 =80	N_2 =20
Gender (%)	M:45(62.1) F:35(37.9)	M:11(55.0) F:9(45.0)
Age (years)	43.2 ± 13.6	31.6 ± 10.4
Age at onset (years)	37.5 ± 11.7	**-**
UHDRS (total motor score)	20	-

Table 2: Basic demographic and clinical details of the initial HD pool that was used for selecting participants of this study.

2.1 Cohorts

The following cohorts were studied in this thesis at baseline. All participants underwent advanced neuroimaging magnetic resonance imaging and a large battery of clinical assessments in the motor, cognitive and neuropsychiatric domains. We also measured serum neurofilament light chain concentration (sNfL) in study participants. Full participant demographics are detailed in Table 2.

Cohort A (premanifest-HD): this cohort comprised of 11 premanifest HD gene carriers recruited from Outpatient Neurogenetics Clinic at Eginition Hospital, National and Kapodistrian University of Athens, Athens, Greece.

Cohort B (manifest-HD): this cohort comprised of 14 manifest HD patients recruited from Outpatient Neurogenetics Clinic at Eginition Hospital, National and Kapodistrian University of Athens, Athens, Greece.

Cohort C (healthy controls): this cohort comprised of 25 age and gender matched healthy controls subjects recruited from all over Greece.

2.1.1 Recruitment &Ethics including Informed Consent Process

Subjects were recruited at the Neurogenetics Unit, 1st Department of Neurology, Eginition Hospital, National and Kapodistrian University of Athens. Imaging and clinical assessments of those subjects took place at the facilities of 1st Department of Neurology, Eginition Hospital. National and Kapodistrian University of Athens and at Research Unit of Radiology, 2nd Department of Radiology, Attikon General University Hospital, National and Kapodistrian

University of Athens. Healthy volunteers were recruited from the family environment of participants and from other patients. We obtained approval to conduct the study from Eginition institutional review board prior to initiating the study. This study was conducted in accordance with all applicable regulatory and privacy requirements. A written informed consent was obtained for each subject before participation in the study. Participants were free to withdraw from the study at any time, without prejudice to further assessments (withdrawal of consent).

2.1.2 Selection Criteria

Main Inclusion criteria

Main inclusion criteria were applied to all participants of this study:

1. Ages 20-70 years, male and female
2. Adequate visual and auditory acuity to complete testing and able to give an informed consent.
3. Females of non-childbearing potential or if child-bearing potential, participant was non-pregnant, non-breastfeeding.
4. Absence of significant comorbidities or clinically significant abnormal laboratory values.

Subjects in Cohort A (Premanifest HD gene carriers)

Premanifest HD gene-carriers were defined at baseline with:

1. positive genetic test with CAG repeat length ≥ 40
2. burden disease score (CAG-35.5) × age >250 (Penney et al. 1997)

3. Unified Huntington's disease rating scale (UHDRS) (Huntington Study Group 1996) Total Motor Score (TMS) ≤ 5 indicating lack of significant motor signs with Unified Huntington's Disease Rating Scale-Diagnostic Confidence Level (UHDRS-DCL) < 4

Subjects in Cohort B (Manifest HD patients)

Manifest gene-carriers were defined at baseline with:

1. positive genetic test with CAG repeat length ≥ 40
2. clinical diagnosis of HD, motor features consistent with HD (UHDRS)/ DCL of 4

Subjects in Cohort C (Healthy controls):

Part of healthy control participants were spouses/partners of individuals with premanifest or manifest HD. All participants were required to be aged between 18-70 years, with an absence of any major health or psychiatric disorder or history of significant head injury at baseline.

Healthy controls were defined at baseline with

1. age and gender matched, and balanced (±8 years) with other cohorts
2. no family history of HD, other neurodegenerative or inherited disease

Main Exclusion criteria

The following main exclusion criteria were applied to all participants of this study:

1. any known intracranial comorbidities (i.e stroke, hemorrhage, neoplasms, demyelinating conditions, etc)
2. a pregnancy or subjects breastfeeding or intend to breastfeed during the study

3. a contraindication to MRI, such as metal devises or implants (e.g. pacemaker, vascular- or heart- valves, stents, clips), metal deposited in the body.
4. claustrophobia
5. any concurrent conditions that could interfere with the safety

2.2 Clinical assessments

All participants underwent a large battery of assessments in the clinical, motor, cognitive, and neuropsychiatric domains. Patients were clinically assessed on the same or the following day of brain MRI screening to ensure that measures depicted each patient's status at the same time. Blood samples were collected also on the same day.

Clinical assessments at baseline and one-year follow up

Motor assessments

For motor assessments, Unified Huntington's Disease Rating Scale (UHDRS) -Total Motor Score (TMS) and UHDRS Diagnostic Confidence Level (DCL) were used in all participants. The UHDRS-TMS and UHDRS-DCL are physician-rated instruments that are used to characterize the clinical HD motor phenotype and to capture the diagnostic confidence of the clinical team. The motor section of the UHDRS assesses motor features of HD with standardized ratings of oculomotor function, dysarthria, chorea, dystonia, gait and postural stability.

UHDRS

UHDRS is a clinical rating scale developed by the Huntington Study Group to prospectively assess clinical features of HD in both manifest HD and premanifest HD.

in four clinical domains in HD, motor function, cognitive function, behavioural disorders, and functional capacity. The UHDRS consists of four parts. each of them scoring separately.

Part I: Motor assessments (31 items with a 5-point ordinal scale. from 0-4 with the highest score defined as inability to perform the task).

Part II: Cognitive function (3 items with higher scores representing better cognitive performance. 1. Verbal Fluency Test, 2. Symbol Digit Modalities Test (SDMT) and 3. Stroop Interference Test.

Part III: Behavioral assessment (10 items with a 5-point ordinal scale. from 0-4 with the highest score indicating severe behavioral symptoms. 4 items yes/no questions assessing confusion, dementia, depression and if treatment is required (1 point for yes).

Part IV: functional capacity. This part is divided into three sections: 1. Huntington's Disease Functional Capacity Scale (HDFCS) or Total Functional Capacity Score (TFC) (25 Yes/No questions) shows the total functional capacity of each case, 2. Independence Scale rated from 10 to 100 with higher scores meaning better functioning, 3. Functional Capacity (5 items with 4-point ordinal scale from 0 to 3 higher scores showing higher functional capacity).

Functional assessments

For functional assessments UHDRS-Total Functional Capacity, UHDRS-Functional Assessment Scale (UHDRS-FAS), and UHDRS - Independence Scale (UHDRS-IS). Physical Performance Test (PPT), HD health-related Quality of Life (HDQoL) questionnaire were applied to all participants.

The Total Functional Capacity (TFC) Scale (Shoulson and Fahn 1979) is used to stage HD progression, reflecting particular the psychosocial and functional effects. The individual's ability to work, to manage money, to perform household chores and activities of daily living are scored.

Table 3: Total Functional Capacity (TFC) Scale

	Stage	**TFC**
Early HD	1	11-13
Early HD	2	7-10
Moderate HD	3	3-6
Advanced HD	4	1-2
Advanced HD	5	0

Physical Performance Test (PPT): PPT is a standardized 9-item test that is completed by the subject and measures the patient's performance on functional tasks. Patients are given 2 chances to complete each of the 9 items, and assistive devices are permitted for the tasks that require a standing position (items 6 to 9). Both the speed and accuracy at which the patients complete the items are taken into account during scoring. The maximum score of the test is 36, with higher scores indicating better performance.

HD health-related Quality of Life questionnaire (HDQoL): The HDQoL is a standardized questionnaire completed by the patient for measuring health-related quality of life. It is a validated disease-specific measure designed for HD that can provide a summary score of overall health-related quality of life, as well as scores on several discrete scales.

Neuropsychiatric assessments

For neuropsychiatric assessments, structured Clinical Interview for DSM-V Axis I Disorders, Problem Behavioral Assessment Short Version, Beck Depression Inventory–II, and Apathy Evaluation Scale were performed in all participants.

Structured Clinical Interview for DSM-V Axis I Disorders (SCID-I): The SCID-I is a physician administered semi-structured interview to determine the major DSM-IV Axis I disorders (major mental disorders). The SCID-I is divided into six self-contained modules that can be administered in sequence: mood episodes, psychotic symptoms, psychotic disorders, mood disorders, substance use disorders and anxiety, adjustment, and other disorders (Osório et al., 2019).

Problem Behavioral Assessment Short Version (PBA-s): The PBA-s, a clinician-rated scale. will be used to perform behavioral assessments and it is designed to assess 10 psychiatric symptoms thought to be potentially most relevant to HD: low mood, suicidal ideation, anxiety, irritability, angry or aggressive behavior, apathy, perseverative thinking or behavior, paranoid/delusional thinking or behavior, hallucinations and behavior suggesting disorientation. In the event that suicidal ideation is detected while administering the PBA-s to a participant, the patient was promptly referred for psychiatric evaluation to the Psychiatric Department of Eginition Hospital (McNally et al., 2015).

Beck Depression Inventory–II (BDI-II): BDI-II is a 21-items questionnaire completed by the patient to measure the severity of depression (Mestre et al., 2018).

Apathy Evaluation Scale (AES-S): AES-S is a self-administered clinical tool to provide global measures of apathy, and the examination of individual items provides qualitative information (Marin et al., 1991).

Cognitive assessments

For cognitive assessments, Mini Mental State Examination, HD Cognitive Assessment Battery: Symbol Digit Modalities Test, Emotion Recognition, Trail Making Test, Hopkins Verbal Learning Test (Revised), Paced Tapping Test, One Touch Stockings of Cambridge, Stroop Color and Word Reading Test, and Interference Test, Circle Tracing Test, Categorical Verbal Fluency Test, Phonemic fluency test, Brief Visuospatial Memory Test-Revised and Vocabulary Subscale of the Wechsler Adult Intelligence Scale-4th Edition were applied to all participants.

Mini Mental State Examination (MMSE): MMSE is a physician administered brief 30-points questionnaire test that is used to screen for cognitive impairment. The MMSE provides measures of spatial and temporal orientation. short-term memory and language functioning (Fountoulakis et al., 2000).

1. Cognitive Assessment Battery (HD-CAB): HD-CAB is a cognitive battery optimized specifically for use in late pre-manifest and early HD clinical trials validated for sensitivity.
    a) Symbol Digit Modalities Test (SDMT): SDMT is an adaptation of the Wechsler Digit Symbol subtest that measures working memory, complex scanning, and processing speed. Participants use a key presented at the top of the test page to match symbols with numbers presented in horizontal rows. The task requires that

the participants fill in the appropriate symbols below the matching number as quickly as possible (Huntington Study Group, 1996).

b) Emotion Recognition: Emotion recognition of facial expressions of emotions is examined using computerized presentations of photographs depicting 6 basic emotions or a neutral expression. Participants are asked to indicate the emotion expressed in each photograph by selecting from the words fear. disgust. happy, sad, surprise, angry, and neutral (6 stimuli per negative emotion, 3 stimuli per positive and neutral emotion).

c) Trail Making Test: Visual attention and task switching are assessed using the Trail Making test which consists of 25 circles on a standard sheet of paper. For Trails A, participants are required to connect, as quickly as possible, circles containing numbers in ascending numerical order. For Trails B, participants are to connect, as quickly as possible, circles containing numbers and letters. alternating between numbers and letters in ascending order (e.g., 1. A. 2. B. 3. C. etc.). Trail A is used only as part of the training (Bowie & Harvey, 2006).

d) Hopkins Verbal Learning Test (Revised): The Hopkins Verbal Learning Test. revised (HVLT-R) is a brief assessment of verbal learning and memory (recognition and recall). Each form consists of a list of 12 nouns (targets) with 4 words drawn from each of 3 semantic categories. The semantic categories differ across the 6 forms, but the forms are very similar in their psychometric properties (Shapiro et al., 1999).

e) Paced Tapping Test: Psychomotor function is assessed in a Paced Tapping test. Participants tap on left and right mouse buttons, alternating between thumbs, at 3.0 Hz. They first listen to a tone presented at the desired tapping rate, and then begin tapping to the tone. After 11 taps with the tone, the repetition of the tone is discontinued, and participants attempt to continue tapping at the same rate until the end of the trial (31 taps later) (Dalla Bella et al., 2017).

f) One Touch Stockings of Cambridge: One Touch Stockings of Cambridge (OTS) is a spatial planning task, which gives a measure of frontal lobe function. OTS is a variant of the Stockings of Cambridge task, and places greater demands on working memory as the participant has to visualize the solution. The participant is shown 2 displays containing 3 coloured balls. The displays are presented in such a way that they can easily be perceived as stacks of coloured balls held in stockings or socks suspended from a beam. This arrangement makes the 3-dimensional concepts involved apparent to the participant, and fits with the verbal instructions. There is a row of numbered boxes along the bottom of the screen. The test administrator first demonstrates to the participant how to use the balls in the lower display to copy the pattern in the upper display, and completes 1 demonstration problem, where the solution requires 1 move. The participant must then complete 3 further problems, 1 each of 2 moves, 3 moves, and 4 moves. Next, the participant is shown further problems, and must work out in their head how many moves the solutions to these problems require, then touch the appropriate box at the bottom of the screen to indicate their response (Stout et al., 2014).

g) Stroop Color and Word Reading Test, and Interference Test: The Stroop Color and Word. and Interference Test consist of three 45-second trials. The first two trials

(colour identification and word reading) measure basic attention. In the first trial, participants must correctly identify the colour of ink patches on a stimulus card. In the second trial, participants read the names of colours printed in black ink. In the third trial, the interference trial, participants must consistently inhibit an overlearned response by identifying the colour of ink (red, green, blue) that the stimulus colour words are printed in. rather than reading the word aloud (Stout et al., 2014).

h) Circle Tracing Test: Tool to measure visuomotor integration deficits. For a circle tracing task, patients are instructed to start at the vertical apex of a predrawn annulus (on a tablet laptop or some other technological device) and to trace circles within the annulus as quickly and accurately as possible in the clockwise direction. Participants may have multiple practice trials in order to ensure that they understand the instructions. Also, direct and indirect conditions may be applied (i.e.. participants can directly observe their hand and the path they are to follow, or the patient's arm as well as the circle they are to trace are obscured from view). Typically, three trials of direct tracing and three trials of indirect tracing are administered. Each terminates after 45 seconds.

2. Brief Visuospatial Memory Test-Revised: The Brief Visual Memory Test – Revised (BVMT-R) is a short task of visual memory. As with the HVLT-R, there are six different versions that allow for repeat testing with reduced practice effects (Duff, 2016).

3. Vocabulary Subscale of the Wechsler Adult Intelligence Scale-4th Edition (WAIS-IV): The WAIS-IV is a battery of tests designed to evaluate intellectual abilities. It is composed of 10 core subtests (Vocabulary, Information, Similarities, Digit Span, Arithmetic, Block Design, Matrix Reasoning, Visual Puzzles, Coding, and Symbol Search) and five optional subtests (Comprehension, Letter–Number Sequencing, Figure Weights, Picture Completion. and Cancellation) (Ruchinskas, 2019).

4. Verbal Fluency Test: Verbal fluency is a commonly used neuropsychological test. which examines the ability to spontaneously produce words orally within a fixed time span. For category fluency, words must be produced according to semantic constraints. Regarding phonemic fluency, in the standard versions of the tasks, participants are given 1 min to produce as many unique words as possible starting with a given letter (letter fluency) (Wahlin et al., 2015).

Other assessments & scores

Disease-burden score (DBS)

Disease-burden score was calculated in all HD participants of this study. DBS was developed by Penney et al. in 1997, and is based on the relationship between observed post-mortem striatal atrophy, age at death and CAG repeat length. These three factors were found to be linearly related with an intercept at 35.5. The CAG repeat 35.5 was thought to be the largest CAG repeat-cutoff whereby no pathology would develop in the striatum, when considered that the process would linearly develop from birth (Penney et al. in 1997).

Disease burden score = (CAG – 35.5) x current age

composite Unified Huntington's Disease Rating (cUHDRS)

cUHDRS score was calculated in all manifest HD patients and premanifest HD expansion carriers of this study. cUHDRS is a novel, multidomain measure encompassing motor, functional, and cognitive scales all of which are independently associated with HD severity. The cUHDRS measures progression in HD, and it is being used as a primary outcome in clinical trials of huntingtin-lowering therapies. The cUHDRS has shown outstanding reliability, superior to its components, particularly regarding sensitivity to disease stage and longitudinally to detecting clinical benefit. cUHDRS is composed of 4 subscales: Total Functional Capacity (TFC); Total Motor Score (TMS); Symbol-Digit Modality Test (SDMT); and Stroop Word Reading (SWR) Test. The cUHDRS correlates with imaging biomarkers. tracking atrophy progression in HD with lower scores over time found to correlate with longitudinal volume decreases in the occipito-parietal cortex and centrum semiovale. Lower baseline scores correlated with decreased volume in the basal ganglia and surrounding WM, as well as reduced FA and increased diffusivity at baseline (Estevez-Fraga et al., 2021).

$$\text{cUHDRS} = \left[\left(\frac{\text{TFC}-10.4}{1.9}\right) - \left(\frac{\text{TMS}-29.7}{14.9}\right) + \left(\frac{\text{SDMT}-28.4}{11.3}\right) + \left(\frac{\text{SWR}-66.1}{20.1}\right)\right] + 10$$

Finger Tapping Test

Finger Tapping Test was performed right and left, in all participants using Digital Finger Tapping Test Version 3.5. Sybu Data, The Digital Finger Tapping Test (Sybu Data; https://appsto.re/us/ehHnA.i) is an iPhone-based software in which subjects are instructed to tap a button as fast as possible with their dominant for a finger over a duration of 10 seconds.

The number of taps is averaged across three trials and reported as a score. The test is a measure of motor performance and is used widely in research settings (Adhikari & Stark, 2017).

Brain MRI Imaging

2.4.1 Brain Magnetic Resonance Imaging: Acquisition Protocol

Brain MRI data were acquired using protocols designed specifically for this study, using the same acquisition protocol at each time point. Brain MRI acquisition protocol included 3D T1-weighted, 30-directional DTI protocol, T2-FLAIR & 3D-FLAIR, 3D ASL rs- fMRI. neuromelanin and SWI that were acquired for all participants on a 3T Philips Achieva-Tx MR scanner (Philips, Best, Netherlands), equipped with an eight- channel head coil. None of the included participants exhibited any indication of other neurological disease (i.e stroke, neoplasm, hemorrhage etc).

T1-weighted sequence had the following parameters: repetition time = 9.90 ms; echo time = 3.69 ms; flip angle = 70◦; 170 contiguous 1 mm slices; field of view = 250 × 250 mm; matrix size = 256 × 256. voxel size = 1 × 1 × 1 mm3; slice thickness = 1 mm. DTI protocol acquisition included an axial single-shot spin-echo echo-planar imaging (EPI) sequence with 30 diffusion encoding directions and the following parameters: repetition time (TR): 7299 ms; echo time (TE): 68 ms; flip angle: 90◦; field of view (FOV): 256 × 256 mm; acquisition voxel size: 2 × 2 × 2 mm. The acquisition consisted of 70 slices and the scan time was 8 min 40s. Moreover, the following MRI sequences were acquired: MP-RAGE: time repetition (TR) = 2300 ms. time echo (TE) = 2.98 ms. flip angle of 9°. time to inversion (TI) = 900 ms. matrix = 240 x 256. and time ~ 6min; FGATIR: TR = 3000 ms. TE = 2.96 ms. flip angle of 8°. TI = 409 ms. matrix =

240 x 256. and time ~ 12min; Arterial Spin labelling (ASL): Whole brain images of regional CBF were acquired using a 3D pCASL sequence. These 3D maps of cerebral tissue perfusion were obtained with a spatial resolution of 2x2x3mm, Effective TE 10.2 ms. TR 4463 ms, 55-60 slice locations were encoded in the 3D Fast Spin Echo (3DFSE) readout where 8 spiral arms were acquired per slice location, 512 points per arm. Labeling time of arterial blood: 1500 ms. post-labeling delay: 1800 ms, number of 'control-label' images: 3. A proton density image was also acquired in the same series to produce the CBF map in quantitative, physiological units of ml blood/100gm tissue/min. The total length of this scan was approximately 6min; Diffusion Tensor Imaging (DTI): Diffusion-weighted data was acquired using echo planar imaging (EPI; TR = 14000 ms. TE = 76 ms. flip angle of 90° and voxel size of 2.0 x 2.0 x 2.0 mm3). The diffusion weighting was isotropically distributed along the 60 directions (b-value = 1500 s/mm2). and a 6 non-DWIs (B0) was acquired at the beginning of each scan. EPI acquisitions are prone to geometric distortions that can lead to errors in tractography. To minimize this, a second 6 non-DWI (B0) image set was acquired with the phase-encoded direction reversed—"blip-up" and "blip-down" (Chang and Fitzpatrick, 1992) that resulted in images with geometric distortions of equal magnitude but in the opposite direction allowing for the calculation of a corrected image (Andersson et al., 2003). Before correcting geometric distortions, each image set (blip-up and blip-down) was corrected for motion and eddy-current-related distortions. The total DTI scan duration was approximately 15min.; Quantitative Susceptibility Mapping (QSM): Quantitative Susceptibility Maps were generated from images acquired using a flow-compensated 3D axial Susceptibility Weighted Angiography (SWAN) sequence with TR = 48.9 ms. nine echoes with TE1 = 4.512 ms. ΔTE = 4.996 ms. flip angle = 20°. 134 1 mm thick slices. FoV = 24 cm. acquisition matrix = 416 x 320 and ASSET factor = 2. total acquisition time = 12' 17". Complex (magnitude, real and imaginary) data were saved

for each image slice; Resting-state function MRI (rs-fMRI): Resting state images were acquired from 32 3.0 mm thick slices with a spacing of 1.0 mm. using a multi-echo, multi-slice with whole head coverage 3D EPI sequence with four echoes and TR = 2.5 s. TE1 = 12 ms. ΔTE = 16 ms. flip angle = 80°. number of volumes = 192 (preceded by four dummy scans), with a total acquisition time of 8' 10". Slices were acquired sequentially in descending order (superior to inferior); Neuromelanin (NM): NM scan consisted of a T1-weighted fast spin echo sequence with on-resonance magnetization transfer preparation pulses; TR = 829 ms, TE = 12 ms, echo train length = 4, voxel size = 0.8x0.8x2.5 mm; flip angle = 123 degrees. slice thickness = 2.5 mm. number of slices = 12, orientation = transversal, acquisition time approximately 5:30 minutes; Susceptibility weighted Imaging (SWI): 3D gradient echo acquisition; magnitude and phase images were obtained with the following parameters: TR = 28ms. TE = 20 ms. FoV = 230 mm. flip angle = 15 degrees. slice thickness = 0.9 mm. voxel size = 0.8x0.7x0.9 mm. phase encoding direction = R >>L, acquisition time approximately 6:30 minutes.

2.5 Imaging analysis

2.5.1 Structural MR Image Analysis

Structural MRI (sMRI) sequences (T1 or T2 weighted) were used to measure static anatomical features of the brain, such as volume and cortical thickness. Different tissue classes such as grey matter or white matter presented different voxel intensities (voxels: 3D array of elements that create an MRI image). Consequently, high between-tissue contrast and high spatial resolution were important to establish the best combination of acquisition length, spatial resolution and tissue contrast during MRI design (Johnson & Gregory, 2019).

Structural MRI Pipeline Analysis

An MRI pipeline analysis of imaging with pre-processing and processing steps is described below.

a. Image quality control

All image quality controls (QC) were carried out using FreeSurfer 6.0.0 (Fischl & Dale, 2000).

Data quality control (QC)

Data quality control was an essential step in MRI pre-processing. Data were checked to evaluate the quality and whether they were sufficient to use in analysis, as well as to identify any data collection issues. Data were anonymized prior to QC analysis, as suggested on the study protocol.

The first step in QC was conversion of data from DICOM format into ANALYZE (.img and .hdr) and/or NIFTI (.nii) formats that were used for imaging analysis. After conversion, data were visually examined for common MRI artifacts (motion artifacts, signal-dropout, intensity inhomogeneity, flow artifacts or wrap-around**).** All data collected were initially checked in Eginition Hospital with Horos v.3.3.6 to ensure reliability and stability of scan acquisition followed by a thorough visual check for artifacts from two individual investigators (M.B. G.A). Visual checks were performed for noise, missing data, brain coverage, motion artefacts, flow, susceptibility and inhomogeneity, and in general image quality. Taking into consideration that HD patients are choreatic, artifacts due to motion were the most common varying from mild to severe, causing imaging blurring, “ringing”, ghosting (multiple images

superimposed on top of each other), and missing slices in raw diffusion data. Field of view (FOV) was positioned carefully, to avoid "wrap around" effect (back of the image wraps into the front). We checked for intensity inhomogeneity artifacts, resulting from the varying magnetic field in the MRI bore causing varying intensity across a smooth spatial gradient within an MRI scan. Factors such as local flip angle variations, participant anatomy and radiofrequency coil homogeneity affect tissue non-uniformity. This affects how well a software, particularly when using automated image processing can delineate different tissue types. Bias correction was applied to all T1-weighted images used in this thesis as previously described to correct these inhomogeneity artifacts using N3 algorithm optimized for 3T data. The N3 correction is a commonly used non-parametric non-uniform intensity normalization method, that demonstrates a high degree of stability, to improve reproducibility and reduce coil-type, pulse-sequence differences system and dependency effects on brain volumetry (Goto et al. 2012, Boyes et al.2008, Arnold et al. 2001).

Finally, we checked tissue contrast quality of T1 and T2 sequences, particularly for regions of interest (ROI), for example within HD it is important that there is good contrast between WM and subcortical structures. All steps were performed in sequence, the precise order depending each time on the type of analysis "whole-brain" vs "region of interest" analysis.

b. Processing - Analysis

All image processing was performed using FreeSurfer 6.0.0. Freesurfer can be used to perform whole-brain analyses on a surface based level or to extract regional values (cortical thickness, volume, surface area) from T1 scans (Dale et al.1999; Fischl et al.1999; Fischl and Dale.2000).

FreeSurfer

FreeSurfer is a software package for the analysis and visualization of structural and functional neuroimaging data, used in Human Connectome Project (https://surfer.nmr.mgh.harvard.edu). It was developed by the Laboratory for Computational Neuroimaging at the Athinoula A. Martinos Center for Biomedical Imaging. It can be used both in cross-sectional or longitudinal studies.

FreeSurfer was operated via the default recon-all pipeline, within 3T scanner mode. There are two main streams in Freesurfer that were also used in this study: 1. the surface-based area, which is mainly used for measuring cortical thickness and 2. the volume-based stream, which is mainly used for calculating volume. The FreeSurfer pipeline includes the automatic calculation of the volume of different regions, combining cortical thickness and volumetric results during processing. The output is a text file for each participant with volumetric results. Based on the FreeSurfer software recommendations. the automatically optimised volumes were extracted for each participant and used in this thesis (https://surfer.nmr.mgh.harvard.edu/fswiki/MorphometryStats).

Segmentation, registration and smoothing, followed by statistical analysis are common processing steps that were applied to our structural MRI data (Johnson & Gregory, 2019)(Figure 3).

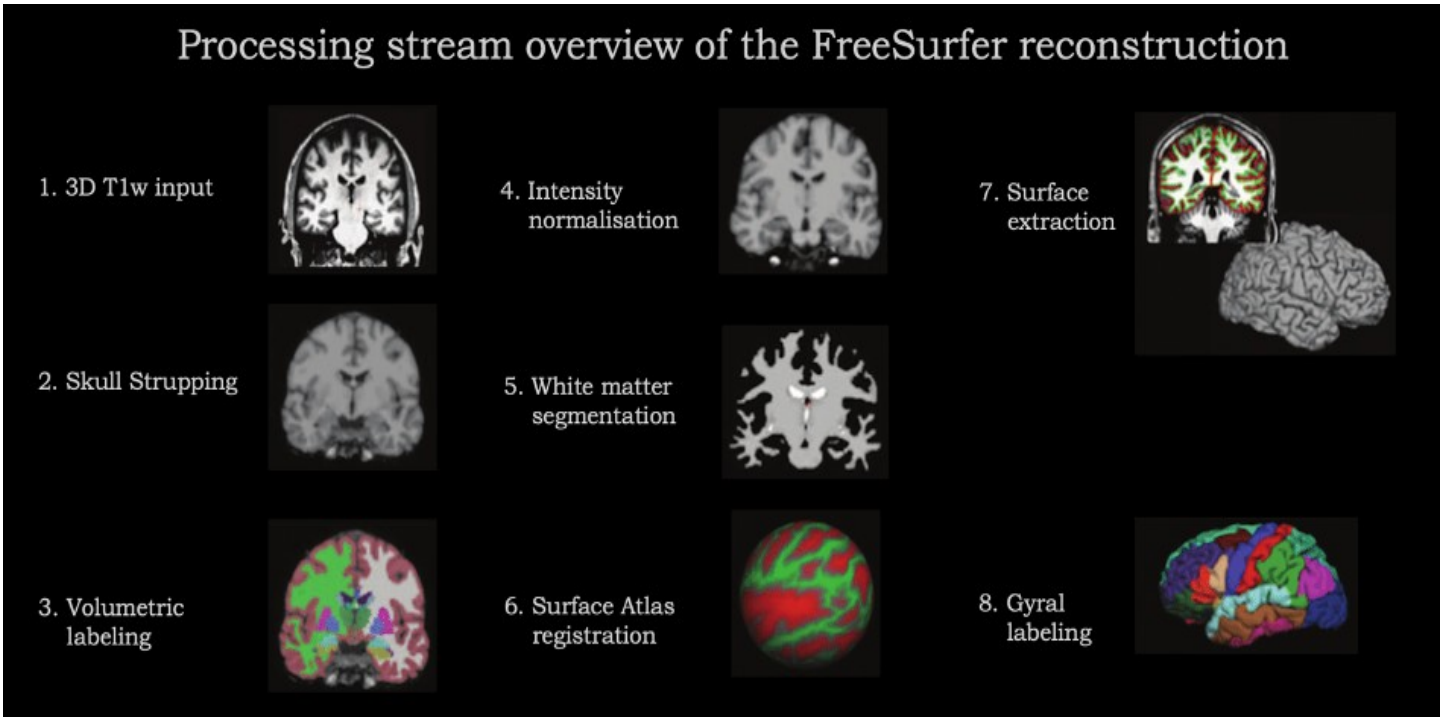

Figure 3: *MRI-analysis pipeline**:** Overview of Freesurfer reconstruction processing stream showing all steps of processing analysis applied in this thesis.*

Registration

Registration, a process of alignment in which scans are moved from one image space to another, was performed between individuals, or/and within individuals to quantify longitudinal change for imaging measures. In detail, scans were registered to a common space to allow the direct comparison between multiple scans and group comparisons. MRI scans can be processed in a range of "spaces," where "space" refers to the location of the head within the FOV. Native space was defined as the space during the image acquisition, where the brain is in the same position within the FOV as on the scanner. Native space was different for each scan, due to differences in positioning, differences or movements of the

participants, or FOV changes. Standard space is defined as a common location to which different scans are aligned. The Montreal Neurological Institute space, MNI13.14 is the most widely used standard space. The registration was performed in two steps: 1. calculation of registration parameters and 2. application to an image. Two types of registration were used: 1. Linear and 2. Non-linear. Linear registrations are applied for a rough spatial alignment between scans, but not an exact correspondence. A non-linear registration was performed for a precise correspondence between two images, warping the scan in many dimensions (Johnson & Gregory, 2019).

Smoothing

Smoothing was performed with the use of an isotropic Gaussian kernel, averaging the signal from neighboring voxels. Smoothing normally distributes the data, which is essential for parametric statistical testing and enhances signal-to-noise ratio (Johnson & Gregory, 2019).

Segmentation – structure parcellation

Structure parcellation was used, that is a specific case of tissue segmentation. After the tissues were correctly segmented, the regions that belong to the same neuroanatomical region inside the same tissue were determined.

We initially conducted group comparisons via whole-brain GLM analyses. For correlations of behavioral and clinical data with cortical indices, we followed a ROI approach, as described below.

Two approaches were perfomed with FreeSurfer 1. a volume-based approach. to calculate volumetric measures and classify subcortical regions, and 2. a surface-based approach to calculate cortical thickness.

1. Whole-brain analysis

Whole-brain techniques are used to perform comparisons between different populations or longitudinally across all regions of the brain. Whole brain cortical reconstruction of T1 MR images was obtained using the standard pipeline of FreeSurfer 6.0.01. Motion correction by linear transformation, accurate skull stripping, and cortical segmentation was performed based on identification of gray/white matter boundaries in native space. All participants' images were registered to the common surface space (i.e.. the fsaverage atlas) and subsequently smoothed with a Gaussian kernel of FWHM 10 mm. Each hemisphere was modeled separately. Cortical thickness was calculated as the closest distance from the gray/white boundary to the gray/CSF boundary at each vertex on the tessellated surface. Additional reconstruction was then conducted using 3D Flair MR images to correct pial surface, separately for each individual (Fischl and Dale. 2000).

Whole-brain analysis registration and segmentation of tissues types was performed as previously described. Following registration and segmentation, statistical analysis and comparison of every voxel of the brain (or of a selected tissue such as white matter) was completed to compare between groups and identify associations with variables included in this study.

Voxel-Based Morphometry (VBM) – Whole-brain analysis

Voxel-based morphometry (VBM) was used to calculate grey matter volume of cortical and subcortical areas, using the Freesurfer software. Volumetric differences were measured with VBM in the GM, WM. CSF between our three cohorts (healthy controls, HD gene carriers, HD manifest) and associations were calculated between volume and covariates, such as motor scores, cognitive scores, fluid biomarkers.

VBM processing included the following steps with Freesurfer images that were segmented into three tissue types (GM, WM and CSF). Gaussian models and tissue probability maps (tissue probability maps, TPM) were used for tissue classification of each voxel. After segmentation, each tissue class for every voxel was classified with a value (from 0 to 1) which represents the probability of each voxel belonging to this specific tissue class. QC was performed again to ensure segmentation was successful for all images. Modulation of all voxels was applied to adjust the volume of the tissue type within each voxel using the warping parameters calculated before so as to preserve the original volume of each voxel from volumetric changes that may have occurred during registration. Images were then aligned and smoothed to avoid errors from registration.

Brain was affine-registered to Talairach space (common standard space). Volumetric labeling and intensity correction were performed, followed by a high dimensional nonlinear volumetric alignment to a Talairach atlas. The volume was labeled in the final step. Finally, a GLM was used to compare voxel volumetric differences between groups and to investigate associations between variables with multiple comparisons correction.

Surface-based Freesurfer pipeline - Whole-brain analysis

Affine-registration and skull stripping was performed after correction for field inhomogeneity. Then, WM voxel were classified in relation to their intensity, neighbors' intensity, and position, building thus a triangular mesh around the WM. Smoothing and topologically corrections were followed, creating an external cortical surface via expansion of the WM. Values were extracted in the final step.

Cortical thickness (CT) – Whole-brain analysis

Cortical thickness was also another whole-brain analysis method that we used with FreeSurfer, in order to quantify the thickness of the cortical layer, measuring the distance between the outer pial-CSF brain surface and the GM-WM surface.

Whole brain differences in the measurements of surface area (SA), cortical thickness (CTh) and gray matter volume (GMV) were examined for both cerebral hemispheres with separate vertex by vertex general linear models (GLMs), in order to identify differences between groups in all brain metrics. Age was included as nuisance variable in all models. Total intracranial volume (TIV) was used as a nuisance variable for between-group designs, for volume and surface area measurements, as previously suggested by Yoo et al. (2016). No covariates were used for cortical thickness analyses, as previously suggested (e.g..Westman et al. 2013).

As whole-brain analysis is an exploratory method to approach differences across all regions of the brain, and every voxel was statistically compared via mass-univariate statistical testing and correlated with several of our variables, correction for multiple-comparisons was applied.

Monte Carlo simulations were used to correct all vertex-wise results at an individual vertex level of $p < 0.05$ (Angelopoulou et al.2020, Johns et al. 2018, Hagler et al. 2006)

2. Region of interest (ROI) analysis

For region of interest (ROI) analyses, an a priori hypothesis is required to segment a structure of interest from which precise measurements of a region were extracted for each participant (e.g.. caudate volume). Volume and cortical thickness were examined within ROIs. An automated segmentation of ROIs was performed to establish boundaries between different regions using FreeSurfer. After segmentation, regions were extracted, ROIs were delineated and values for each region were extracted for statistical analyses. The extracted volumes were then analyzed using Freesurfer and SPSS v.26.

2.5.2 Neuromelanin (NM-MRI) imaging analysis

The analysis of the NM-MRI was performed with Analyze Software V.14.0 (Analyze, Biomedical Imaging Resources, Mayo Clinic, USA). The images were analyzed in subjects' native space. The substantia nigra (SN) was defined bilaterally on two consecutive axial slices comprising of the SN and the red nucleus (RN), over the superior colliculus.

The region of interest corresponding to the locus coeruleus (LC) was delineated in the axial slice adjacent to the fourth ventricle, where the LC has high signal intensity. This generally lies about 7 mm below the inferior colliculus, in agreement with the typical neuroanatomical location of the LC. The pontine reference region was manually drawn on the same slice.

To define the areas of NM-MRI high signal intensity in the LC and SN, a threshold of intensity higher than 1.5 SD of the mean of the reference regions was used. The areas of the right and

left LC and SN were calculated and averaged. The area (in mm^2) and the volume (in mm^3) of the SN and LC were sampled using Analyze software. Measures of area and volume were compared between groups and associations between all variables were investigated using multiple comparisons correction.

2.6 Measurement of plasma neurofilament light chain concentration (sNfL)

Plasma NfL concentrations were measured in this study for all HD participants (premanifest HD and HD manifest) at baseline examination. BD Vacutainer tubes with EDTA were used to collect blood. Plasma was isolated with sample processing as previously described and samples were frozen then stored at −20°C (Borowsky et al.2013).

NfL quantification

The quantification of NfL was performed externally in Jehn Kuhle's lab, University of Basel. Switzerland. Plasma NfL concentrations were measured with ultrasensitive single-molecule array (Simoa) technology by an in-house method (Quanterix, Lexington, MA, USA, Kuhle J et al., 2016). All NfLvalues were within the linear ranges of the assays.

To minimise the number of statistical comparisons between variables, we assessed firstly the most robust markers that were chosen *a priori* from previous publications (volumetric imaging measures, SDMT, SWR, UHDRS, TMS and TFC). After this analysis, sNFL values were compared between groups and associations between all variables were investigated with multiple comparisons correction. Only values that were above 65% percentile of healthy controls values are considered to be abnormal, in accordance to relevant tables as shown below (Barro et al., 2018, Khalil et al., 2018, Siller et al., 2019), Figure 4.

NfL of 18.5 pg/ml at age 75 years: level above 65−th percentile

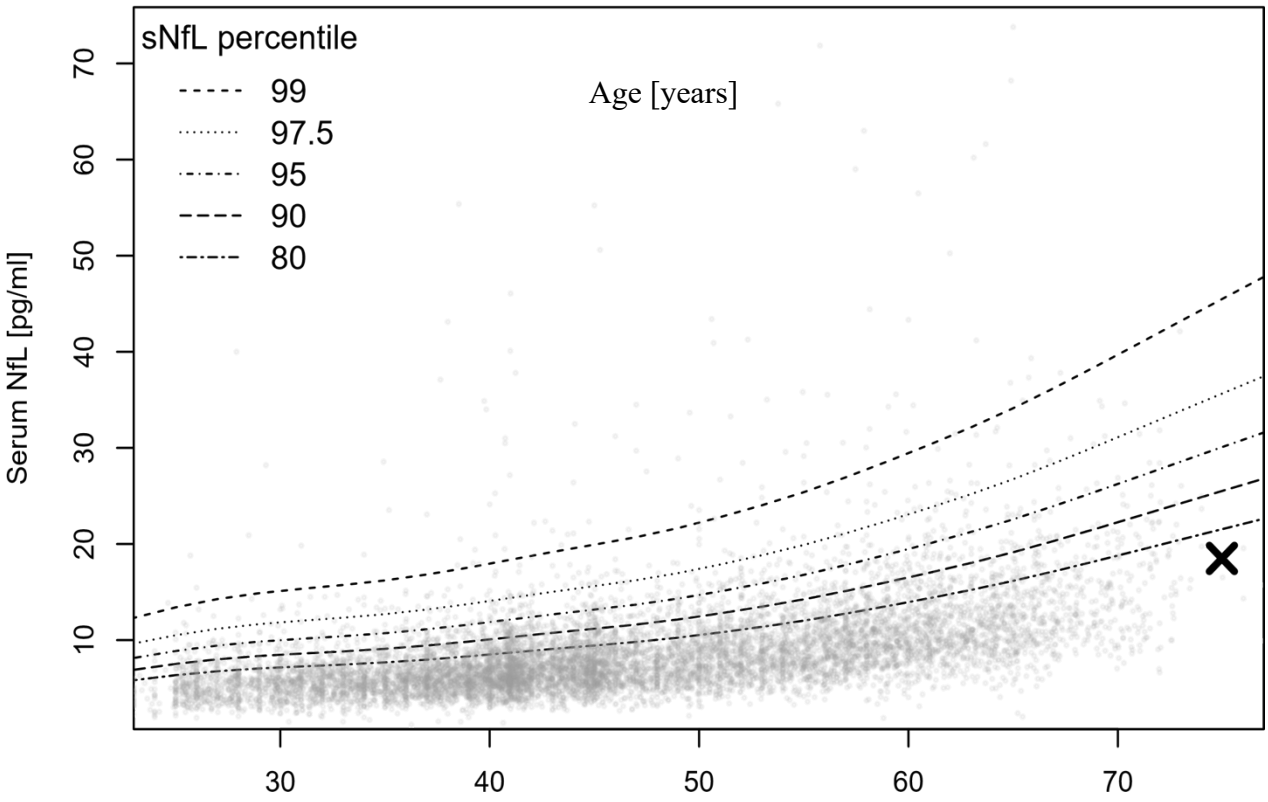

Figure 4: Example of sNfL value is shown in the table (NfL-18.5 pg/ml at age 75 years). Percentiles above 65% percentile of healthy controls values are considered to be abnormal. in accordance to relevant percentiles shown in this figure. (Barro et αl.,Brain. 2018, Simoa NF-light®).

A-synuclein measurements

Patients & controls

In the present study, a total of 34 consecutive symptomatic patients were included with molecularly confirmed HD and 4 asymptomatic subjects positive for the HD expansion (premanifest), recruited while attending a specialist Neurogenetics outpatient clinic. 36 control subjects were also included, 12 of which were at-risk of developing HD but tested negative for the expansion and had no other comorbidities, and 24 of which were non-blood relatives of patients attending the clinic without any significant morbidities. 120 consecutive samples were initially collected from manifest HD patients, premanifest HD expansion carriers and controls but several samples were excluded to exclude hemolysis.

All patients were examined neurologically and assessed using the Unified HD Rating Scale (UHDRS) motor score, CAG repeat expansion size in *HTT* was calculated with fragment analysis on an ABI 310 genetic analyzer using standard molecular diagnostic techniques. To estimate exposure to mutant Htt, Disease Burden Score (DBS) was calculated using the longer CAG-repeat length and the age of subjects DBS = age x (CAGn - 35.5). The study was approved by the Ethics Committee of Eginition Hospital and written informed consent was obtained from all patients for the performance of molecular genetic testing (Tabrizi et al., 2009).

Serum a-synuclein measurement

Peripheral blood was collected during clinic visits, allowed to coagulate then immediately centrifuged and stored at -80^{o}C. Visibly hemolyzed serum samples were excluded. All serum samples were measured following a 60x dilution in TBST buffer (10mM Tris-Cl, pH 7.6. 100

mM NaCl. 0.1% Tween-20) using an ELISA assay developed in-house for the accurate quantification of a-synuclein concentration. Two commercially available a-synuclein-specific antibodies were used: the monoclonal Syn-1 (BD Transductions) as the capture antibody and the polyclonal C-20 (Santa Cruz). as previously described (Emmanouilidou et al., 2011, Kapaki et al. 2013).

Briefly, non-transparent white ELISA plates (Corning Costar) were coated with 0.5 lg/ml of Syn-1 antibody (50 ll per well) in 100 mM NaHCO3 (pH 9.3) for 24 h at ambient temperature. ELISA plates were washed three times in wash buffer (50 mM Tris-HCl. 150 mM NaCl and 0.04% Tween-20). Samples were added appropriately diluted in TBST/BSA (10mM Tris-Cl. pH 7.6. 100 mM NaCl. 0.1% Tween-20 and 1% BSA) and plates were incubated at 37 C for 2.5 h to allow antigen binding. Following washing, 50ll of C-20 antibody (10.000 diluted in TBST/BSA) were added to each well and further incubated for 1h at ambient temperature. The wells were washed and 50 ll of anti-rabbit IgG conjugated with HRP (goat polyclonal. Dako). 15.000 diluted in TBST/BSA were added to each well. Wells were incubated at 4 C for 30 min and washed again. Finally, 50 ll of HRP sub- strate (SuperSignal ELISA Femto Substrate. Thermo Fisher Scientific) were added and incubated for 5 min at ambient temperature according to the manufacturer's instructions. Chemiluminescence was measured by a Spark 10 M microplate reader (Tecan) following integration for 10 ms. To avoid the matrix effect, the standard addition method was implemented; each sample was assessed in the presence of 0. 0.03 and 0.09 ng/ml recombinant human a-synuclein (Chemicon) as standard. Each standard addition was measured at least in duplicate. The final concentration for each sample was estimated as the mean value of the concentration obtained in the presence of the two standard additions. A standard concentration of recombinant a-synuclein (0.14ng/ml) was included in each assay to assure day-to-day reproducibility (Emmanouilidou et al., 2011).

Statistical analysis for a-synuclein measurements

For statistical analysis symptomatic HD patients and asymptomatic HD gene carriers were grouped together. Chi-square tests, ANOVA and ANCOVA were used as appropriate to investigate differences between the HD group and controls. Correlations between variables were investigated using Pearson's method. The threshold for statistical significance was set to $p < 0.05$. All statistical analysis was performed on SPSS v.24.

2.6 Statistical analysis

Statistical analysis was performed using R v4.0. All data underwent a normality test (Shapiro–Wilk), and were found to be non-normally distributed. Spearman's method was used to correlate the different indices. The Benjamini–Hochberg false discovery rate correction was applied in the resulting P values to account for the multiple numbers of tests. Adjusted p-values less than 0.05 were deemed significant.

Analyses to detect baseline differences

Data were analyzed from all markers using a GLM, with the absolute values of the MRI, clinical and genetic marker as dependent variable, and a 3-subgroup (premanifest, manifest and control groups) categorical variable as independent. Gender, age and educational level were included as covariates in the model. Benjamini–Hochberg (BH) false discovery rate correction at 0.1 was used to correct for multiple testing. Marginal means, and standardized effect sizes were used to report differences across groups. Partial correlations were applied across different markers and clinical measurements, correcting for age, gender, and educational level where needed.

Regression

Regression analysis was used to investigate the relationship between variables by fitting models to data (an outcome and one or more predictors). Linear regression analysis was used in this thesis. Multiple regression uses a GLM to estimate the relationship between predictor variables (e.g. UHDRS) and measured variables (e.g. grey matter volume), so that the unique contribution of variables to a predictor can be better understood.

Covariates

To prevent confounding or interacting effects on the results, confounding covariates were controlled for where possible. All analyses in this thesis were controlled for age and gender. For cognitive variables, data were controlled for education level (measured using the International Standard Classification of Education. ISCED). HD premanifest investigations also included disease-burden score as an adjustment. Regarding variations in head size, cross-sectional between-group analyses of regional volumes were adjusted for total TIV, using the automated method with statistical parametric mapping where needed, expressing each volume as a TIV percentage (Barnes et al. 2010, Penney et al. 1997).

Correlation analysis

Correlation analysis was used to examine the relationship between two variables. We used Spearman's correlation analysis, that is a non-parametric correlation measuring the extent to which one variable tends to increase or decrease as the other variable increases. The Spearman coefficient is more robust than the more commonly used Pearson, making it more appropriate for small sample sizes and it is not influenced so much by data outliers.

Correction for Multiple Comparisons

As we evaluated many variables and several statistical tests were performed simultaneously, the risk to identify a false-positive result for all statistical comparisons was significantly increased. The Family-Wise Error (FWE) rate is the probability of making a false-positive discovery (type I error) when performing multiple tests. FWE correction aims to reduce this probability by adjusting the p-value threshold (e.g. $p<0.05$) according to the number of tests being made.

For multiple comparisons correction, an available R script was used. Non-parametric permutation tests similar to Nichols and Holmes were implemented, resulting in a family-wise error (FWE)-corrected alpha value and cluster threshold which were used to identify significant differences between our cohorts. First, we extracted numerical data for each participant for left or right hemisphere clusters (either cortical or subcortical) or tract bins that significantly differed between premanifest HD, manifest HD and healthy controls. Partial correlation analyses then followed between clinical, neuropsychological and other variables that differed between our groups, controlling for age and years of education.

Phenotypic clustering

Data were assessed for evidence of phenotypic clustering in HD by using two different approaches: 1. By grouping the variables into 3 main domains: imaging variables, cognitive variables, and motor variables and with all variables grouped together. Premanifest HD and manifest HD subjects were initially pooled into one HD group and then data were investigated in subgroups.

Computational analysis of genetic HD modifiers & RNA-seq datasets

RNA-seq data on HD gene expression data were obtained via the Gene Expression Omnibus (GEO) repository either via direct inquiry or via the RNA-seq Experiments Interactive Navigator (GREIN) back-end pipeline. GREIN uses its back-end computational pipeline to extract knowledge from Sequence Read Archive (SRA) runs and generate gene signatures that may be subsequently used in gene set enrichment analyses (GSEA). GREIN is accessible at: https://shiny.ilincs.org/grein, the source code at: https://github.com/uc-bd2k/grein and the Docker container at: https://hub.docker.com/r/ucbd2k/grein (Mahi et al. 2019).

Pathway analyses (with a focus to a-synuclein pathway), head-to-head comparisons and visualization of GREIN-extracted gene signatures were subsequently analyzed via GeneTrail 3.0 and GeneMania. GeneTrail applies a modified Kolmogorov-Smirnov on previously extracted data, Independent Samples Shrinkage T-test scores, and the Benjamini Yekutieli procedure were performed to adjust p-values for multiple comparisons. For all tests, false discovery rates (FDRs) and q-values<0.05 were considered statistically significant (Gerstner et al. 2020). Genetrail 3 interrogates curated pathway databases such as GO BP, GO MF, KEGG. Reactome to retrieve significantly enriched pathways.

GWAS HD data provided by Bettencourt et al 2016 study (UCL) were re-analyzed with advanced techniques in combination with RNA datasets to discover interactions and potential pathways (Bettencourt et al 2016).

2.11 *Literature Review*

Search strategy and selection criteria

References were identified by searching PubMed until March 15, 2021, and by further examining the reference lists from relevant articles. Combinations of the following search terms were used: “Huntington’s disease; neuroimaging; imaging; MRI; neurodegeneration; neurological disorders; rare diseases; neurofilaments; markers; biomarkers; volume; surface area; cortical thickness; finger tapping; UHDRS; cUHDRS; MoCA; neuromelanin; a-synuclein; transcriptomics; GWAS; computational; mitochondria; immunological pathways; DNA repair”. There were no language restrictions. Articles were generated on the basis of the relevance to each theme of interest included in this thesis.

3. Results

3.1 Descriptive statistics of this study

Table 2 presents descriptive statistics of the most important variables used in this study across all three groups (premanifest HD n_1=11, manifest HD n_2=14 and healthy controls n_3=25). Demographic, clinical, cognitive, psychiatric and biofluid measures as previously described in detail in the methods section were assessed and their medians with standard deviation, standard error and confidence intervals are presented here in table 2.

Variables	Group	Median	Standard Dev.	Standard Error	CI.lower	CI.upper
Age	HD	41.5	11.26	3.01	39.71	52.72
Age	controls	36	11.75	2.40	35.12	45.05
Age of onset	HD	38	10.22	-	-	-
Disease burden score	HD	388	71.64	19.15	368.03	450.76
Disease burden score	pre-HD	272	77.93	23.50	245.24	349.94
AES	HD	42.5	15.74	4.55	37.83	57.84
AES	pre-HD	27	4.07	1.23	25.53	31.01
Allele 1 CAG repeat length smaller allele	HD	18	3.29	0.88	16.81	20.61
Allele 1 CAG repeat length smaller allele	pre-HD	17	2.61	0.79	15.52	19.03
Allele 2 CAG repeat length larger allele	HD	45	2.85	0.76	43.21	46.50
Allele 2 CAG repeat length larger allele	pre-HD	43	2.04	0.62	41.81	44.55
NfL	controls	2.9	1.27	0.25	2.63	3.68
NfL	HD	29.755	11.83	3.42	25.49	40.53
NfL	pre-HD	7.6677	10.27	3.25	3.66	18.35
PPT	controls	36	0.00	0.00	36.00	36.00
PPT	HD	26	11.68	3.12	13.54	27.03
PPT	pre-HD	36	0.00	0.00	36.00	36.00
Problem Behaviours Total	controls	1	0.00	0.00	1.00	1.00
Problem Behaviours Total	HD	39.5	28.69	8.28	36.94	73.39
Problem Behaviours Total	pre-HD	11	3.72	1.12	8.14	13.14
UHDRS FAS	controls	25	0.00	0.00	25.00	25.00

Variables	Group	Median	Standard Dev.	Standard Error	CI.lower	CI.upper
UHDRS FAS	HD	21.5	8.29	2.22	12.21	21.79
UHDRS FAS	pre-HD	25	0.00	0.00	25.00	25.00
UHDRS IS	controls	100	0.00	0.00	100.00	100.00
UHDRS IS	HD	85	20.07	5.36	66.27	89.44
UHDRS IS	pre-HD	100	0.00	0.00	100.00	100.00
UHDRS TFC	controls	13	0.00	0.00	13.00	13.00
UHDRS TFC	HD	11	4.11	1.10	7.06	11.80
UHDRS TFC	pre-HD	13	0.00	0.00	13.00	13.00
UHDRS TMS Bradykinesia Body	controls	0	0.00	0.00	0.00	0.00
UHDRS TMS Bradykinesia Body	HD	1	0.62	0.16	0.57	1.28
UHDRS TMS Bradykinesia Body	pre-HD	0	0.00	0.00	0.00	0.00
UHDRS TMS Dysarthria	controls	0	0.00	0.00	0.00	0.00
UHDRS TMS Dysarthria	HD	1	0.61	0.16	0.36	1.07
UHDRS TMS Dysarthria	pre-HD	0	0.00	0.00	0.00	0.00
UHDRS TMS Finger Taps left	controls	0	0.00	0.00	0.00	0.00

UHDRS TMS Finger Taps left	HD	2	0.96	0.26	1.45	2.55
UHDRS TMS Finger Taps left	pre-HD	0	0.40	0.12	-0.09	0.45
UHDRS TMS Finger Taps right	controls	0	0.00	0.00	0.00	0.00
UHDRS TMS Finger Taps right	HD	2	0.84	0.23	1.16	2.13
UHDRS TMS Finger Taps right	pre-HD	0	0.40	0.12	-0.09	0.45
UHDRS TMS Fist Hand Palm Sequence	controls	0	0.00	0.00	0.00	0.00
UHDRS TMS Fist Hand Palm Sequence	HD	2	0.74	0.20	1.21	2.07
UHDRS TMS Fist Hand Palm Sequence	pre-HD	0	0.00	0.00	0.00	0.00
UHDRS TMS Gait	controls	0	0.00	0.00	0.00	0.00
UHDRS TMS Gait	HD	0.5	0.83	0.22	0.24	1.19
UHDRS TMS Gait	pre-HD	0	0.00	0.00	0.00	0.00
UHDRS TMS Maximal Chorea bucco oral lingual	controls	0	0.00	0.00	0.00	0.00
UHDRS TMS Maximal Chorea bucco oral lingual	HD	1	1.03	0.27	0.55	1.74
UHDRS TMS Maximal Chorea bucco oral lingual	pre-HD	0	0.00	0.00	0.00	0.00
UHDRS TMS Maximal Chorea Face	controls	0	0.00	0.00	0.00	0.00
UHDRS TMS Maximal Chorea Face	HD	1	0.77	0.21	0.70	1.59
UHDRS TMS Maximal Chorea Face	pre-HD	0	0.00	0.00	0.00	0.00
UHDRS TMS Maximal Chorea left lower limb	controls	0	0.00	0.00	0.00	0.00
UHDRS TMS Maximal Chorea left lower limb	HD	2	0.74	0.20	1.21	2.07
UHDRS TMS Maximal Chorea left lower limb	pre-HD	0	0.00	0.00	0.00	0.00
UHDRS TMS Maximal Chorea left upper limb	controls	0	0.00	0.00	0.00	0.00
UHDRS TMS Maximal Chorea left upper limb	HD	2	0.85	0.23	1.01	1.99
UHDRS TMS Maximal Chorea left upper limb	pre-HD	0	0.00	0.00	0.00	0.00
UHDRS TMS Maximal Chorea right lower limb	controls	0	0.00	0.00	0.00	0.00
UHDRS TMS Maximal Chorea right lower limb	HD	2	0.65	0.17	1.12	1.88
UHDRS TMS Maximal Chorea right lower limb	pre-HD	0	0.00	0.00	0.00	0.00
UHDRS TMS Maximal Chorea right upper limb	controls	0	0.00	0.00	0.00	0.00
UHDRS TMS Maximal Chorea right upper limb	HD	2	0.73	0.19	1.29	2.13
UHDRS TMS Maximal Chorea right upper limb	pre-HD	0	0.00	0.00	0.00	0.00
UHDRS TMS Maximal Chorea trunk	controls	0	0.00	0.00	0.00	0.00
UHDRS TMS Maximal Chorea trunk	HD	1	1.00	0.27	0.50	1.65

UHDRS TMS Maximal Chorea trunk	pre-HD	0	0.00	0.00	0.00	0.00
UHDRS TMS Maximal Dystonia left lower limb	controls	0	0.00	0.00	0.00	0.00
UHDRS TMS Maximal Dystonia left lower limb	HD	0.5	1.03	0.27	0.26	1.45
UHDRS TMS Maximal Dystonia left lower limb	pre-HD	0	0.00	0.00	0.00	0.00
UHDRS TMS Maximal Dystonia left upper limb	controls	0	0.00	0.00	0.00	0.00
UHDRS TMS Maximal Dystonia left upper limb	HD	0	1.05	0.28	0.18	1.39
UHDRS TMS Maximal Dystonia left upper limb	pre-HD	0	0.00	0.00	0.00	0.00
UHDRS TMS Maximal Dystonia right lower limb	controls	0	0.00	0.00	0.00	0.00
UHDRS TMS Maximal Dystonia right lower limb	HD	0.5	1.03	0.27	0.26	1.45
UHDRS TMS Maximal Dystonia right lower limb	pre-HD	0	0.00	0.00	0.00	0.00
UHDRS TMS Maximal Dystonia right upper limb	controls	0	0.00	0.00	0.00	0.00
UHDRS TMS Maximal Dystonia right upper limb	HD	1	0.86	0.23	0.64	1.64
UHDRS TMS Maximal Dystonia right upper limb	pre-HD	0	0.00	0.00	0.00	0.00
UHDRS TMS Maximal Dystonia trunk	controls	0	0.00	0.00	0.00	0.00
UHDRS TMS Maximal Dystonia trunk	HD	0	0.51	0.14	0.13	0.73
UHDRS TMS Maximal Dystonia trunk	pre-HD	0	0.00	0.00	0.00	0.00
UHDRS TMS Ocular Pursuit horizontal	controls	0	0.00	0.00	0.00	0.00
UHDRS TMS Ocular Pursuit horizontal	HD	1	0.77	0.21	0.41	1.30
UHDRS TMS Ocular Pursuit horizontal	pre-HD	0	0.00	0.00	0.00	0.00
UHDRS TMS Ocular Pursuit vertical	controls	0	0.00	0.00	0.00	0.00
UHDRS TMS Ocular Pursuit vertical	HD	1	0.77	0.21	0.41	1.30
UHDRS TMS Ocular Pursuit vertical	pre-HD	0	0.00	0.00	0.00	0.00
UHDRS TMS Pronate Supinate Hands left	controls	0	0.00	0.00	0.00	0.00
UHDRS TMS Pronate Supinate Hands left	HD	1	0.77	0.21	0.70	1.59
UHDRS TMS Pronate Supinate Hands left	pre-HD	0	0.40	0.12	-0.09	0.45
UHDRS TMS Pronate Supinate Hands right	controls	0	0.00	0.00	0.00	0.00
UHDRS TMS Pronate Supinate Hands right	HD	1	0.83	0.22	0.59	1.55

UHDRS TMS Pronate Supinate Hands right	pre-HD	0	0.30	0.09	-0.11	0.29
UHDRS TMS Retropulsion Pull Test	controls	0	0.00	0.00	0.00	0.00
UHDRS TMS Retropulsion Pull Test	HD	1.5	0.83	0.22	0.81	1.76
UHDRS TMS Retropulsion Pull Test	pre-HD	0	0.00	0.00	0.00	0.00
UHDRS TMS Rigidity Arms left	controls	0	0.00	0.00	0.00	0.00
UHDRS TMS Rigidity Arms left	HD	1	0.86	0.23	0.36	1.36
UHDRS TMS Rigidity Arms left	pre-HD	0	0.00	0.00	0.00	0.00
UHDRS TMS Rigidity Arms right	controls	0	0.00	0.00	0.00	0.00
UHDRS TMS Rigidity Arms right	HD	0.5	0.97	0.26	0.22	1.35
UHDRS TMS Rigidity Arms right	pre-HD	0	0.00	0.00	0.00	0.00
UHDRS TMS Saccade Initiation horizontal	controls	0	0.00	0.00	0.00	0.00
UHDRS TMS Saccade Initiation horizontal	HD	1	0.70	0.19	0.38	1.19
UHDRS TMS Saccade Initiation horizontal	pre-HD	0	0.00	0.00	0.00	0.00
UHDRS TMS Saccade Initiation vertical	controls	0	0.00	0.00	0.00	0.00
UHDRS TMS Saccade Initiation vertical	HD	1	0.77	0.21	0.41	1.30
UHDRS TMS Saccade Initiation vertical	pre-HD	0	0.00	0.00	0.00	0.00
UHDRS TMS Saccade Velocity horizontal	controls	0	0.00	0.00	0.00	0.00
UHDRS TMS Saccade Velocity horizontal	HD	1	0.77	0.21	0.41	1.30
UHDRS TMS Saccade Velocity horizontal	pre-HD	0	0.00	0.00	0.00	0.00
UHDRS TMS Saccade Velocity vertical	controls	0	0.00	0.00	0.00	0.00
UHDRS TMS Saccade Velocity vertical	HD	1	0.77	0.21	0.41	1.30
UHDRS TMS Saccade Velocity vertical	pre-HD	0	0.00	0.00	0.00	0.00
UHDRS TMS Tandem Walking	controls	0	0.00	0.00	0.00	0.00
UHDRS TMS Tandem Walking	HD	1	1.07	0.29	0.67	1.90
UHDRS TMS Tandem Walking	pre-HD	0	0.00	0.00	0.00	0.00
UHDRS TMS Tongue Protrusion	controls	0	0.00	0.00	0.00	0.00
UHDRS TMS Tongue Protrusion	HD	1	0.89	0.24	0.70	1.73
UHDRS TMS Tongue Protrusion	pre-HD	0	0.00	0.00	0.00	0.00
UHDRS TMS Total	controls	0	0.00	0.00	0.00	0.00
UHDRS TMS Total	HD	37	18.88	5.05	23.39	45.19
UHDRS TMS Total	pre-HD	0	1.73	0.52	-0.16	2.16
cUHDRS	HD	9.736	4.74	1.43	3.91	10.28
cUHDRS	pre-HD	17.109	1.99	0.60	15.00	17.67
Finger Tapping Test L	controls	48	8.27	1.65	45.79	52.61

Finger Tapping Test L	HD	20.5	6.84	1.98	15.15	23.85
Finger Tapping Test L	pre-HD	41	8.48	2.56	37.21	48.61
Finger Tapping Test R	controls	54	7.78	1.56	50.83	57.25
Finger Tapping Test R	HD	26	6.80	1.96	19.68	28.32
Finger Tapping Test R	pre-HD	50	6.74	2.03	47.02	56.08

Variables	**Group**	**Median**	**Standard Dev.**	**Standard Error**	**CI.lower**	**CI.upper**
WAIS IV DIGIT SPAN Score	controls	9	1.99	0.40	8.46	10.10
WAIS IV DIGIT SPAN Score	HD	4	1.65	0.48	3.95	6.05
WAIS IV DIGIT SPAN Score	pre-HD	8	1.97	0.59	6.22	8.87
BDI II Total	controls	0	4.19	0.84	1.47	4.93
BDI II Total	HD	8	15.91	4.59	4.89	25.11
BDI II Total	pre-HD	4	6.25	1.88	2.53	10.92
MOCA	controls	29	1.11	0.22	27.90	28.82
MOCA	HD	17.5	5.33	1.54	15.03	21.81
MOCA	pre-HD	24	2.76	0.83	23.15	26.85
SDMT O Total Correct	controls	62	12.20	2.44	58.24	68.32
SDMT O Total Correct	HD	20	6.53	1.97	16.62	25.38
SDMT O Total Correct	pre-HD	50	11.48	3.46	41.01	56.44
SDMT W Total correct	controls	53	9.57	1.91	50.53	58.43
SDMT W Total correct	HD	20	4.99	1.50	14.56	21.26
SDMT W Total correct	pre-HD	39	9.67	2.92	33.41	46.40
SNST Colour Word Correct	controls	112	9.14	1.83	102.27	109.81
SNST Colour Word Correct	HD	46	20.97	6.32	24.55	52.73
SNST Colour Word Correct	pre-HD	92	20.36	6.14	77.41	104.77

Comparisons between groups

In total, 25 controls were compared to 14 manifest HD and 11 premanifest HD expansion carriers. Kruskal-Wallis one-way analysis of variance was performed and to checkwhich groups were significantly different. Dunn's Multiple Comparison Test was applied. Dunn's Multiple Comparison Test is a post hoc non parametric test. Three main group

comparisons were applied: healthy control subjects versus premanifest HD expansion carriers, healthy control subjects versus manifest HD, and also premanifest HD versus manifest HD.

A difference was significant for all manifest HD variables presented in Table 3, in comparison with healthy controls, after correcting for multiple comparisons ($p<0.005$, table 2). No significant differences were detected between controls and premanifest HD in UHDRS TMS total score and UHDRS subscores ($p>0.005$, table 2). We note that there were no significant group differences in age, handedness and years of education. Correlations between demographic, clinical, cognitive and psychiatric variables did not reach statistical significance, due to the small size of cohort and the number of variables ($p>0.005$). Between HD manifest and premanifest HD groups, significant differences were noted in the following variables: UHDRS TMS total, FAS, IS, finger tapping test R,L, cUHDRS, Problem Behaviour's Total, MOCA, SDMT oral, WAIS IV, and NfL.

Variable	*Group Comparisons*
UHDRS TMS total	Controls - HD : p. 0.000* Controls - pre-HD: p. 0.260 HD - pre-HD: p. 0.000*
UHDRS TFC	Controls – HD: p. 0.000* Controls - pre-HD: p. 0.000* HD - pre-HD: p. 0.100

UHDRS FAS	Controls – HD: p. 0.000* Controls - pre-HD: p. 0.000* HD - pre-HD: p. 0.032*	
UHDRS IS	Controls – HD: p. 0.000* Controls - pre-HD: p. 1.000 HD - pre-HD: p. 0.000*	
PPT	Controls – HD: p. 0.000* Controls - pre-HD: p. 1.000 HD - pre-HD: p. 0.100	
Finger Tapping Test R	Controls – HD: p. 0.000* Controls - pre-HD: p. 0.054* HD - pre-HD: p. 0.0000	
Finger Tapping Test L	Controls – HD: p. 0.000* Controls - pre-HD: p. 0.160 HD - pre-HD: p. 0.000*	
Problem Behaviour's Total	Controls – HD: p. 0.000* Controls - pre-HD: p. 0.000* HD - pre-HD: p. 0.032*	
MOCA	Controls – HD: p. 0.000* Controls - pre-HD: p. 0.006* HD - pre-HD: p. 0.040*	
AES	Controls – HD: p. 0.000* Controls - pre-HD: p. 0.000* HD - pre-HD: p. 0.082	
TMT difference	Controls – HD: p. 0.000* Controls - pre-HD: p. 0.008* HD - pre-HD: p. 0.086	
SDMT Oral Total	Controls – HD: p. 0.000* Controls - pre-HD: p. 0.020* HD - pre-HD: p. 0.008*	
SNST Colour	Controls – HD: p. 0.000* Controls - pre-HD: p. 0.000* HD - pre-HD: p. 0.080	

WAIS IV Score	Controls – HD: p. 0.000* Controls - pre-HD: p. 0.030* HD - pre-HD: p. 0.026*
NfL	Controls – HD: p. 0.000* Controls - pre-HD: p. 0.012* HD - pre-HD: p. 0.024*
cUHDRS	Controls – HD: p. 0.014* Controls - pre-HD: p. 0.000* HD - pre-HD: p. 0.000*

Table 3: Comparisons between groups with Dunn's Multiple Comparison Test. Groups compared were healthy control subjects (controls) versus premanifest HD (pre-HD), healthy control subjects versus manifest HD (HD) and premanifest HD (pre-HD) versus manifest HD (HD).

**statistically significant*

3.2 Structural T1 Sequence analysis results

- ***Surface based analysis - Whole-brain analysis***

Group comparisons (T1 images only)

Whole brain analysis GLMs for cortical thickness, surface area and grey matter volume demonstrated several significant differences between manifest and premanifest HD groups and healthy controls (Monte Carlo corrected, $p < 0.05$). In detail, the manifest HD group revealed significantly reduced cortical thickness in both left and right hemisphere compared to healthy controls group and premanifest HD group. No significant differences were identified when

comparing premanifest HD group and healthy controls (Figure 5 and Table 1 for specific clusters).

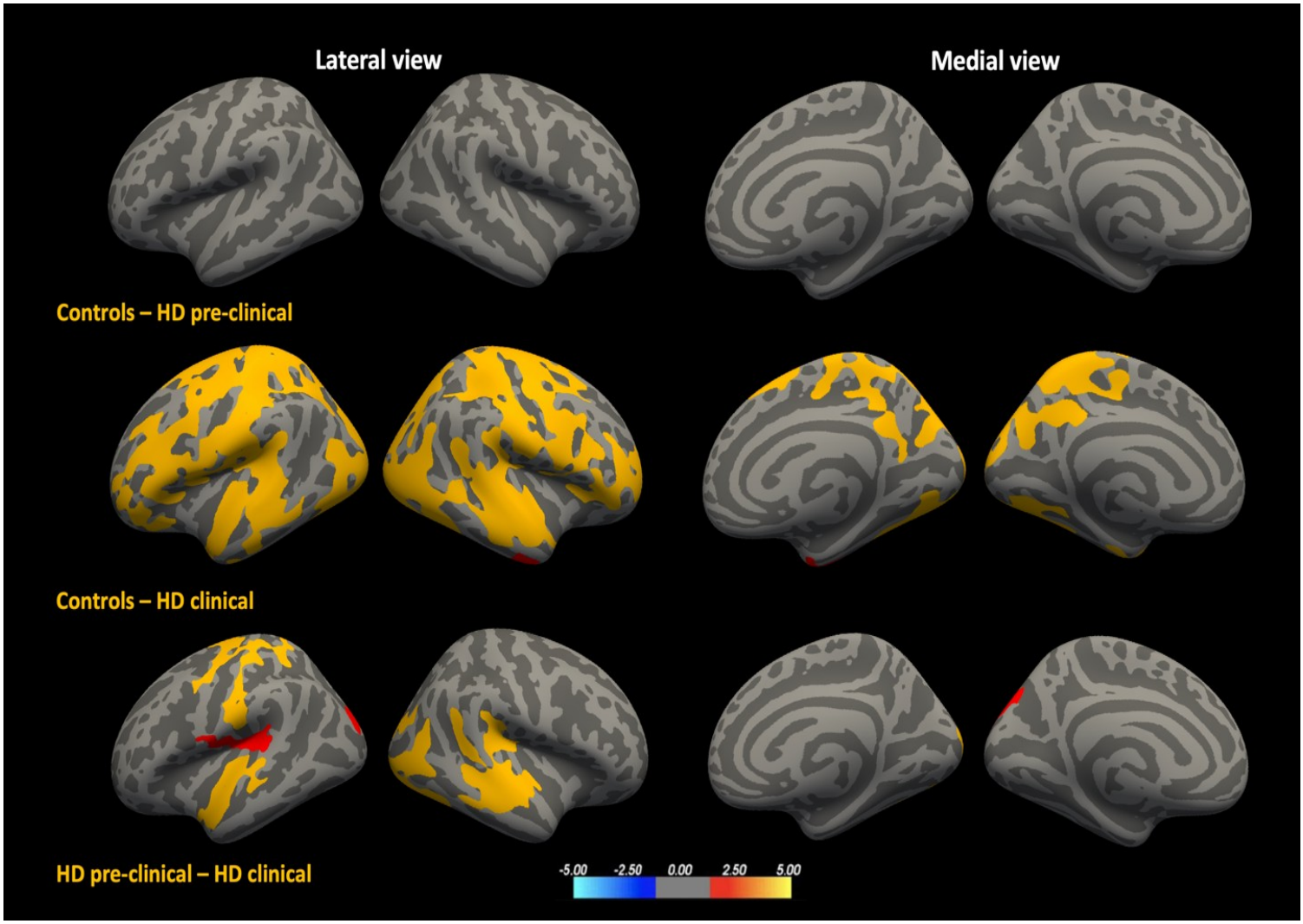

Figure 5. *Cortical thickness maps from general linear model analyses performed on the following contrasts: Upper row: healthy control subjects versus premanifest HD; middle row: control subjects versus manifest HD; bottom row: premanifest HD versus manifest HD. The*

color bar represents the tenth logarithm of p-value. Clusters significant after multiple comparison correction with Monte Carlo simulations ($p < 0.05$).

***Table 4**. Significant clusters in cortical thickness for group comparisons: healthy controls versus premanifest HD, healthy controls versus manifest HD and premanifest HD versus manifest HD.*

Hemisphere		Cluster	Area (mm2)	t	p	x	y	z
LH	Controls – HD premanifest	No significant clusters						
RH		No significant clusters						
LH	Controls – manifest HD	Precuneus	6012.01	5.065	0.00020	-13.4	-53.6	33.6
		Lateral occipital gyrus	5285.26	3.730	0.00020	-26.2	-90.7	-0.3
		Supramarginal gyrus	1088.11	3.748	0.01792	-45.2	-41.8	20.9
		Banks ssperior temporal sulcus	1067.93	3.311	0.02010	-56.1	-36.3	3.7
RH		Precentral gyrus	4028.71	3.700	0.00020	47.0	3.4	22.6
		Lateral occipital gyrus	3564.38	4.034	0.00020	45.6	-74.3	3.5
		Superior parietal gyrus	2029.91	4.622	0.00020	20.4	-85.4	37.2
		Superior temporal gyrus	1336.43	3.978	0.00300	56.1	-11.5	-6.2
		Post central gyrus	1316.76	3.748	0.00360	35.4	-34.5	63.4
		Entorhinal cortex	1207.06	3.615	0.00719	22.3	-7.9	-30.5
		Fusiform gyrus	1017.83	2.640	0.02879	31.3	-76.3	-9.2
LH	HD premanifest - HD manifest	Post central gyrus	3286.06	3.536	0.00020	-45.6	-27.6	59.5
		Superior temporal gyrus	1967.62	5.218	0.00020	-51.1	6.0	-14.4
			1377.94	3.756	0.00120	-7.4	-89.2	29.8
		Superior parietal gyrus	1083.68	3.898	0.00878	-50.9	-11.1	15.5
		Post central gyrus						

RH	Fusiform gyrus	3982.84	4.306	0.00020	43.4	-56.5	-9.9
	Superior temporal gyrus	3610.73	4.957	0.00020	59.0	-8.2	-6.1

Group comparisons (pial surface corrected by 3D FLAIR images)

Cortical thickness

Whole brain analysis GLMs for cortical thickness. surface area and grey matter volume, using corrected pial surface as suggested by Freesurfer for more accurate results, demonstrated several significant differences between manifest and premanifest HD groups and healthy controls (Monte Carlo corrected, $p < 0.05$). More specifically, with regards of cortical thickness manifest HD group revealed again significant clusters indicating reduced cortical thickness in both left and right hemisphere, compared to healthy controls group and significant reduced cortical thickness in right hemisphere compared to premanifest HD group. Premanifest HD group also showed reduced cortical thickness compared to healthy controls (Figure 6, Table 5 for specific clusters).

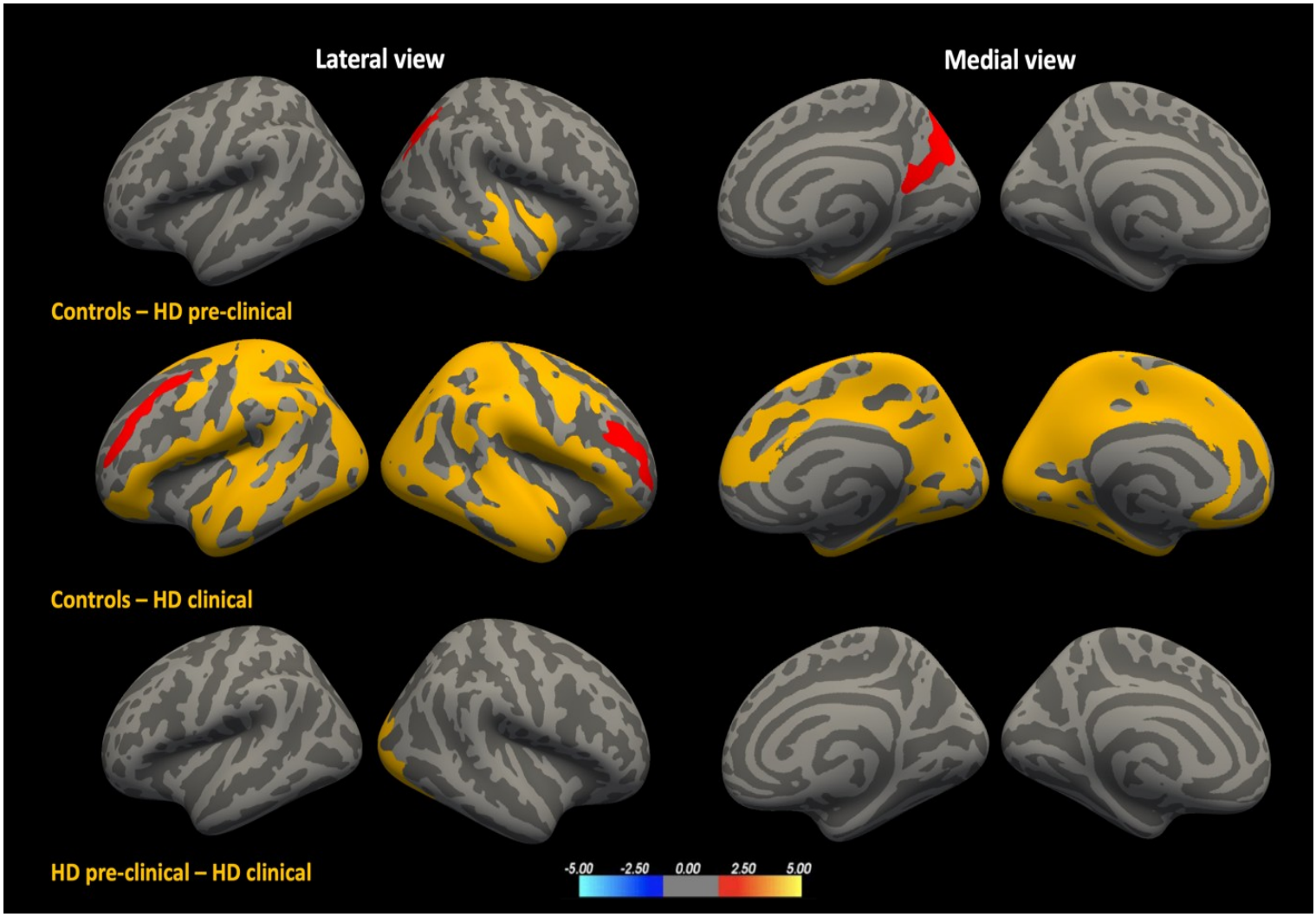

Figure 6. *Cortical thickness maps for pial surface corrected by FLAIR images from general linear model analyses performed on the following contrasts: Upper row: healthy control subjects versus premanifest HD; middle row: control subjects versus manifest HD; bottom row: premanifest HD versus manifest HD. The color bar represents the tenth logarithm of p-value. Clusters significant after multiple comparison correction with Monte Carlo simulations ($p < 0.05$), (Table 5).*

***Table 5**. Significant clusters in cortical thickness for group comparisons: Control vs premanifest HD. Controls vs manifest HD and premanifest HD vs manifest HD contrasts using pial surface corrected with 3D FLAIR images.*

**mni coordinates*

	Hemisphere	Cluster	Area (mm2)	t	p	x	y	z*
Controls – premanifest HD	LH	No significant clusters						
	RH	Middle temporal gyrus	5489.02	3.729	.00020	62.4	-9.2	-
		Precuneus	1583.65	2.824	.00719	20.6		
		Superior parietal gyrus	1290.85	2.877	.03253	17.0	-69.2	
						36.8		
						26.4	-60.7	
						31.4		
Controls – manifest HD	LH	Postcentral gyrus	47107.62	9.316	.00020	-48.1	-26.2	
		Rostral middle frontal	1618.27	4.000	.00579	49.8		
						-39.4	38.6	
						26.8		
	RH	Precentral gyrus	47393.14	6.352	.00020	47.0	3.4	
		Rostral middle frontal	1424.73	4.724	.01653	22.6		
						41.8	32.3	
						30.2		
premanifest HD - manifest HD	LH	No significant clusters						
	RH	Fusiform gyrus	1963.04	3.219	.00020	21.0	-94.4	
						17.9		

ROI analysis

As seen in Figure 6, cortical thickness clusters in controls versus manifest HD group cover large brain areas including each of the 32 regions of interest of Desikan-Killiany Atlas (Desikan et al.. 2006) in the left hemisphere and 30 regions (excluding insula and medial orbitofrontal cortex) on the right hemisphere (see also Figure 5 for cortical thickness map using labels annotation of Desikan-Killiany Atlas). Thus, cortical thickness values for each ROI were extracted based on Desikan-Killiany Atlas (Desikan et al., 2006) for both hemispheres.

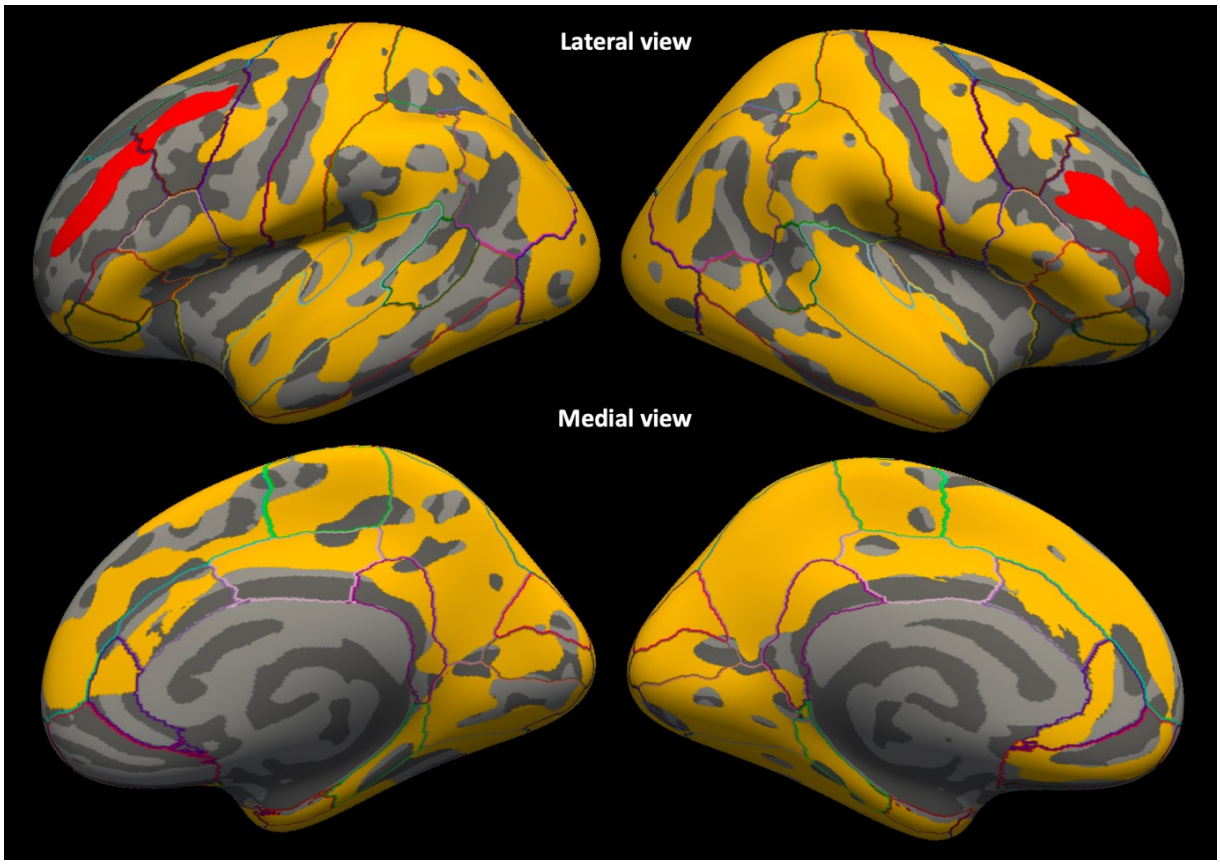

Figure 6. *Cortical thickness maps using Desikan-Killiany Atlas ROIs annotation for the contrast healthy control subjects versus* manifest HD. *Clusters significant after multiple comparison correction with Monte Carlo simulations ($p < 0.05$).*

Surface areas

The manifest HD group revealed significant clusters indicating reduced surface area in both left and right hemisphere compared to healthy controls group and premanifest HD group. Premanifest HD group did not differ significantly in surface area compared to healthy controls (Figure 7, Table 6 for specific clusters).

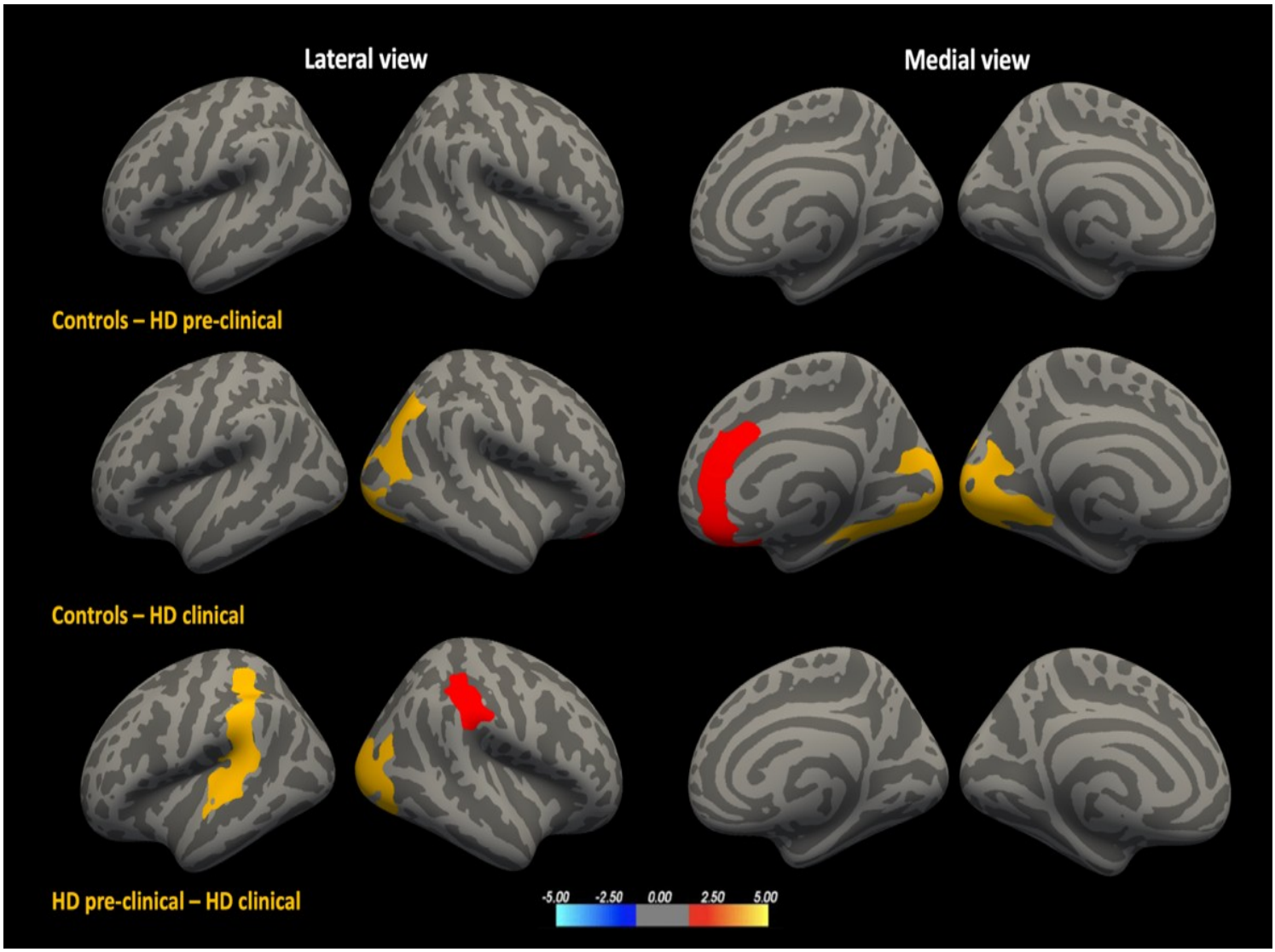

***Figure** 7. Surface area maps for pial surface corrected by FLAIR images. GLM analyses performed on the following contrasts: Upper row: healthy control subjects versus premanifest HD; middle row: control subjects versus manifest HD; bottom row: premanifest HD versus manifest HD. The color bar represents the tenth logarithm of p-value. Clusters significant after multiple comparison correction with Monte Carlo simulations ($p < 0.05$), (table 6).*

***Table 6**. Significant clusters in surface area for group comparisons: Controls vs premanifest HD. controls vs manifest HD and premanifest HD vs manifest HD using pial surface corrected with 3D Flair images.*

**mni coordinates*

	Hemisphere	Cluster	Area (mm2)	t	p	x	y	z*
controls – premanifest HD	LH	No significant clusters						
	RH	No significant clusters						
controls – manifest HD	LH	Lingual	5146.37	4.151	0.00020	-11.8	-81.7	
						-6.0		
	RH	Lateral occipital	8103.01	4.598	0.00020	17.4	-98.5	
		Rostral anterior	1424.73	4.724	0.00200	-11.6		
		cingulate				6.9	37.9	
						-2.1		
manifest HD – premanifest HD	LH	Superior parietal	47107.62	3.976	0.00020	-32.4	-42.5	
		lobe				44.7		
	RH	Lateral occipital	4083.72	4.337	0.00020	29.9	-91.7	
		Supramarginal	1470.70	6.883	0.01177	-1.3		
		gyrus						

	44.5	-37.0
	40.5	

Grey matter volume

Finally, manifest HD group revealed significant clusters indicating reduced grey matter volume in both left and right hemisphere, compared to healthy controls group and premanifest group. Premanifest HD group did not differ significantly in surface area compared to healthy controls (Figure 8, Table 7 for specific clusters).

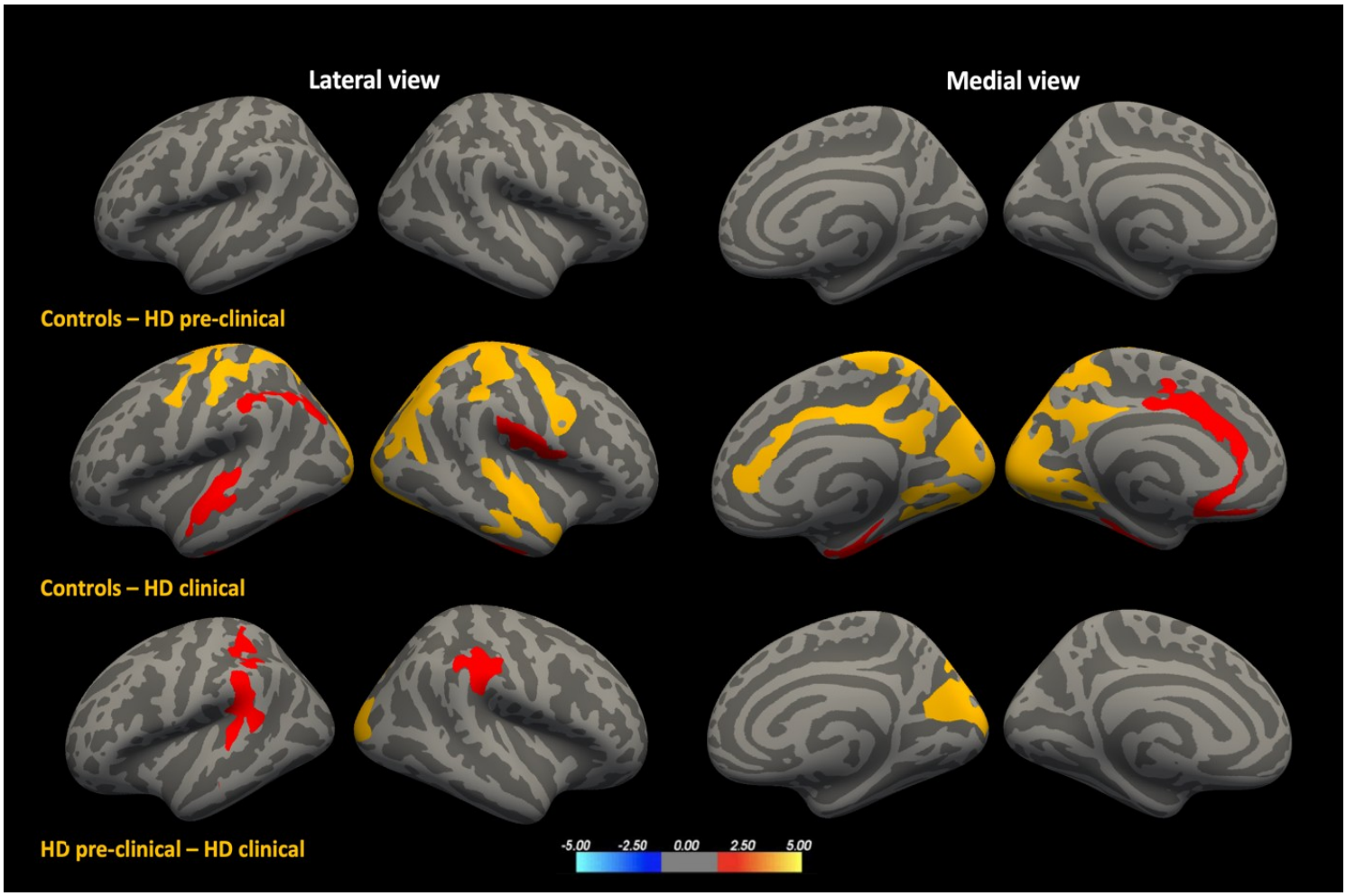

***Figure 8**. Grey matter maps for pial surface corrected by FLAIR images from general linear model analyses performed on the following contrasts: Upper row: healthy control subjects versus premanifest HD; middle row: control subjects versus manifest HD; bottom row: premanifest HD versus manifest HD. The color bar represents the tenth logarithm of p-value. Clusters significant after multiple comparison correction with Monte Carlo simulations ($p < 0.05$).*

**mni coordinates*

Subcortical structures & brainstem – ROI analysis

Volume values for subcortical areas including thalamus, caudate, putamen, pallidum, hippocampus and amygdala of both hemispheres along with brainstem were extracted and group comparisons were conducted using one-way ANCOVA. Covariates included total intracranial volume, age and sex. Results indicated that the effect of group was significant for all subcortical regions of interest (see table 8). Post-hoc comparisons using Sidak criterion showed that manifest HD group had significantly reduced volume compared to healthy control group and premanifest HD group. However, premanifest HD group presented significantly reduced volume in only left and right caudate, left and right putamen, right pallidum, right nucleus accumbens and brainstem compared to controls (See Figures 9-22 for error bar charts for between groups differences).

***Table** 7. One way Analysis of covariates models for subcortical values indicating differences between healthy control group, premanifest HD and manifest HD group.*

Subcortical areas	Healthy group (n=24)		Premanifest HD group (n=10)		Manifest HD group (n=14)		F(1.47)	η^2
	Mean	SD	Mean	SD	Mean	SD		
Left Thalamus	7936.65	796.1	7290.47	593.9	6306.36	514.7	24.45***	.54
Right Thalamus	7371.62	747.0	7041.61	616.2	6238.59	550.4	10.22***	.33
Left Caudate	3328.17	447.80	2679.06	543.3	1887.97	323.1	38.31***	.65
Right Caudate	3433.04	485.6	2825.09	527.0	1937.25	284.9	38.67***	.65
Left Putamen	4734.48	581.1	3865.52	812.4	2295.40	309.1	77.35***	.79
Right Putamen	4825.86	490.3	3991.29	808.7	2518.65	217.0	93.28***	.82
Left Pallidum	1984.38	226.6	1678.21	270.0	1141.10	191.5	53.41***	.72
Right Pallidum	1968.11	235.5	1623.39	263.6	1072.13	127.6	67.77***	.76
Left Hippocampus	4231.93	338.0	3892.65	305.1	3538.76	291.6	14.94***	.42
Right Hippocampus	4282.53	368.4	4045.38	377.1	3731.09	328.4	6.694**	.24
Left Amygdala	1618.84	240.0	1464.02	199.1	1206.74	118.0	15.83***	.43
Right Amygdala	1751.76	222.6	1648.03	167.8	1401.65	132.1	13.51***	.39
Left Nucleus Accumbens	429.89	90.9	355.25	70.5	228.82	37.83	24.42***	.54
Right Nucleus Accumbens	503.06	75.7	424.38	76.0	286.55	41.7	33.71***	.62
Brainstem	21279.81	2216.0	19936.03	2277.8	17559.09	2144.51	12.21***	.37

Table 9. *Between groups subcortical values comparisons between healthy control group, pre manifest HD and manifest HD groups using Sidak corrections.*

Subcortical areas	Healthy controls versus premanifest HD group		Healthy controls versus manifest HD group		Premanifest HD versus manifest HD group	
	Mean Difference (stand.error)	p	Mean Difference (stand.error)	p	Mean Difference (stand.error)	p
Left Thalamus	290.08 (188.9)	.346	1165.84 (169.2)	<.000	875.76 (199.7)	<.000
Right Thalamus	-16.35 (193.6)	.999	718.58 (173.4)	<.000	734.93 (204.7)	.003
Left Caudate	446.27 (159.7)	.023	1249.00 (143.0)	<.000	802.73 (168.8)	<.000
Right Caudate	426.67 (168.3)	.045	1318.98 (150.7)	<.000	892.31 (177.9)	<.000
Left Putamen	609.78 (190.6)	.008	2103.78 (170.6)	<.000	1494.00 (201.4)	<.000
Right Putamen	577.43 (163.7)	.003	1984.91 (146.6)	<.000	1407.48 (173.0)	<.000
Left Pallidum	194.07 (81.5)	.064	744.37 (73.0)	<.000	550.30 (86.1)	<.000
Right Pallidum	237.44 (76.2)	.010	788.90 (68.3)	<.000	551.46 (80.6)	<.000
Left Hippocampus	179.26 (110.1)	.297	536.73 (98.6)	<.000	357.47 (116.4)	.011
Right Hippocampus	58.99 (124.0)	.952	392.23 (111.0)	.003	333.29 (131.04)	.044
Left Amygdala	23.52 (60.9)	.973	290.89 (54.5)	<.000	267.37 (64.4)	<.000
Right Amygdala	-16.33 (56.52)	.988	237.19 (50.6)	<.000	253.53 (59.8)	<.000

Left Nucleus Accumbens	60.93 (27.1)	.087	169.24 (24.3)	<.000	108.30 (28.7)	.001
Right Nucleus Accumbens	65.59 (26.3)	.049	192.57 (23.5)	<.000	126.98 (27.8)	<.000
Brainstem	-187.33 (619.2)	.987	2453.64 (554.4)	<.000	2640.96 (654.5)	.001

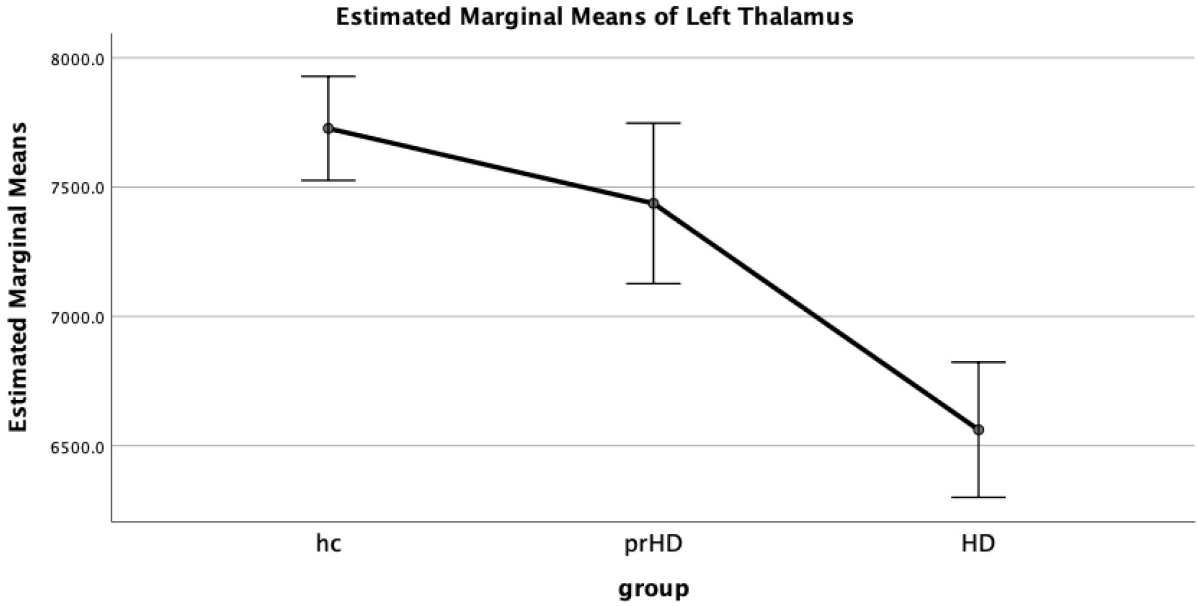

Figure 9. *Error bar chart for left thalamus volume indicating differences between healthy control group, premanifest HD and manifest HD groups.*

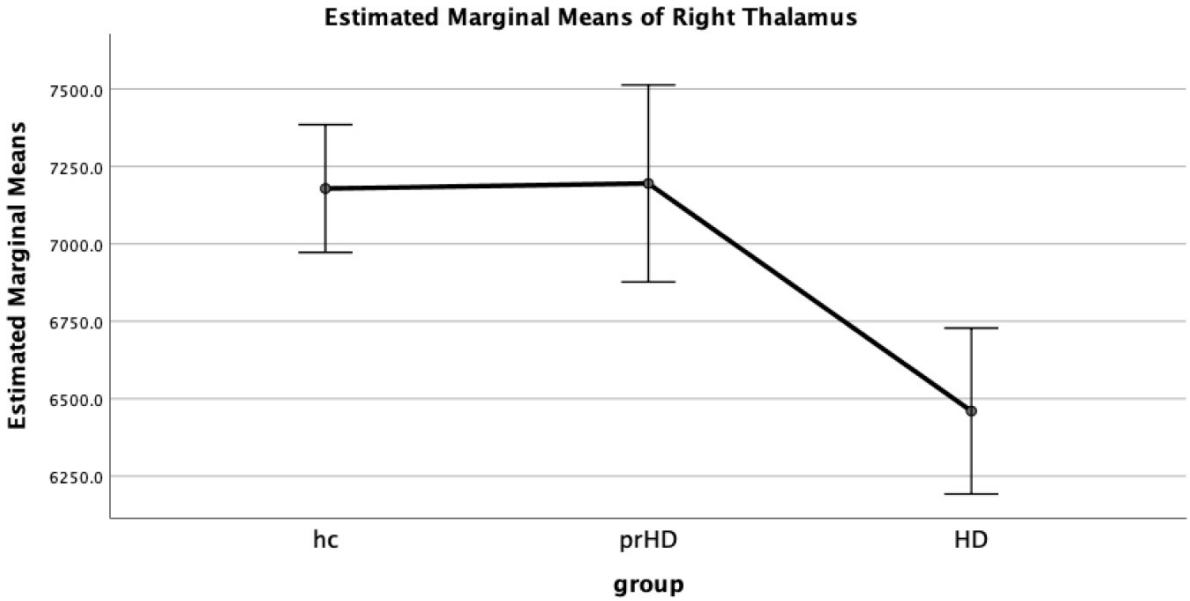

Figure 10. *Error bar chart for right thalamus volume indicating difference between healthy control group, premanifest HD and manifest HD groups.*

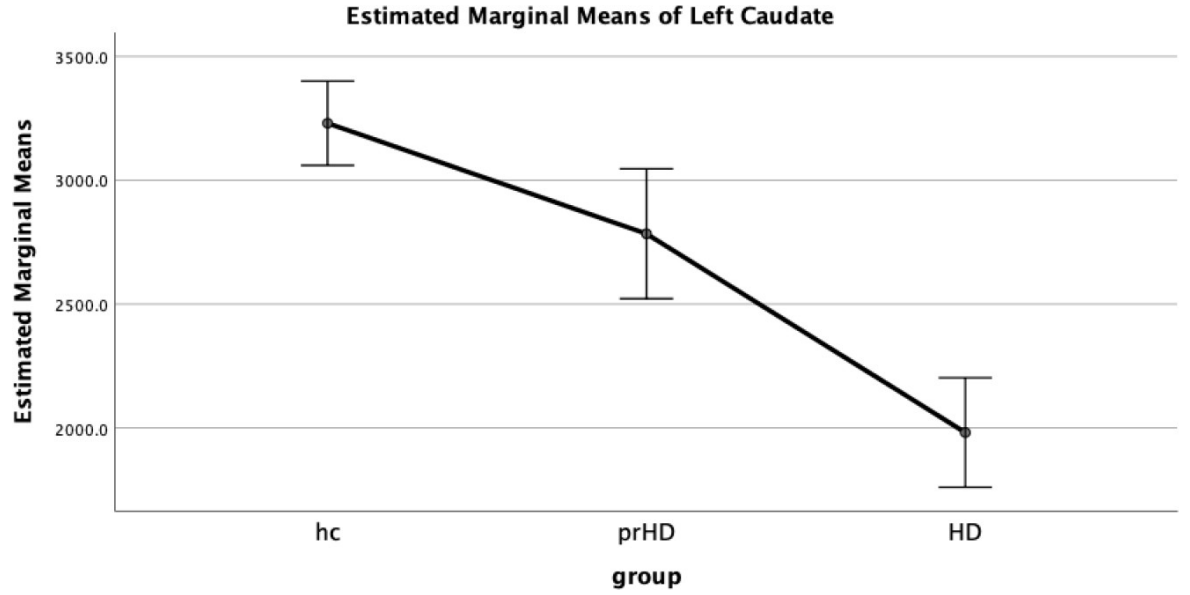

Figure 11. *Error bar chart for left Caudate volume indicating difference between healthy control group, premanifest HD and manifest HD groups.*

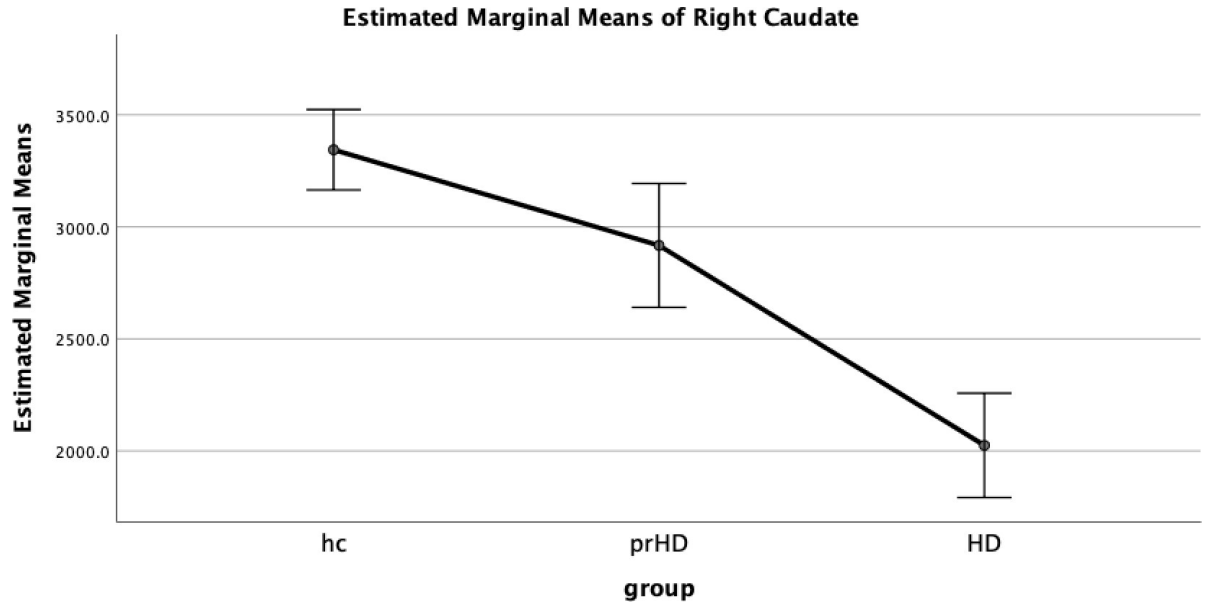

Figure 12. *Error bar chart for right caudate volume indicating difference between healthy control group, premanifest HD and manifest HD groups.*

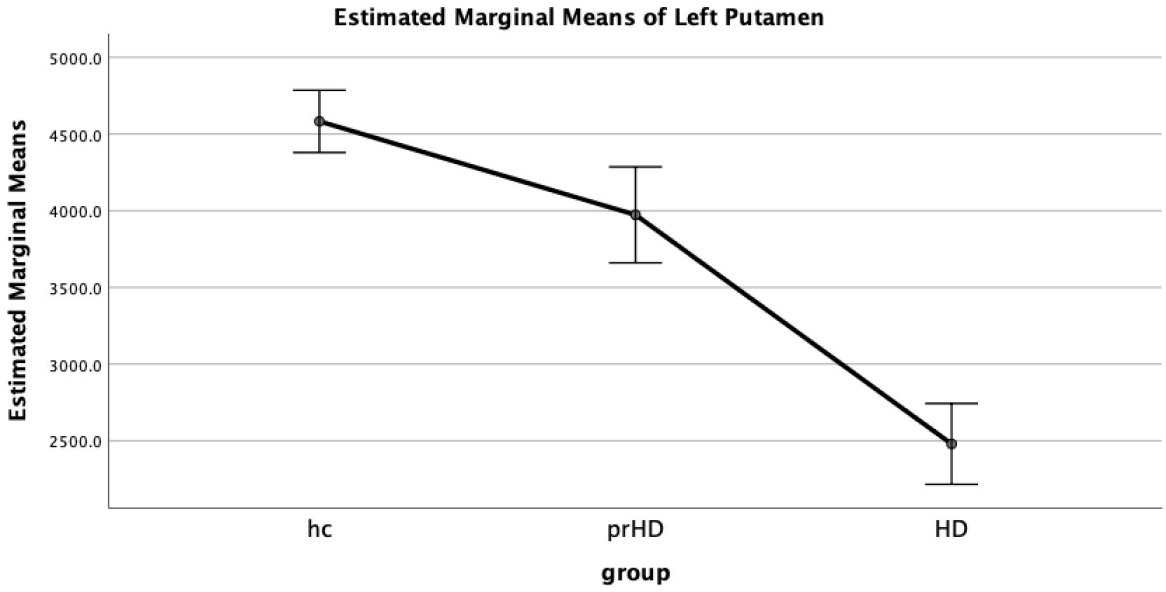

Figure 13. *Error bar chart for left putamen volume indicating difference between healthy control group, premanifest HD and manifest HD groups.*

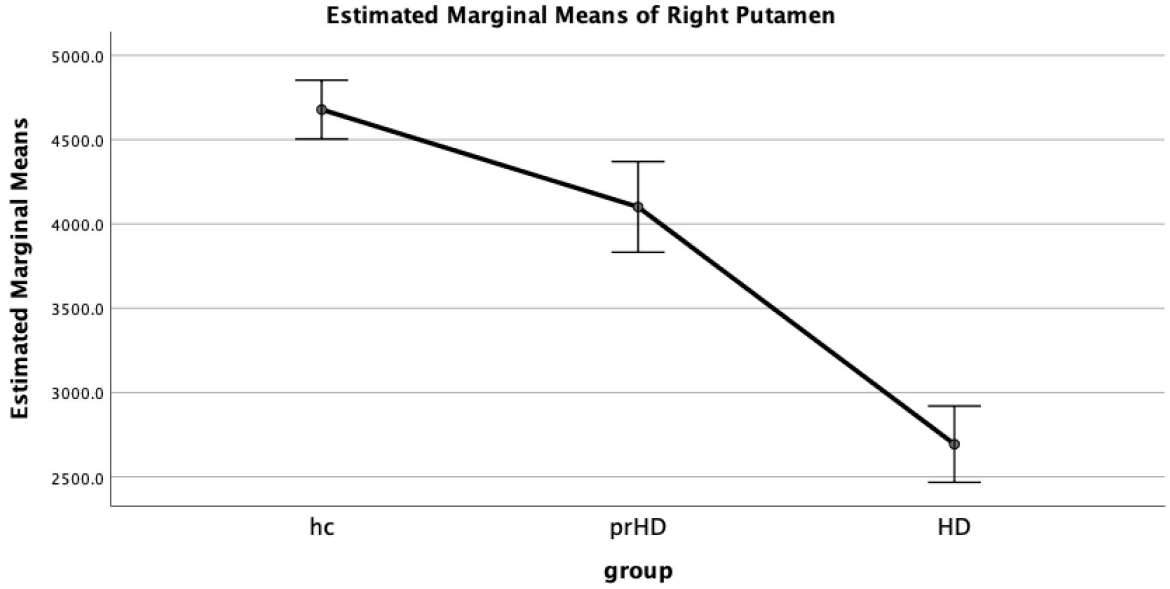

Figure 14. *Error bar chart for right putamen volume indicating difference between healthy control group, premanifest HD and manifest HD groups.*

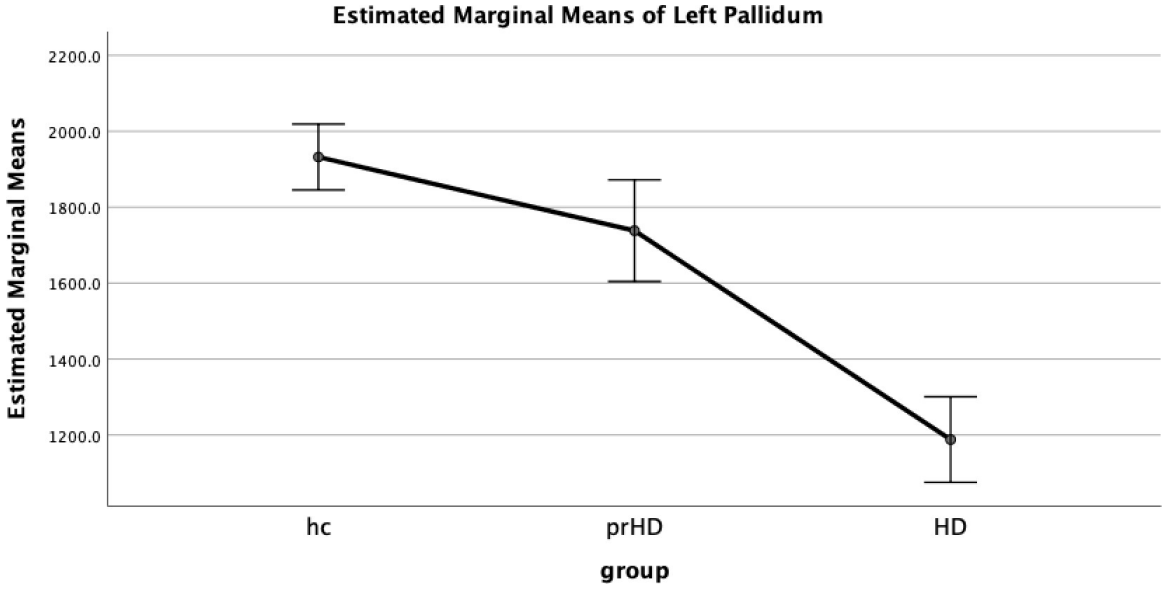

Figure 15. *Error bar chart for left pallidum volume indicating difference between healthy control group, premanifest HD and manifest HD groups.*

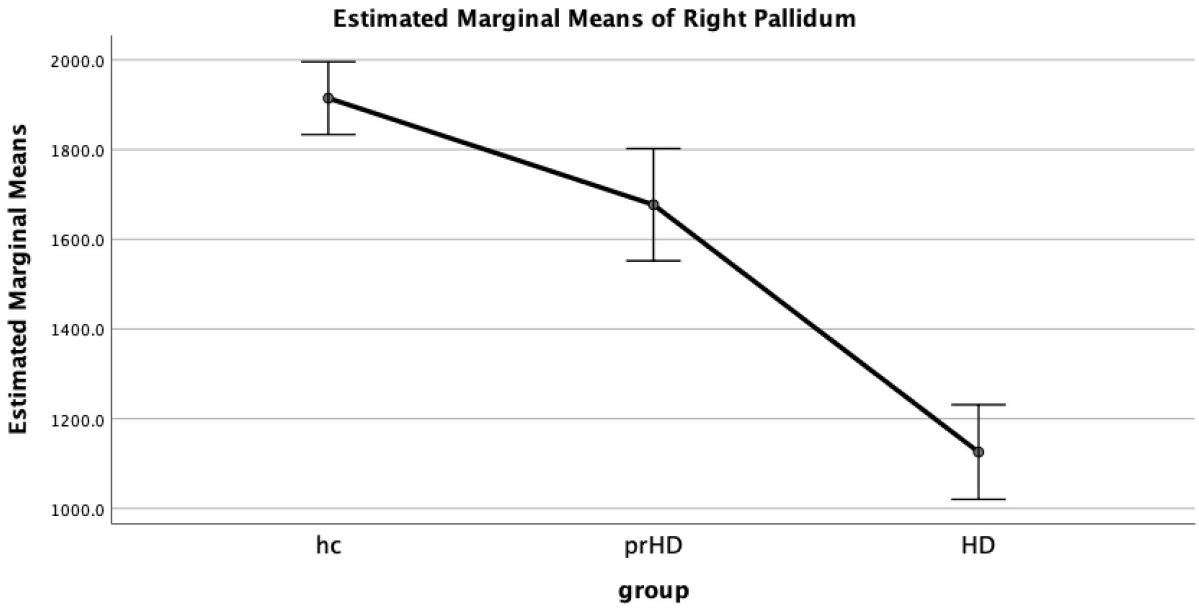

Figure 16. *Error bar chart for right pallidum volume indicating difference between healthy control group, premanifest HD and manifest HD groups.*

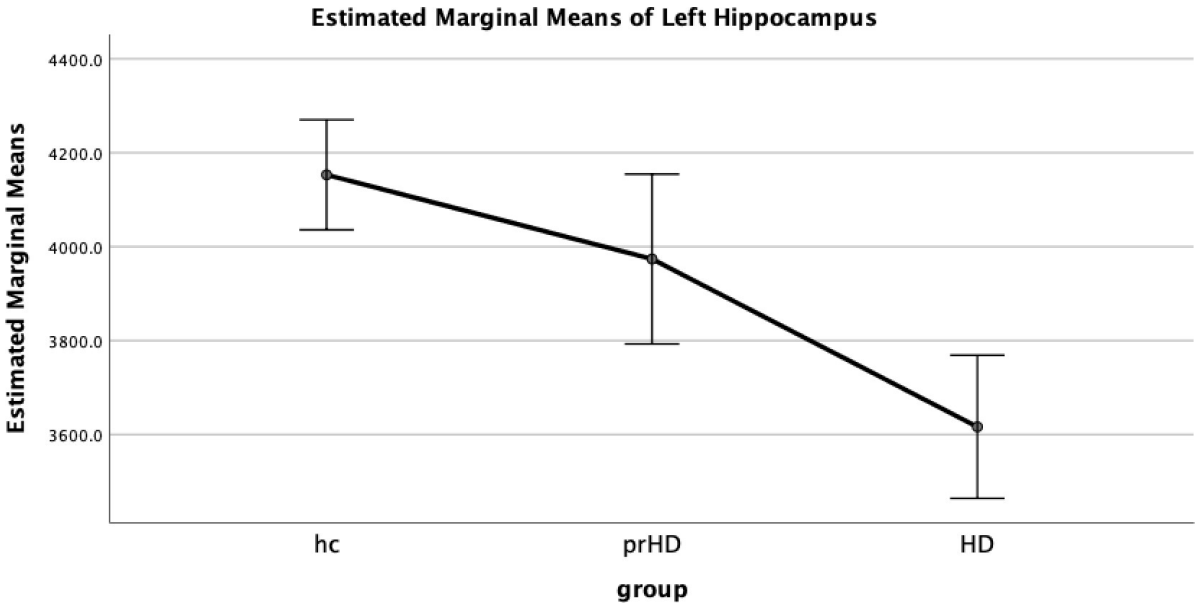

Figure 17*. Error bar chart for left hippocampus volume indicating difference between healthy control group, premanifest HD and manifest HD groups.*

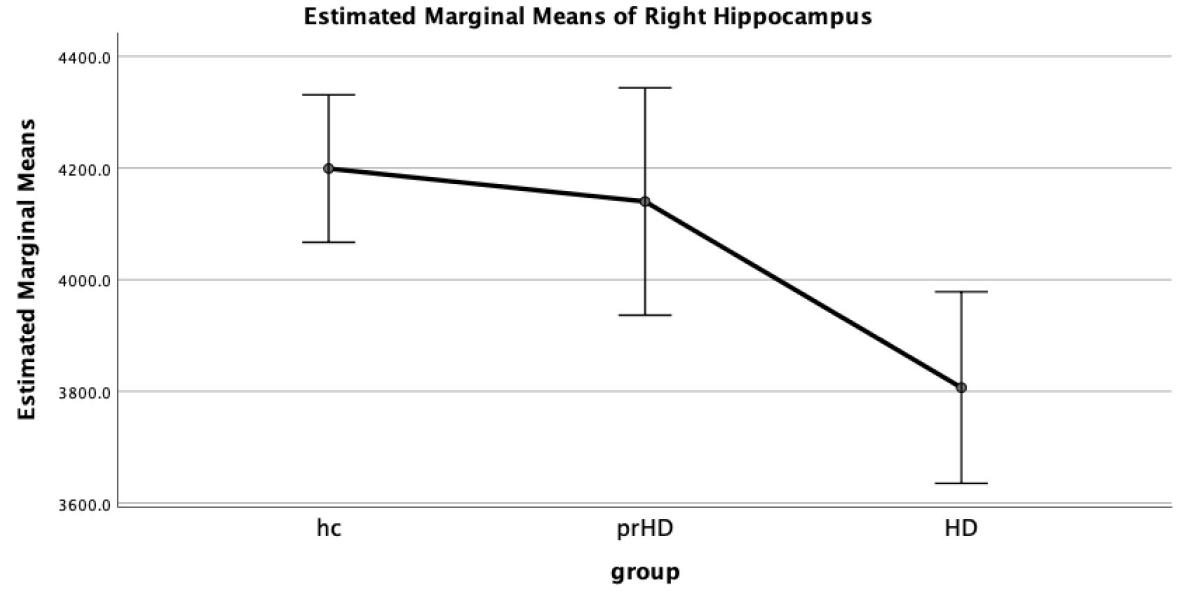

Figure 18. *Error bar chart for right hippocampus volume indicating difference between healthy control group, premanifest HD and premanifest HD groups.*

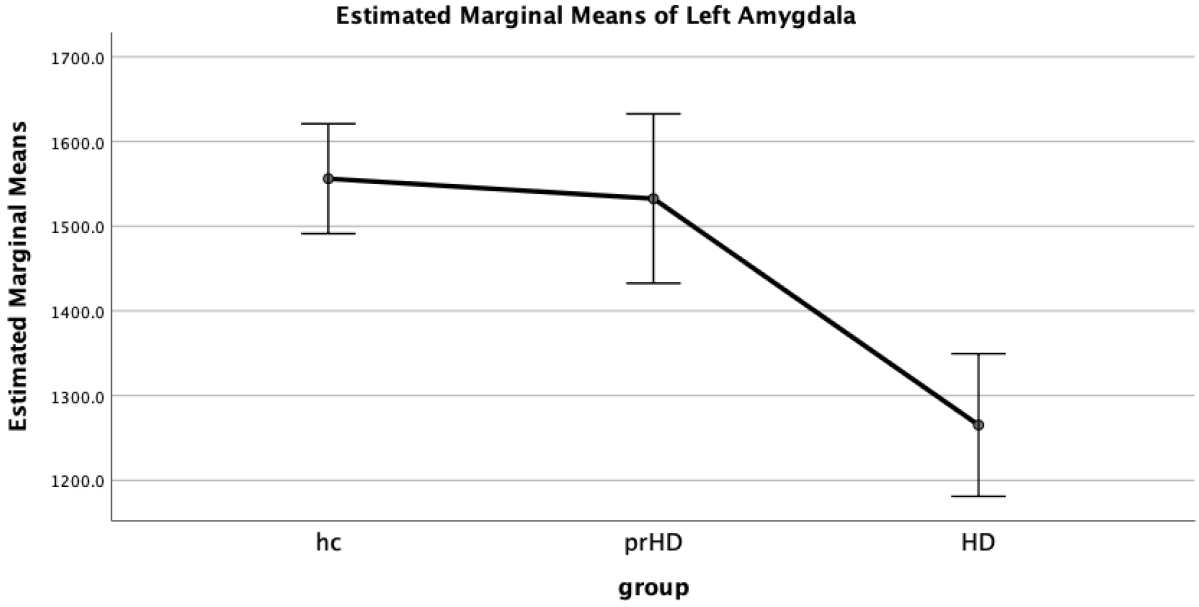

Figure 19. *Error bar chart for left amygdala volume indicating difference between healthy control group, premanifest HD and manifest HD groups.*

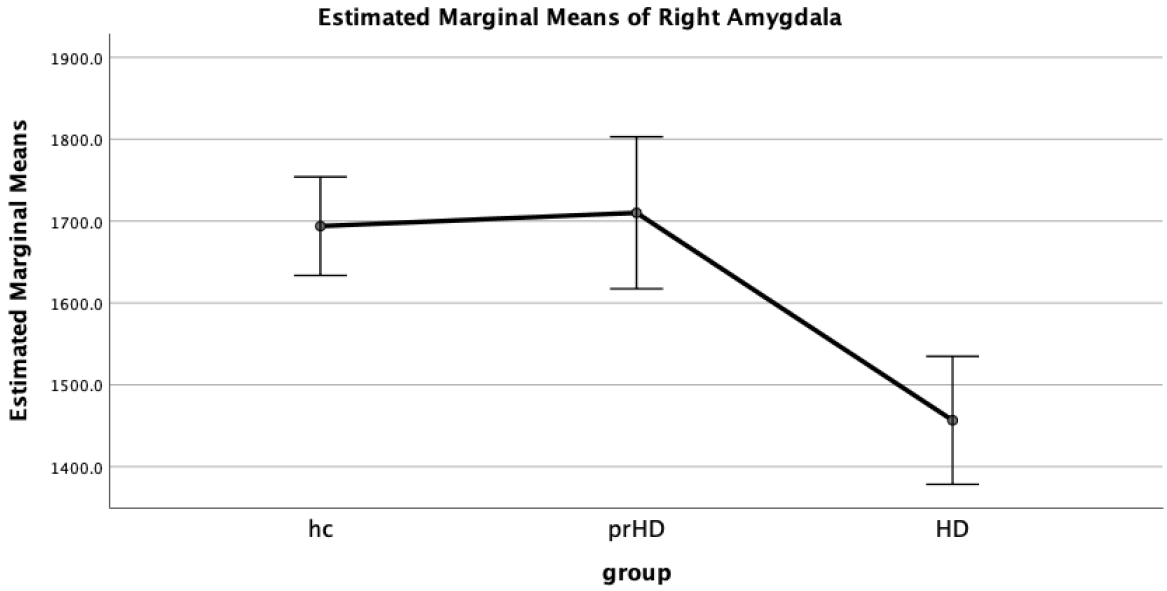

Figure 20. *Error bar chart for right amygdala volume indicating difference between healthy control group, premanifest HD and manifest HD groups.*

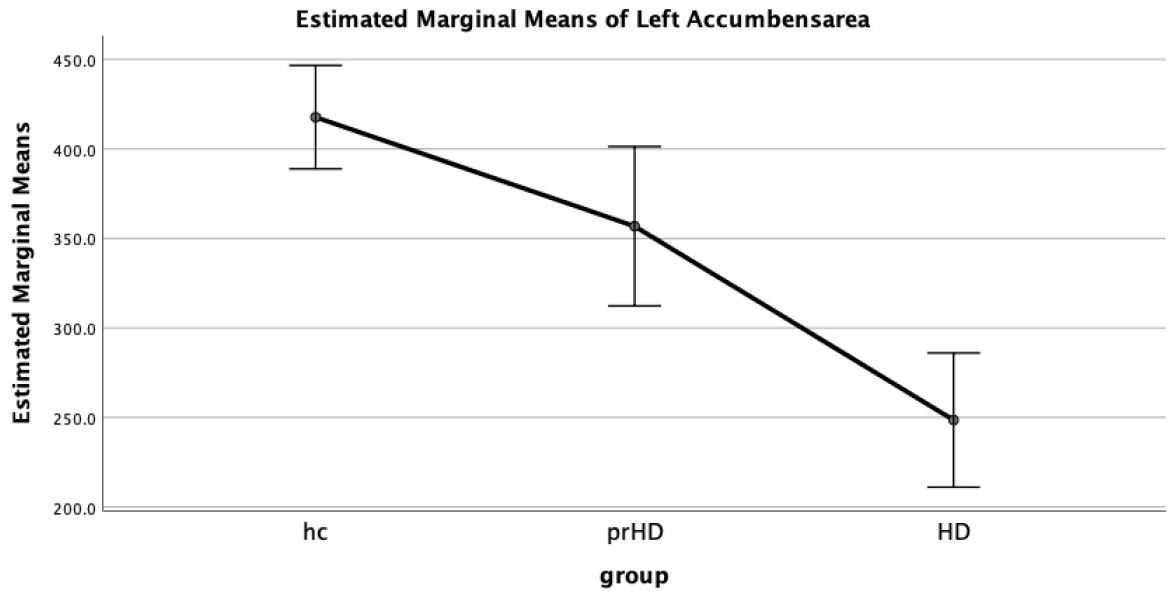

Figure 21. *Error bar chart for left Nucleus accumbens volume indicating difference between healthy control group, pre* manifest HD *and* manifest HD *groups.*

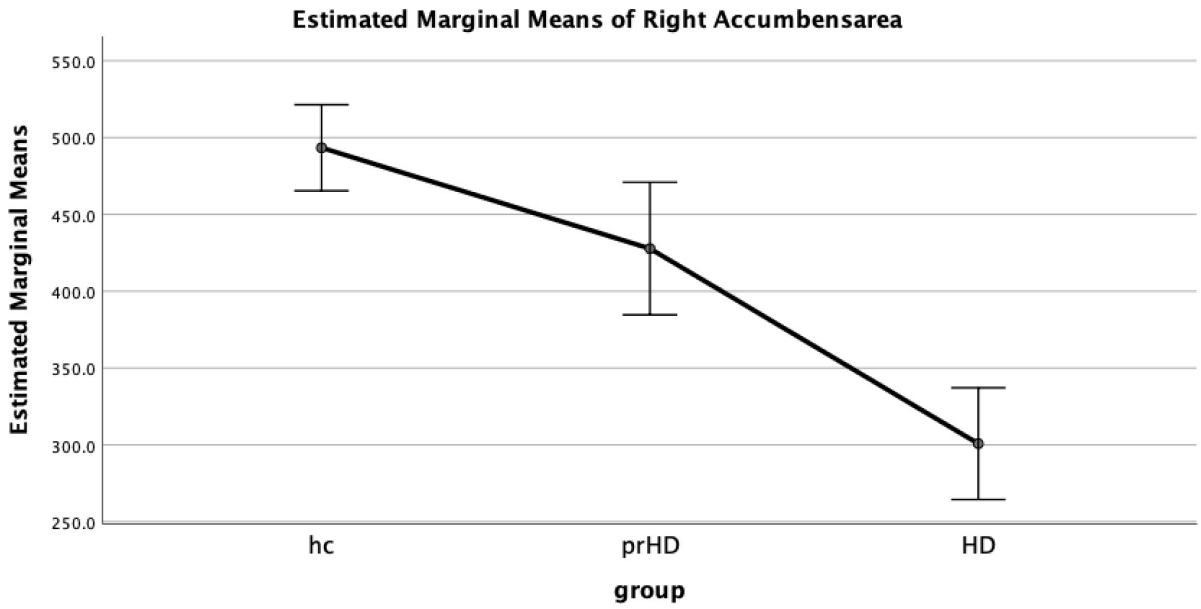

Figure 22. *Error bar chart for right Nucleus accumbens volume indicating difference between healthy control group, premanifest HD and manifest HD groups.*

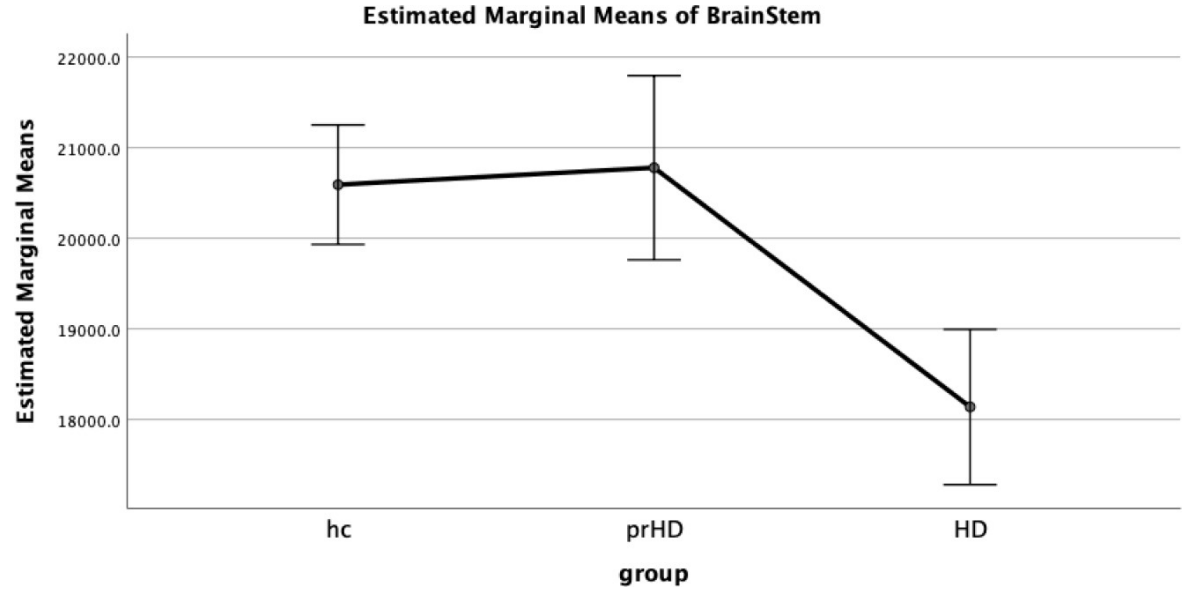

Figure 23. *Error bar chart for Brainstem volume indicating difference between healthy control group, premanifest HD and manifest HD groups.*

Neuromelanin sequence analysis results

All groups were analyzed for differences in the neuromelanin sequence (Prof. Politis Lab). Table 11 shows values of locus coeruleus (LC) and substantia nigra (SN) area in groups as well as between groups comparisons. All three groups' analyses produced statistically significant differencesfor both metrics surface area and volume (both $p<0.001$) in the premanifest HD (pre HDGECs) versus the control group analysis or versus the manifest HD (m HDGECs) group analysis.

Group	**Values SN area (mm^2)**	**Comparison**	**p-value**
Healthy	100.8±12.39	**Healthy vs pre HDGECs**	0.00024
Pre HDGECs	77.99±9.18	**Healthy vs m HDGECs**	<0.00001
m HDGECs	63.62±10.1	**Pre HDGECs vs m HDGECs**	0.002
Group	**Values SN volume(mm^3)**	**Comparison**	**p value**
Healthy	255.35±28.14	**Healthy vs pre HDGECs**	<0.00001
Pre HDGECs	195.49±22.73	**Healthy vs m HDGECs**	<0.00001
m HDGECs	159.04±25.26	**Pre HDGECs vs m HDGECs**	0.002
Group	**Values LC volumes(mm^3)**	**Comparison**	**p value**

Healthy	**14.14±2.4**	Healthy vs pre HDGECs	0.02
Pre HDGECs	**12.2±1.3**	Healthy vs m HDGECs	<0.00001
m HDGECs	**10.13±1.7**	Pre HDGECs vs m HDGECs	0.004
Group	**Values LC area (mm^2)**	**Comparison**	**p value**
Healthy	5.56±0.81	Healthy vs preHDGECs	0.021
Pre HDGECs	4.88±0.52	Healthy vs mHDGECs	<0.00001
mHDGECs	4.05±0.67	Pre HDGECs vs m HDGECs	0.004

Table 11: Neuromelanin sequence analysis - Comparisons of values of locus coeruleus (LC). substantia nigra (SN) area and volume in groups as well as between groups (premanifest HD or pre-HDGECs) versus the control group analysis or versus manifest HD (mHDGECs) group analysis. or premanifest HD (pre- HDGECs) versus manifest HD (mHDGECs).

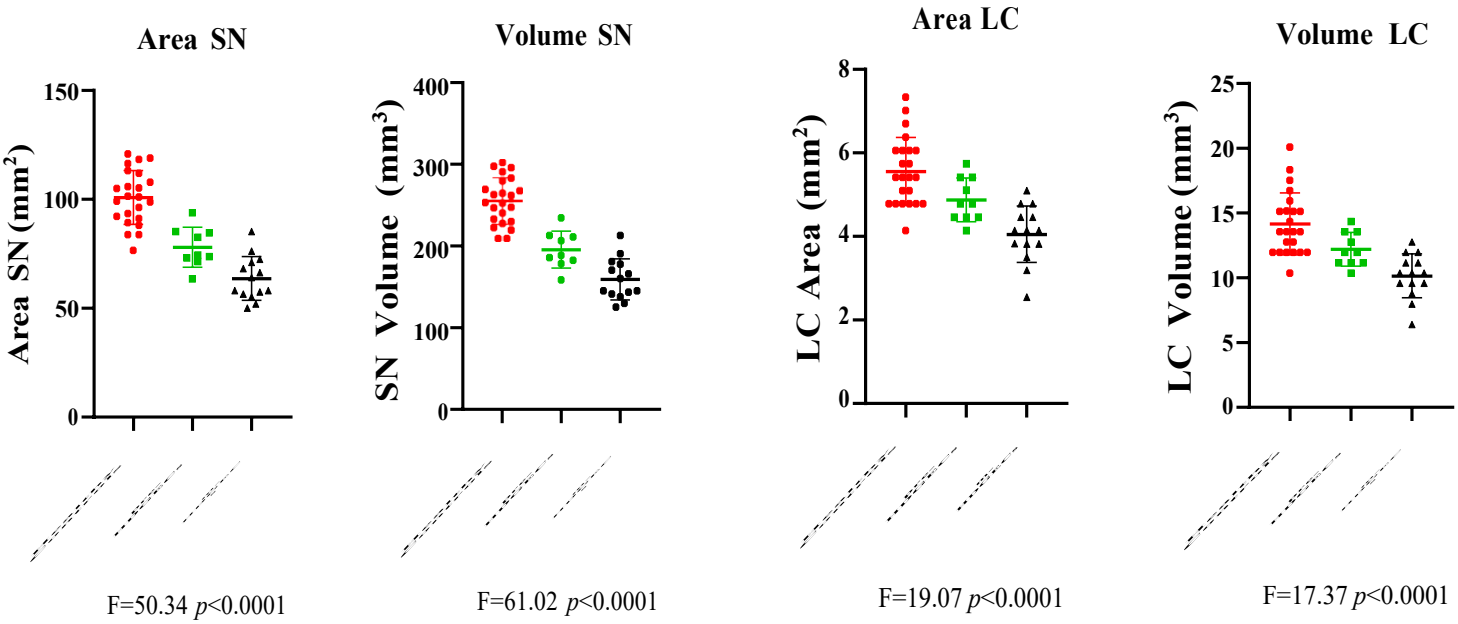

Figure 24: Scatter-plot showing neuromelanin sequence analysis results. Values of locus coeruleus (LC and. substantia nigra (SN) areas and volumes in groups (pre HDGECs. mHDGECs and healthy controls) are depicted.

Statistically significant correlations were identified between SN area, volume, LC area, volume and finger tapping test. HDQoL, PBA, AES-s and BDI-II Values were correlated

with all significant variables using Spearman's rank correlation coefficient as seen in Table 11 & Figure 5.

	BDI-II	AES-s	PBA	HDQoL	Finger Tapping
SN Area	Rho= -0.7 p= 0.02	Rho= -0.49 p= 0.02	Rho= -0.54 p= 0.008	Rho= -0.6 p= 0.002	Rho= 0.64 p= 0.0009
SN Volume	Rho= -0.48 p= 0.02	Rho= -0.49 p= 0.017	Rho= -0.54 p= 0.0076	Rho= -0.61 p= 0.002	Rho= 0.66 p= 0.0007

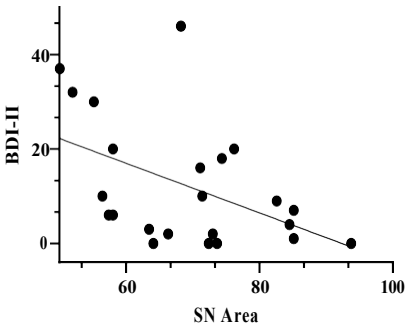

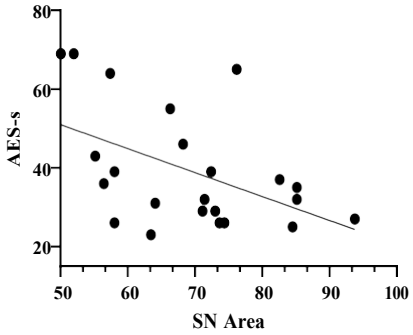

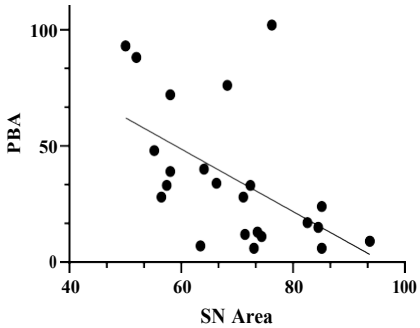

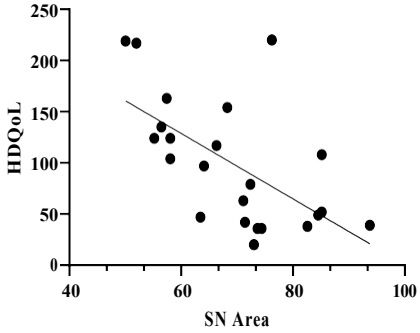

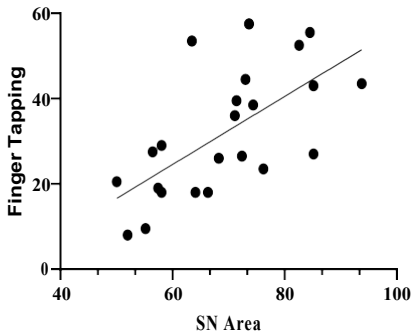

Table 12 & Scatter-plot Figure 6: *SN, LC area and volume values in correlation with finger tapping test. HDQoL, PBA, AES-s and BDI-II. ($p<0.05$ statistically significant).*

However, statistically significant correlations were not identified between SN area, volume, LC area, volume and UHRDS or PPT.

	UHDRS-TMS	**UHDRS-TFC**	**UHDRS-FAS**	**UHDRS-IS**	**UHDRS-TMS (brady)**	**PPT**
SN Area	Rho= -0.46 p= 0.09	Rho= 0.35 p= 0.12	Rho= 0.3 p= 0.29	Rho= 0.35 p= 0.22	Rho= -0.49 p=*0.07*	Rho= 0.35 p=0.21
SN Volume	Rho= -0.47 p= 0.09	Rho= 0.35 p= 0.21	Rho= -0.3 p= 0.29	Rho= 0.35 p= 0.21	Rho= -0.49 p= *0.07*	Rho= 0.35 p= 0.22
LC Area	Rho= -0.42 p= 0.13	Rho= 0.46 p= 0.09	Rho= 0.45 p= 0.1	Rho= 0.43 p= 0.12	Rho= -0.41 p= 0.14	Rho= 0.42 p= 0.13
LC Volume	Rho= -0.42 p=0.13	Rho= 0.46 p= 0.09	Rho= 0.45 p= 0.1	Rho= 0.43 p= 0.13	Rho= -0.41 p= 0.14	Rho= 0.43 p= 0.13

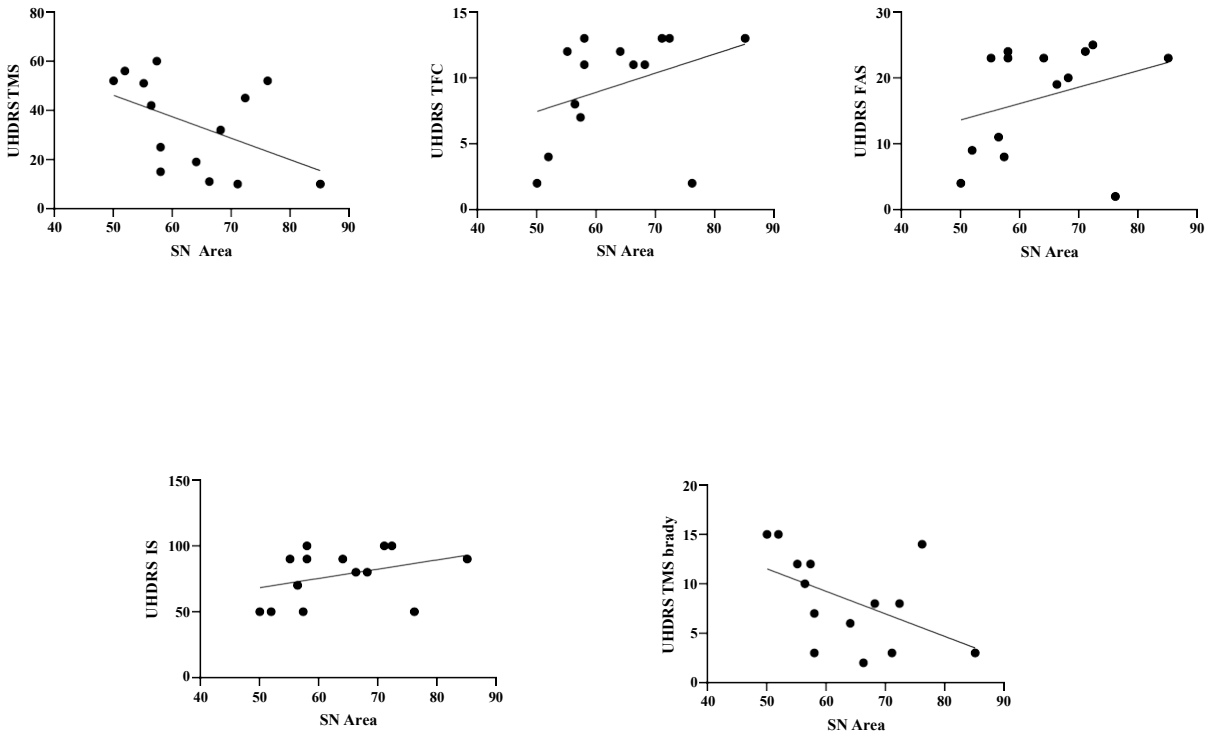

Table 13 & Scatter-plot Figure 7 : *SN, LC area and volume values in correlation UHDRS-TMS, UHDRS-TFC, UHDRS-FAS, UHDRS-IS, UHDRS-TMS, PPT (p<0.05 statistically significant).*

Furthermore, statistically significant correlations were also identified between SN area, Volume, LC area, volume and cognitive scales such as MoCA, TMT-A, SDMT words. SDMT oral, HTLV-R.

	MoCA	**TMT-A**	**SDMT W**	**SDMT O**	**HTLV-R**
SN Area	Rho= 0.49 p= 0.01	Rho= 0.57 p= 0.0047	Rho= 0.46 p= 0.03	Rho= 0.63 p= 0.0017	Rho= 0.75 p <0.0001

SN Volume	Rho= 0.5 p= 0.015	Rho= -0.51 p= 0.01	Rho= 0.47 p= 0.027	Rho= 0.64 p= 0.0014	Rho= 0.76 p <0.0001
	TMT-A	**SDMT W**	**SDMT O**	**HTLV-R**	
LC Area	Rho= -0.54 p= 0.008	Rho= 0.49 p= 0.01	Rho= 0.43 p= 0.04	Rho= 0.47 p= 0.02	
LC Volume	Rho= -0.54 p= 0.008	Rho= 0.5 p= 0.01	Rho= 0.43 p= 0.04	Rho= 0.47 p= 0.023	

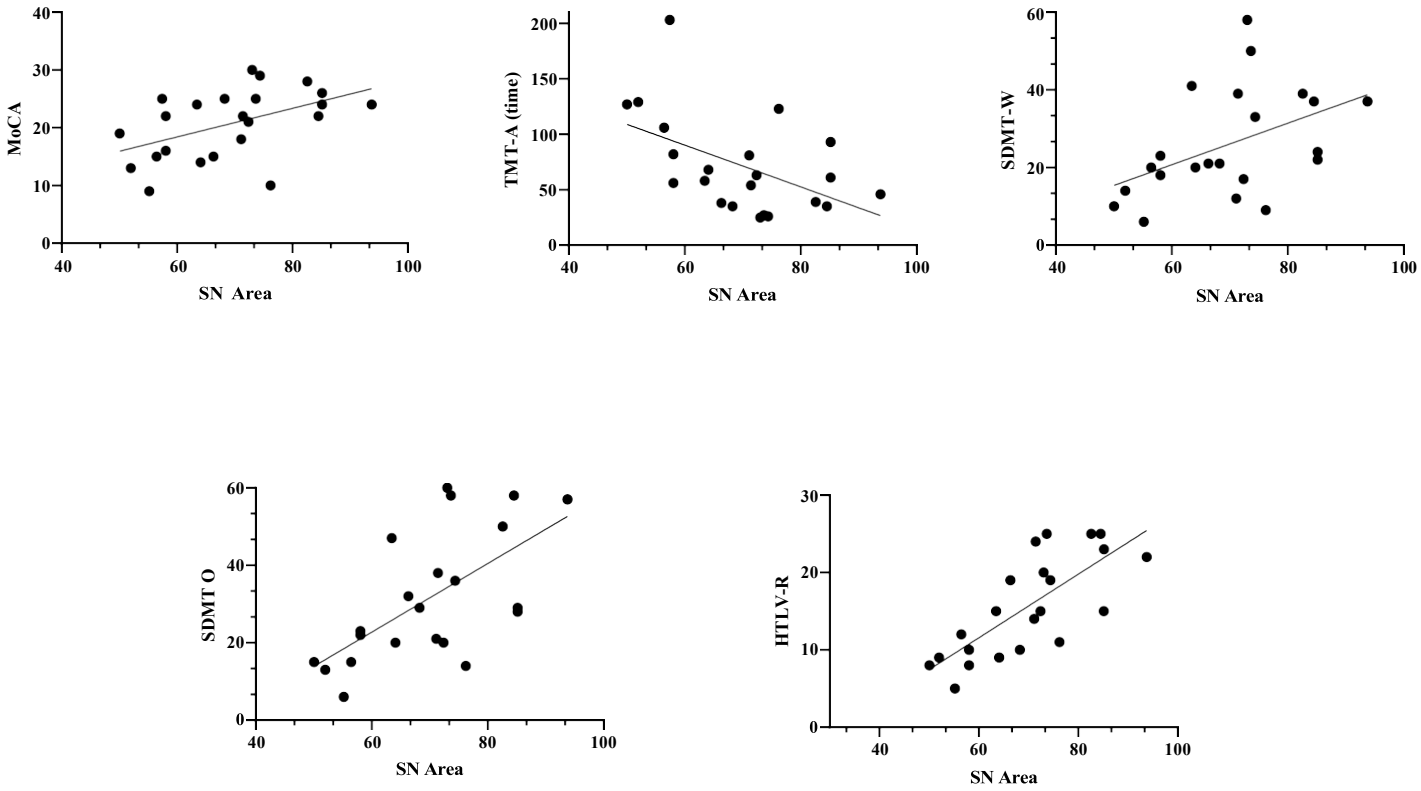

Table 14 & Scatter-plot 8 Figure 25: *SN.LC area and volume values in correlation with MoCA. TMT-A, SDMT Word, SDMT Oral, HTLV-R, PPT (p<0.05 statistically significant).*

Finger-Tapping Test

Finger Tapping values were also investigated in focus groups. Values from right and left finger tapping were categorized in two main groups HD (manifest HD and pre-manifest HD) and controls were correlated with all significant variables. Results were corrected for multiple comparisons as previously described. Table 15 presents only statistically significant correlations identified with subcortical ROIs. Values were corrected for multiple comparison as described in the Methods section.

Variable 1	ROI	Effect size	p.value	Multiple comparison adjustment
Finger Tapping Test L	RightPutamen	0.77178805	1.349E-10	3.2589E-09
Finger Tapping Test L	LeftPutamen	0.7674427	1.9778E-10	4.539E-09
Finger Tapping Test L	RightPallidum	0.74750842	1.0352E-09	1.5839E-08
Finger Tapping Test L	LeftAccumbensarea	0.74144505	1.662E-09	2.2815E-08
Finger Tapping Test L	RightCaudate	0.72887774	4.2586E-09	4.7675E-08
Finger Tapping Test L	RightAccumbensarea	0.72589031	5.2857E-09	5.5774E-08
Finger Tapping Test L	LeftCaudate	0.71665645	1.013E-08	9.2074E-08
Finger Tapping Test L	LeftPallidum	0.70802007	1.8198E-08	1.5613E-07
Finger Tapping Test L	LeftThalamusProper	0.66185075	3.0172E-07	1.5388E-06
Finger Tapping Test L	LeftAmygdala	0.64870608	6.1543E-07	2.7968E-06
Finger Tapping Test L	RightAmygdala	0.62920633	1.6673E-06	6.541E-06
Finger Tapping Test L	LeftHippocampus	0.57170031	2.1913E-05	5.2387E-05
Finger Tapping Test L	RightThalamusProper	0.56712218	2.6357E-05	6.141E-05
Finger Tapping Test L	BrainStem	0.50960064	0.00021606	0.00039828
Finger Tapping Test L	RightHippocampus	0.4470126	0.00144655	0.00215224
Finger Tapping Test R	LeftAccumbensarea	0.7328556	3.1797E-09	3.6949E-08
Finger Tapping Test R	RightPutamen	0.72229366	6.8309E-09	6.7429E-08
Finger Tapping Test R	LeftPutamen	0.71414259	1.204E-08	1.0731E-07
Finger Tapping Test R	RightPallidum	0.69854687	3.3791E-08	2.585E-07
Finger Tapping Test R	RightAccumbensarea	0.69055882	5.5919E-08	3.7745E-07
Finger Tapping Test R	LeftThalamusProper	0.68050583	1.0308E-07	6.436E-07
Finger Tapping Test R	LeftPallidum	0.64186975	8.798E-07	3.7048E-06
Finger Tapping Test R	RightCaudate	0.63812026	1.0663E-06	4.4294E-06
Finger Tapping Test R	LeftCaudate	0.63746817	1.1023E-06	4.5583E-06
Finger Tapping Test R	LeftAmygdala	0.63399038	1.314E-06	5.338E-06
Finger Tapping Test R	RightAmygdala	0.62122037	2.4593E-06	8.8535E-06
Finger Tapping Test R	LeftHippocampus	0.58194799	1.4349E-05	3.6188E-05

Finger Tapping Test R	RightThalamusProper	0.55688124	3.9446E-05	8.7257E-05
Finger Tapping Test R	BrainStem	0.5071597	0.00023433	0.00042513
Finger Tapping Test R	RightHippocampus	0.4988048	0.00030796	0.0005304

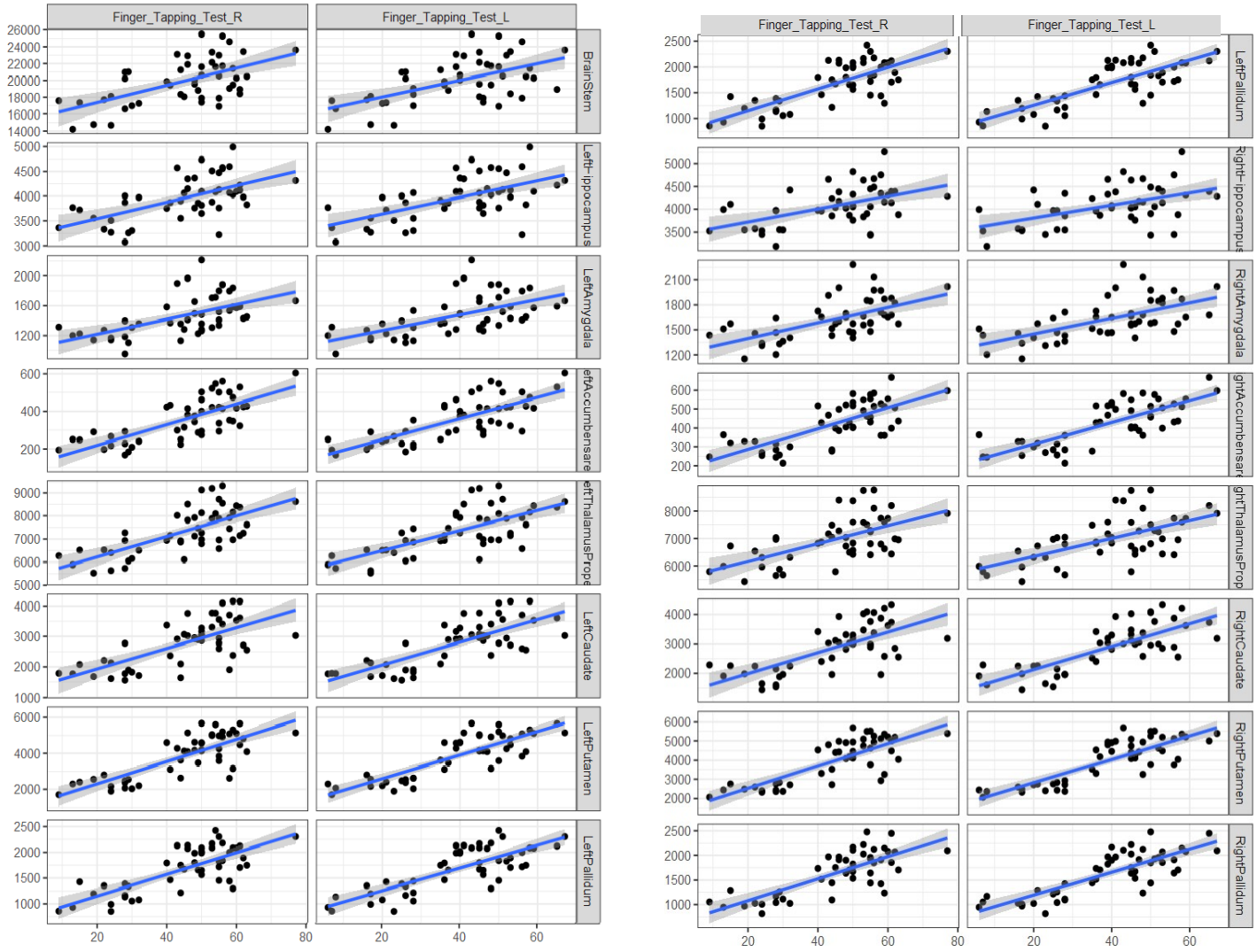

Table 15 & Scatter-plot Figure 26: Finger Tapping test values that correlated statistically significantly with subcortical ROIs. (p<0.05 statistically significant).

cUHDRS

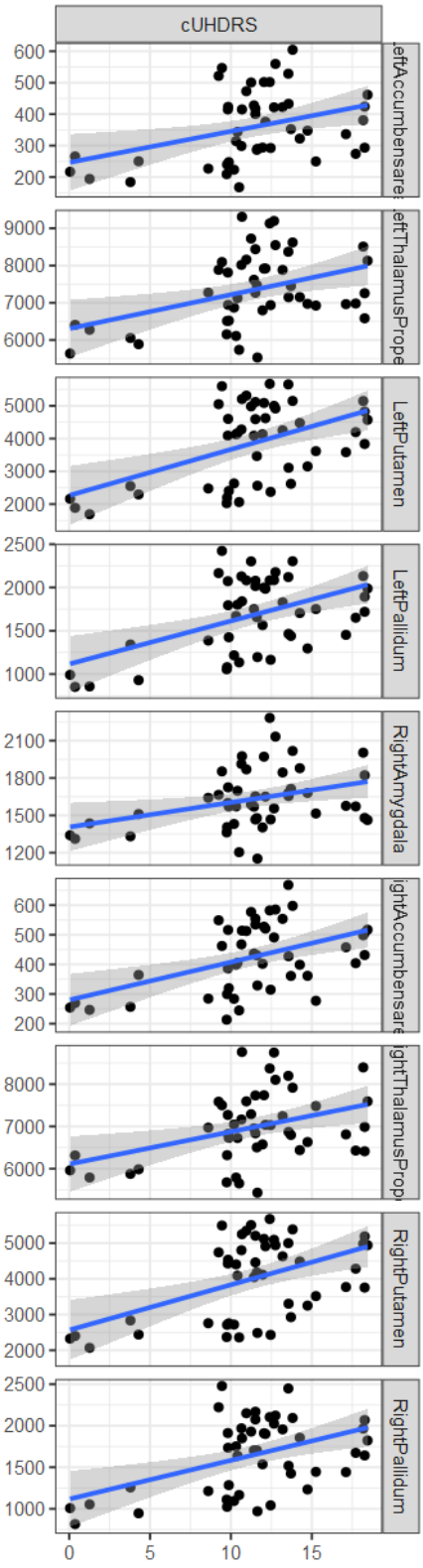

cUHDRS values were also analysed separately (table 16). Values from cUHDRS were categorized in two main groups HD (manifest HD and pre-manifest HD) and controls, and were correlated with all significant variables. Results were corrected for multiple comparisons as previously described.

Variable 1	ROI	Effect size	p.value	Multiple comparison adjustment
cUHDRS	Right Accumbens area	0.41653657	0.00358696	0.00498159
cUHDRS	Left Accumbens area	0.38283847	0.00790828	0.01037059
cUHDRS	Left Putamen	0.38190228	0.00807484	0.01054439
cUHDRS	Right Putamen	0.37583117	0.00923042	0.01193455
cUHDRS	Left Thalamus Proper	0.36652212	0.01127851	0.014319
cUHDRS	Right Amygdala	0.35067939	0.0156621	0.01961502
cUHDRS	Right Thalamus Proper	0.34391443	0.01793424	0.02221813
cUHDRS	Left Pallidum	0.33171437	0.02273854	0.02783198
cUHDRS	Right Pallidum	0.31731714	0.02975402	0.03584539

Table 16 & Scatter-plot Figure 10: cUHDRS values statistically significant correlated with subcortical ROIs. (p<0.05 statistically significant).

NfL

Baseline plasma NfL samples were available for the HD participants (premanifest HD and manifest HD) of this study. Plasma NfL concentrations are presented by disease group in Table 1. Plasma NfL levels were significantly elevated in manifest HD, as well as in premanifest HD, in comparison to controls. Plasma NfL concentrations were 3 times higher in manifest HD group than in premanifest HD (mean 33.00 [11.83] log pg/mL vs 11.00 [10.26] log pg/mL. p<0.00) (Figure 27)

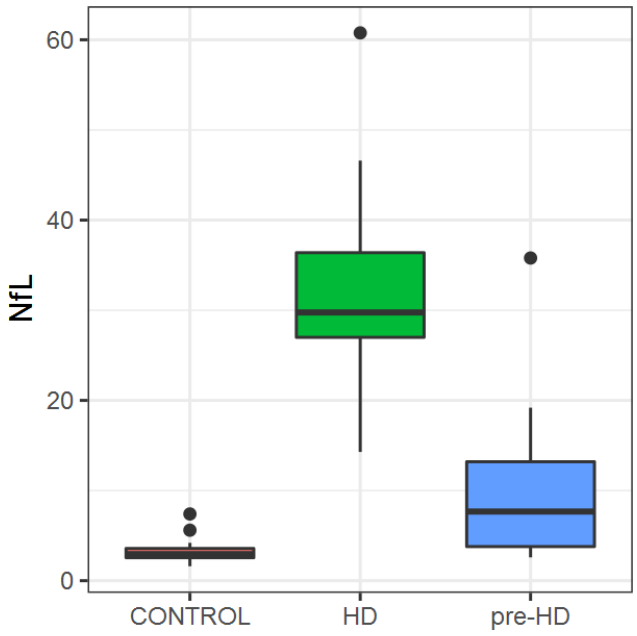

Figure 27: Box-plot showing differences of plasma NfL levels between groups (manifest HD, healthy controls and pre-manifest HD).

NfL values were also analysed separately. NfL values were categorized in two main groups HD (manifest HD and pre-manifest HD) and controls and correlated with the most significant

variables. Results were corrected for multiple comparisons as previously described. NfL values were significantly correlated with subcortical ROIs (pallidum, accumbens area, hippocampus, putamen, caudate, amygdala, thalamus and braistem. ($p<0.05$ statistically significant).

Variable 1	ROI	Effect size	p-value	Multiple comparison adjustment
NfL	Right Pallidum	-0.6710664	3.3293E-07	1.6886E-06
NfL	Right Accumbens area	-0.6363412	2.0026E-06	7.5345E-06
NfL	Left Pallidum	-0.6294949	2.7797E-06	9.5931E-06
NfL	Left Hippocampus	-0.6149268	5.4432E-06	1.6668E-05
NfL	Left Putamen	-0.6107445	6.5609E-06	1.8908E-05
NfL	Left Caudate	-0.6100043	6.7794E-06	1.9388E-05
NfL	Left Accumbens area	-0.5981804	1.1318E-05	3.0203E-05
NfL	Right Caudate	-0.5982237	1.1297E-05	3.0203E-05
NfL	Right Amygdala	-0.5949547	1.2971E-05	3.3636E-05
NfL	Right Putamen	-0.5897736	1.6096E-05	3.9828E-05
NfL	Left Thalamus Proper	-0.5849627	1.9604E-05	4.7609E-05
NfL	Left Amygdala	-0.5840375	2.0354E-05	4.917E-05
NfL	BrainStem	-0.4819589	0.00069511	0.00109079
NfL	Right Thalamus Proper	-0.4760994	0.00082453	0.00127214
NfL	Right Hippocampus	-0.4567939	0.00141727	0.00211498

Table 18 : NfL values statistically significant correlated with subcortical ROIs. ($p<0.05$ statistically significant).

Pilot study a-synuclein: Results

Table 19 summarizes the demographic, clinical, genetic and serum a-synuclein data of participants with corresponding p-values. HD and control groups were well matched for sex but not for age or medication. The types of symptomatic treatment received by HD patients included dopamine agonists, tetrabenazine and anti-depressants. Asymptomatic HD gene carriers were drug naive. There was no significant difference in serum a-synuclein levels between symptomatic HD patients and asymptomatic HD gene carriers (Table 19, $p = 0.826$, ANOVA) and the two were grouped together for further statistical analysis.

Table 19. Demographic, clinical, genetic and serum a-synuclein data in Huntington disease (HD) patients and controls

*Data are mean ± SD; NA: not applicable; chi-square test; *ANOVA; HD: Huntington's disease; UHDRS: Unified HD Rating Scale; DA: dopamine antagonists; SSRI:serotonin-specific reuptake inhibitors; SNRI: serotonin and noradrenaline reuptake inhibitors; TBZ: tetrabenazine; CAG1: CAG repeat number in allele 1 of HTT gene; CAG2:CAG repeat number in allele 2 of HTT gene; DBS: Disease Burden Score = age x (CAGn-35.5).*

Variable	**Huntington disease**			**Controls**	**p-value (All HD vs controls)**
	Symptomatic	**Premanifest**	**All HD**		
N	34	4	38	36	-
Sex (male/female)	14/20	1/3	15/23	15/21	0.848†
Age (years)	51.4 ± 12.7	39.3 ± 5.6	50.1 ± 12.6	41.6 ± 13.5	0.006*
Age at motor onset (years)	44.2 ± 11.6	NA	NA	NA	-
Disease duration (years)	6.6 ± 4.5	NA	NA	NA	-
On medication (%)	28 (82.4)	0 (0.0)	28 (73.7)	0 (0.0)	<0.001†
UHDRS motor score	44.7 ± 25.0	NA	NA	NA	
DBS	422.7 ± 111.2	268.6 ± 85.5	406.1 ± 118.7	NA	-
Serum α-synuclein (ng/ml)	2.47 ± 1.43	2.64 ± 2.00	2.49 ± 1.47	1.40 ± 1.16	0.001*

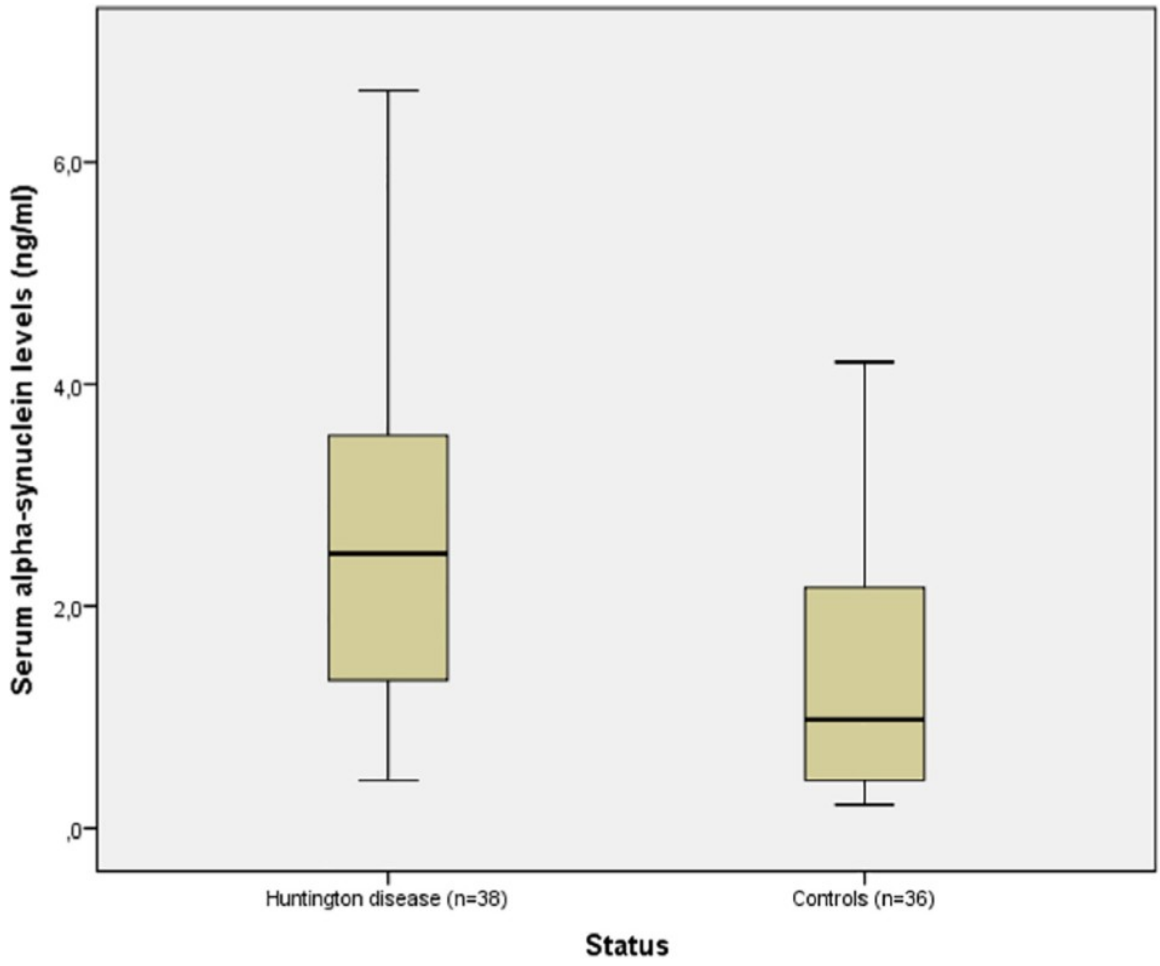

Fig. 28 Box plots of serum α-synuclein levels (ng/ml) in Huntington's disease patients (34 symptomatic and 4 premanifest) vs. controls; differences were significant with $p = 0.001$, ANOVA.

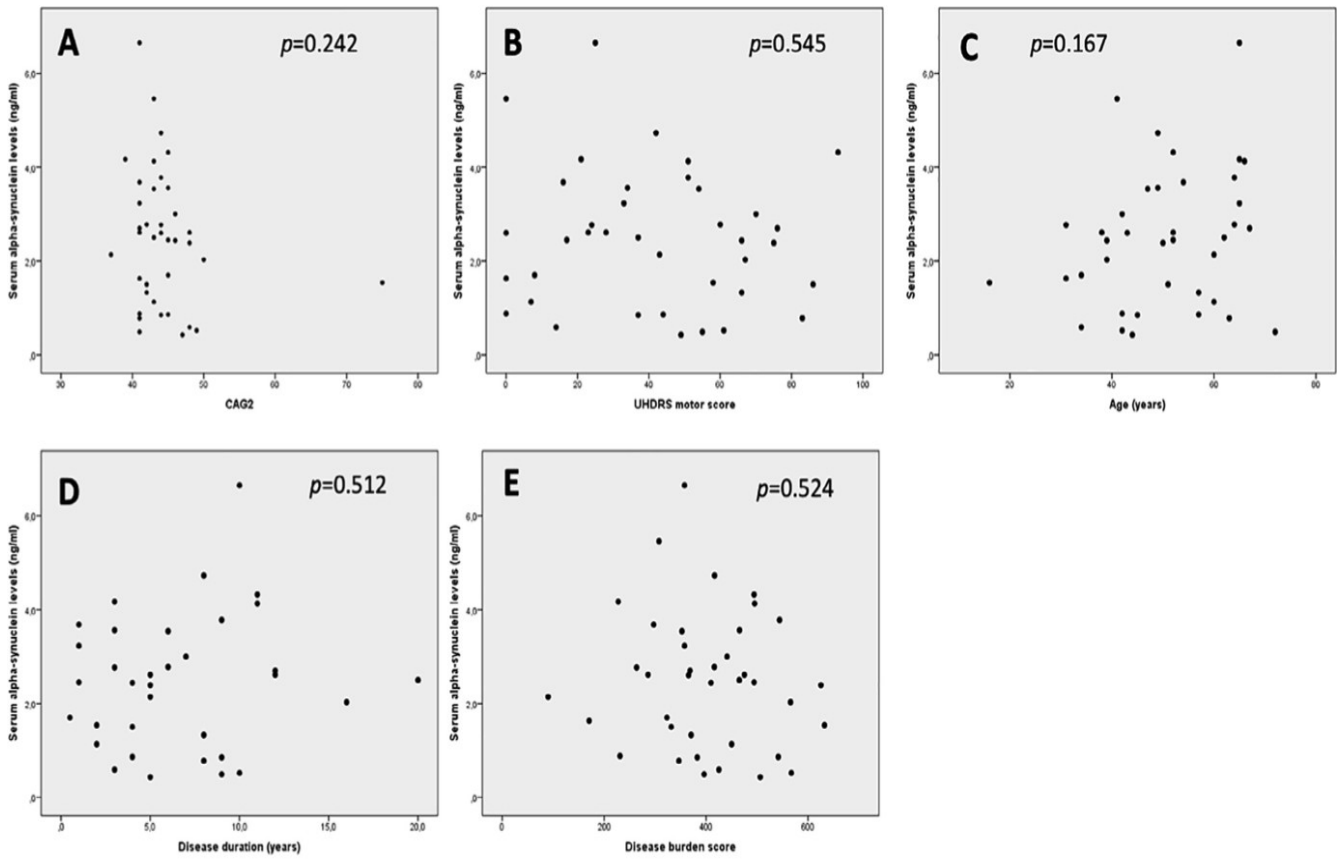

Fig. 29 Pearson correlations between serum α-synuclein levels (ng/ml) and **(A)** CAG2 score; **(B)** Unified Huntington disease rating scale motor score; **(C)** age; **(D)** disease duration (n = 34, premanifest cases excluded); and **(E)** disease burden score in Huntington's disease patients (34 symptomatic and 4 premanifest). No significant correlations were found.

Serum a-synuclein levels were significantly higher in HD patients vs. controls (2.49 ± 1.47 vs. 1.40 ± 1.16 ng/ml. p = 0.001; Table 1, Figure 28). In order to control for the age difference between HD patients and controls, we used ANCOVA with age as covariate which did not affect the significance of the result (p = 0.002). Serum a-synuclein levels did not differ significantly between male and female HD patients (2.58 ± 1.54 vs. 2.43 ± 1.45 ng/ml; p = 0.765. ANOVA), nor between HD patients receiving medication and HD patients that were treatment naïve (2.42 ± 1.46 vs. 2.68 ± 1.57 ng/ml; p = 0.629, ANOVA) nor between HD patients with psychotic features and HD patients with purely depressive and/or anxious features (2.21 ± 1.23 vs. 2.67 ± 1.54 ng/ml; p = 0.383. ANOVA). Within the HD group serum a-synuclein levels did not correlate significantly with CAG2. Unified HD Rating Scale (UHDRS) motor score, age, disease duration or disease burden score (Figure 29). There was also no correlation between serum a-synuclein levels and UHDRS motor subscores for parkinsonism (rigidity, bradykinesia, finger tapping and retropulsion).

Computational analysis of genetic HD modifiers & RNA-seq datasets

Differentially expressed genes detected (Appendix) were subsequently supplied to GeneTrail 3.0 for GSEA – gene set enrichment analysis. The results of these analyses revealed a statistically significant enrichment of immune system – associated pathways. corroborated by multiple databases (Appendix, Tables 1-3) as well as the depletion of pathways associated with neuronal survival, synaptogenesis and metal ion homeostasis.

Comparisons revealed significant overlap between mRNA surveillance, DNA repair, protein trafficking, regulation of exocytosis and natural immunity pathways (FDR<0.05, Appendix, Figure 3 and Supplementary Materials 3).

The *SNCA* gene was significantly enriched only in the peripheral blood dataset GSE1751 and involved in pathways associated with mitochondrial bioenergetics, transport and the regulation of exocytosis. (FDR<0.05, Supplementary Materials 4).

The *FAN1* gene was significantly enriched only in peripheral blood dataset GSE1751 and was associated with pathways involved in the pathway «cellular response to DNA damage stimulus» (FDR= 2.800e-2, Supplementary Materials 5).

4. Discussion

In this thesis, known and potential biomarkers were analyzed cross-sectionally in three groups: premanifest HD expansion carriers, manifest HD patients and healthy controls. Clinical, cognitive, neuroimaging and biofluid values were analyzed as markers. Each participant underwent clinical and neuropsychological assessments, blood sample collection and a specifically designed brain MRI protocol. In total, 25 controls were compared to 14 manifest HD patients and 11 premanifest HD expansion carriers. Using a tailored framework, neuroimaging potential markers for characterization of patients with manifest HD as well as premanifest HD were obtained and, interestingly, we showed for the first time that neuromelanin-MRI values were correlated in HD with finger-tapping, apathy scale, HD-QoL, BDI-II, MoCA, TMT-A, SDMT words, SDMT oral, and HTLV-R. We also confirmed NfL levels as a marker in HD, showing a 3-fold increase in manifest HD patients in comparison to controls.

All demographic, clinical, cognitive, neuroimaging and biofluid values, were analyzed in between-groups comparisons and correlations. We note that our analyses are based on small-sized cohorts of manifest HD patients and premanifest HD and multiple variables were studied simultaneously and, consequently, multiple corrections had to be applied. As expected no statistically significant differences were detected between controls and premanifest HD in UHDRS TMS total score and UHDRS subscores. This characterized our premanifest group as an “early” premanifest group far from disease onset, without motor or other evident symptoms. However, the observed differences in premanifest HD when compared with controls in cognitive and psychiatric scales reflect the well-established knowledge that psychiatric and cognitive impairment precedes motor disease onset by up to 10 years. In the premanifest HD group, all cognitive and psychiatric scales were significantly

different from controls (AES, PBS, MoCA, SNST, BDI, SDMT, WAIS), (Papoutsi et al. 2014, Tabrizi et al.2012, Paulsen et al.2008).

In the manifest HD group, all clinical and functional assessments (UHDRS TMS total score and UHDRS subscores, PPT, FAS, finger tapping test) were significantly different when compared with controls, as were cognitive measures such as TMT, SDMT, MOCA, WAIS and also psychiatric scales like AES. This is in line with the HD phenotypic spectrum, typically characterized by a triad of psychiatric, movement and cognitive impairment (Ross et al., 2014).

Symbol Digit Modalities Test (SDMT) and finger tapping were found to be impaired both in premanifest HD group and manifest HD group, as previously described in HD studies (Ross et al., 2014; Tabrizi et al., 2012). Of note, finger tapping test (right), as this was assessed by special designed software, was found affected even in our "early" premanifest HD patients. Finger tapping is a measurement commonly used in neurodegenerative disorders, such as HD. Recent technological advances in the software equipment allow it to be quickly and easily analyzed but further studies are needed. In comparison of healthy controls with premanifest patients, finger tapping was significantly different only for the right hand probably because right hand was the dominant hand in the majority of our participants, and subtle differences could be more easily detected. Finger tapping was found to correlate well with all subcortical ROIs volumes in HD ($p.<0.05$), (Bechtel et al. 2010).

We have also calculated cUHDRS scale, a novel scale recently introduced in HD clinical trials (Estevez-Fraga et al., 2021). The cUHDRS in this thesis was found to correlate well

with all subcortical ROIs volumes (p.<0.05) (table 17). A recent study has shown lower baseline scores correlating with decreased volume in the basal ganglia and surrounding WM, as well as with increased diffusivity at baseline and with longitudinal volume decreases in the occipito-parietal cortex and centrum semiovale (Estevez-Fraga et al., 2021). cUHDRS score was calculated in all manifest HD patients and premanifest HD expansion carriers of this study identifying differences in between groups comparisons. cUHDRS is a novel, multidomain measure encompassing motor, functional, and cognitive scales, all of which are independently associated with HD severity. The cUHDRS measures progression in HD, and combines TFC, TMS, SDMT and Stroop, providing more representative values (Estevez-Fraga et al., 2021).

Plasma NfL levels were also measured and analyzed in this study. Plasma NfL are known as one of the most robust biomarkers of Huntington's Disease (Zeun et al., 2019b). Plasma NfL levels were significantly elevated in manifest HD, as well as in premanifest HD, in comparison to controls. More specifically, plasma NfL concentrations were 3 times higher in manifest HD group than in premanifest HD (p<0.00). To minimize the number of statistical comparisons between variables, we assessed firstly the most robust markers that were chosen a priori from previous publications (volumetric imaging measures, SDMT, SWR, UHDRS TMS and TFC)(Tabrizi et al., 2012). After this analysis, plasma NFL values were compared between groups and associations between all variables were investigated with multiple comparisons correction. Only subcortical ROIs volumes correlated with NfL values and this could be attributed to the small sample size of the cohorts included in this study. NfL appears to be a robust biomarker of HD disease progression and neuronal damage and has been

shown to be higher in the plasma and CSF of HD patients in several different cohorts (Wild et al., 2015, Waldö et al., 2013).

Other known correlations in HD with variables measured in this thesis such as age of onset and CAG repeat number were not replicated. This is attributed to the small sample size of the cohorts included.

The cortical morphology of manifest HD patients was compared with premanifest HD expansion carriers and healthy controls using novel surface-based techniques. Quantitative measures of cortical morphometry, surface area and cortical thickness were assessed in this study. The main findings were a reduced cortical thickness in manifest HD group in both left and right hemisphere when compared to healthy controls group and premanifest-HD group. More specifically, for cortical thickness the following statistically significant clusters were identified in the manifest HD group, showing a diffuse brain atrophy*:* precuneus, lateral occipital gyrus, supramarginal gyrus, superior temporal sulcus, precentral gyrus, superior parietal gyrus, superior temporal gyrus, post central gyrus, entorhinal cortex and fusiform gyrus ($p < 0.05$)*.* Cortical thickness analysis of the premanifest HD group in comparison to manifest HD group revealed the following statistically significant clusters: post central gyrus, superior temporal gyrus, superior parietal gyrus and fusiform gyrus. No significant differences were identified when comparing pre-manifest HD group and healthy controls. Areas such as precuneus and occipital gyrus that were significantly different between manifest HD and pre-manifest HD but not in premanifest HD versus controls, are reported to be more susceptible to cortical thickness, as degeneration has been described initially occurring in the posterior-cortical region (Tan et al. 2021, Paulsen et al. 2014, Dominguez et al.2013).

A few studies have assessed cortical morphometry in HD, like cortical thickness, with controversial findings (Tan et al., 2021). Furthermore, in the early stages of manifest HD cortical thinning was noted mainly in the precuneus, primary motor and visual cortex. Taking into consideration that our manifest HD patients were mainly early HD, we also noted in this study thinning in these areas, but also widespread thinning of the cortex. However, the comparison between pre-manifest HD and manifest HD group showed a significant difference between the cortical thickness of temporo-parietal and not occipital regions, implicating that cortical thinning in the premotor, parieto-occipital, and entorhinal regions were already thinned in premanifest HD more than other areas, as this has been previously described in other HD studies (Tan et al., 2021). We didn't observe any differences between controls and pre-manifest HD, but our premanifest-HD group was an "early" pre-manifest HD that is a possible explanation for the differences with those included in previous studies. TRACK-HD showed that cortical thinning was evident in premanifest-HD closer to estimated clinical diagnosis, whereas identified thinning throughout the cortex was reported in manifest HD. After clinical conversion, it is well-established that atrophy becomes much more evident, and is widespread throughout the brain. Neuroimaging in these patients could provide more data for clinical trials. However, as disease progresses, imaging cannot be performed successfully due to motor artifacts and poor cooperation of the patients. Performing volumetric measures from MRI is dependent on good quality data without artifacts (Tan et al.2021).

In this direction, we applied a novel analysis technique that has been recently introduced in imaging studies but not until now in HD studies (Angelopoulou et al., 2020). 3D Flair MR images were used to correct pial surface, separately for each individual, so as to provide more

accurate results. Findings with 3D Flair correction revealed again significant clusters indicating reduced cortical thickness in both left and right hemisphere, compared to healthy controls group and significant reduced cortical thickness in specific clusters when compared to premanifest HD group. Interestingly, after corrections with 3D Flair, statistically significant differences were also identified in the premanifest HD group showing reduced cortical thickness compared to healthy controls in specific clusters like precuneus, superior parietal gyrus and middle temporal gyrus. Different contrast of T1 sequence and FLAIR images helps to better define pial and white matter and this correction has been recently introduced in the field and was used in analysis of other diseases (Angelopoulou et al., 2020). Interestingly, after applying this correction our statistically significant clusters for cortical thickness changed. This supports the fact that all neuroimaging analysis findings vary based on methodology and pipeline used, and could explain controversial findings in different HD studies (Popescu et al. 2016).

It is well-established that atrophy in the striatum (caudate and putamen) is the predominant neuropathological feature of HD. Striatal atrophy has been found to occur several years before the onset of motor symptoms. Herein, we also showed that volume values for subcortical areas including thalamus, caudate, putamen, pallidum, hippocampus and amygdala of both hemispheres along with brainstem were significantly lower in manifest HD group compared to healthy control group and premanifest HD group. However, premanifest HD group presented significantly reduced volume in only left and right caudate, left and right putamen, right pallidum, right nucleus accumbens and brainstem compared to controls. The fact that the amygdala and hippocampus are smaller structures and thus more difficult to reconstruct in

neuroimaging analysis, as well as the small cohort size, could be the reasons for these differences.

In this study, a neuromelanin sequence (NM-MRI) was analyzed. To the best of our knowledge, only one study exists in HD which includes NM-MRI sequence and our results are in line with these authors showing significant differences between HD patients and healthy controls in Locus Coeruleus (LC) and Substantia Nigra (SN) volume and area (Leitão et al., 2020). Of note, we showed here for the first time that NM-MRI correlated in HD with finger-tapping, apathy scale, HD-QoL, BDI-II, MoCA, TMT-A, SDMT words, SDMT oral, HTLV-R. Further studies are needed in larger HD cohorts to validate the use of NM-MRI as a potential biomarker but the results of the previous and this study are promising. NM-MRI correlates well in this study with selected motor, cognitive and neuropsychiatric measures and this could provide a robust marker in premanifest HD, in which psychiatric and cognitive decline can precede motor onset by up to 10 years (Estevez-Fraga et al., 2021).

In this thesis, we also found elevated serum a-synuclein in HD patients when compared to controls. To the best of our knowledge, this is the first study to investigate serum a-synuclein in HD. Our findings may be used to complement previous data regarding the role of a-synuclein in HD animal models and HD post mortem tissue (Charles et al., 2000, Corrochano et al., 2012, Toma´s-Zapico et al.,2012, St-Amour et al., 2018).

The use of serum or plasma a-synuclein as a more accessible biomarker in PD compared to CSF a-synuclein has been recently investigated in several studies, but remains controversial. A major factor in conflicting reports is thought to be the possibility of hemolysis during collection or processing, given that erythrocytes are a major source of a-synuclein,

accounting for more than 99% of its blood levels. Additionally, contamination by platelets in plasma, differences in detection methods and sensitivity or accuracy of antibodies may also influence the detected peripheral a-synuclein (Atik et al. 2016, Simonsen et al. 2016, Barbour et al. 2008).

Overall, it seems unlikely that peripheral a-synuclein can be considered a proximal marker of neurodegeneration. Nevertheless, the difference in serum a-synuclein between HD and controls needs to be explained. A possible explanation may relate to a membrane abnormality, originally observed several decades ago. It was speculated to affect peripheral tissues like erythrocytes, in patients with HD (Pettegrew et al., 1980). Recent studies have shown that mutant Htt may insert more than wild-type Htt into lipid bilayers resulting to increased cell membrane fluidity (Kegel et al., 2009, Sameni et al., 2018). Another explanation could be that lymphocyte or platelet membranes may make them more fragile during processing and result in a rise in extracellular a-synuclein. Futhermore, elevated levels of a-synuclein in HD may represent a non-specific stress response (Tagliafierro and Chiba-Falek, 2016). Further studies are needed in larger cohorts and novel more accurate techniques of a-synuclein measurements.

This study has some limitations that should be acknowledged. First, our analyses are based on small-number cohorts of manifest HD patients and premanifest HD, as it is a rare disease with pronounced motor and cognitive manifestations. This has limited our ability to screen many patients as we selected only “early” manifest HD patients and even these patients could not complete the full MRI and neuropsychological protocol of the study. Movement during scan acquisition compromises scan quality and a few participants were excluded after image quality screening. MRI scan quality is essential when measuring neuroimaging markers as

borders of structures like pial matter and subcortical areas need to be reconstructed so as to measure volume and area values. In addition, it is difficult to scan HD patients in the later disease stages as they are bedridden. Consequently, most MRI studies like ours are limited to individuals who are in early or mid-stage of disease progression. Furthermore, we have no longitudinal data at one-year follow-up yet to study how these markers vary with disease course and compare their potential to predict disease progression. Larger sample size and follow-up data could provide more evidence for clinical prognosis. Likewise, having additional time points would allow comparison of change rates of markers of clinical decline. Moreover, the range of HD participants in this study does not cover the extreme phenotypes (juvenile HD and late-onset HD) and the whole spectrum of HD, as later stages of disease were excluded. In addition, we should note that a lack of clear transition between premanifest and manifest states makes age at onset difficult to determine. For example, it was found that motor age of onset in TRACK-HD study was two years earlier than observed in EHDN Registry study. This difference could affect results of studies and of clinical trials where age of onset is crucial (Lahiri et al.,2013).

Whole-brain exploratory methods are widely used in HD brain MRI studies to measure cortical thickness and volume, and are considered as more accurate neuroimaging techniques to approach differences in patients, although ROIs analysis is the gold standard for analyzing subcortical structures. Although whole-brain analysis approach has been automated, many differences exist between studies in processing steps, software and statistical models, amongst many other factors. Changes in data processing of MRI for example could result in findings mimicking biological changes that are not real. Consequently, results should be interpreted with caution. ROI analyses reconstruct subcortical structures to provide

measurements of differing characteristics of a region. However, in order to obtain accurate data, the ROIs need to be precisely defined. Although the manual measurement of ROIs is a highly accurate method it is not possible to be applied when measuring multiple anatomically complex regions. Automated measures are used that are more convenient. However, they often bring an increased level of error. Finally, statistical analysis of all neuroimaging sequences involves a great number of statistical tests that run simultaneously for every voxel of image, and corrections for multiple comparisons are applied.

The involvement of DNA repair pathways in neurodegenerative diseases and in HD is well-established and presents numerous opportunities for therapeutic intervention. However, the exact mechanism that they contribute to the pathophysiology remains to be explored. *FAN1* variants are the strongest modifiers but how any of the *FAN1* variants modify disease is unknown. As previously stated, in this thesis we have performed an in silico analysis of DNA and RNA datasets. We also replicated here *FAN1* gene enrichment but only in the peripheral blood dataset.

We have shown elevated a-synuclein levels in peripheral blood of HD patients in this thesis. Of note, the *SNCA* gene was significantly enriched only in the peripheral blood and not in CNS. This is compatible with the elevated protein expression we have detected in HD serum, and suggests that the source of this increased a-synuclein is excessive mRNA production from peripheral sources, likely erythrocytes, where a-synuclein is most abundantly expressed (Breza et al., 2020).

Conclusions

This thesis has provided data for neuromelanin-MRI values, a novel MRI sequence and their potential use as a biomarker in HD. These results provide important validation of NM-MRI sequence and present new data that NM-MRI values could be used in parallel with motor, cognitive and psychiatric scales. Furthermore, this thesis has advanced the knowledge in HD cortical morphometry presenting more data in this research area of HD with contradictory findings. The patterns of atrophy clusters identified across the cortex reveal the complex nature of cortical change in HD. In addition, these results offer confirmation of NfL as a robust biomarker in HD.

Overall, it seems unlikely that peripheral a-synuclein can be considered a proximal marker of neurodegeneration. Nevertheless, the difference in serum a-synuclein between HD and controls needs to be explained. A possible explanation may relate to a membrane abnormality, originally observed several decades ago. As Htt associates with membranes and polyglutamine expansion, it is speculated that it may modify membrane function in Huntington disease through a mechanism that remains to be elucidated (Kegel et al., 2009). Further studies are needed in larger cohorts and novel more accurate techniques of a-synuclein measurements.

The findings have implications for the overall understanding of HD, but also could offer potential value in developing new more accurate and effective biomarkers that could be used effectively in clinical trials. Together with the increasing availability of high field MRI and the advent of more advanced automated neuroimaging techniques, such findings may provide more insights into the mechanisms of the disease. Further studies are needed in larger HD populations and with novel techniques to explore potential biomarkers.

Future directions

This study was designed as a longitudinal study. We aim to analyze longitudinal differences across groups and we will hopefully follow-up all HD patients included in this study and perform the same protocol as in baseline. We have already screened at follow-up (one-year) 5 manifest HD and 4 premanifest HD. However, due to COVID pandemic the follow-up of these patients included in this study hasn't been completed yet. Linear regression will be used to explore associations between variables and to predict accuracy of these markers.

In this thesis, we found elevated serum a-synuclein in HD patients compared to controls. To the best of our knowledge, this is the first study to investigate serum a-synuclein in HD. Our findings may be used to complement previous data regarding the role of a-synuclein in HD animal models and HD post mortem tissue (Charles et al., 2000; Corrochano et al., 2012; St-Amour et al., 2018).

REFERENCES

Adhikari, S., & Stark, D. E. (2017). Video-based eye tracking for neuropsychiatric assessment. *Annals of the New York Academy of Sciences*, *1387*(1), 145–152. https://doi.org/10.1111/nyas.13305

Ahmad, R., Bourgeois, S., Postnov, A., & Schmidt, M. E. (2014). *Clinical / Scientific Notes*. 279–282.

Angelopoulou, G., Meier, E. L., Kasselimis, D., Pan, Y., Tsolakopoulos, D., Velonakis, G., Karavasilis, E., Kelekis, N. L., Goutsos, D., Potagas, C., & Kiran, S. (2020). Investigating Gray and White Matter Structural Substrates of Sex Differences in the Narrative Abilities of Healthy Adults. *Frontiers in Neuroscience*, *13*(January), 1–15. https://doi.org/10.3389/fnins.2019.01424

Aylward, E. H., Nopoulos, P. C., Ross, C. A., Langbehn, D. R., Pierson, R. K., Mills, J. A., Johnson, H. J., Magnotta, V. A., Juhl, A. R., & Paulsen, J. S. (2011). Longitudinal change in regional brain volumes in prodromal Huntington disease. *Journal of Neurology, Neurosurgery and Psychiatry*, *82*(4), 405–410. https://doi.org/10.1136/jnnp.2010.208264

Aylward, E. H., Schwartz, J., Machlin, S., & Pearl, G. (1991). Bicaudate Ratio as a Measure of Caudate Volume on MR Images AJNR 1991; 12:1217-1222. *American Journal of Neuroradiology*, *12*, 18–22.

Barro, C., Benkert, P., Disanto, G., Tsagkas, C., Amann, M., Naegelin, Y., Leppert, D., Gobbi, C., Granziera, C., Yaldizli, Ö., Michalak, Z., Wuerfel, J., Kappos, L., Parmar, K., & Kuhle, J. (2018). Serum neurofilament as a predictor of disease worsening and brain

and spinal cord atrophy in multiple sclerosis. *Brain*, *141*(8), 2382–2391. https://doi.org/10.1093/brain/awy154

Bashir, H., & Jankovic, J. (2018). Treatment options for chorea. *Expert Review of Neurotherapeutics*, *18*(1), 51–63. https://doi.org/10.1080/14737175.2018.1403899

Bates, G. P., Dorsey, R., Gusella, J. F., Hayden, M. R., Kay, C., Leavitt, B. R., Nance, M., Ross, C. A., Scahill, R. I., Wetzel, R., Wild, E. J., & Tabrizi, S. J. (2015). Huntington disease. *Nature Reviews Disease Primers*, *April*, 15005. https://doi.org/10.1038/nrdp.2015.5

Bettencourt, C., Moss, D. H., Flower, M., Wiethoff, S., Brice, A., Goizet, C., Stevanin, G., Koutsis, G., Karadima, G., Panas, M., Yescas-Gómez, P., García-Velázquez, L. E., Alonso-Vilatela, M. E., Lima, M., Raposo, M., Traynor, B., Sweeney, M., Wood, N., Giunti, P., … Jones, L. (2016). DNA repair pathways underlie a common genetic mechanism modulating onset in polyglutamine diseases. *Annals of Neurology*, 983–990. https://doi.org/10.1002/ana.24656

Björkqvist, M., Wild, E. J., Thiele, J., Silvestroni, A., Andre, R., Lahiri, N., Raibon, E., Lee, R. V., Benn, C. L., Soulet, D., Magnusson, A., Woodman, B., Landles, C., Pouladi, M. A., Hayden, M. R., Khalili-Shirazi, A., Lowdell, M. W., Brundin, P., Bates, G. P., … Tabrizi, S. J. (2008). A novel pathogenic pathway of immune activation detectable before clinical onset in Huntington's disease. *Journal of Experimental Medicine*, *205*(8), 1869–1877. https://doi.org/10.1084/jem.20080178

Bougea, A., Stefanis, L., Paraskevas, G. P., Emmanouilidou, E., Vekrelis, K., & Kapaki, E. (2019). Plasma alpha-synuclein levels in patients with Parkinson's disease: a systematic review and meta-analysis. *Neurological Sciences*, *40*(5), 929–938.

https://doi.org/10.1007/s10072-019-03738-1

Bowie, C. R., & Harvey, P. D. (2006). Administration and interpretation of the Trail Making Test. *Nature Protocols*, *1*(5), 2277–2281. https://doi.org/10.1038/nprot.2006.390

Breza, M., Emmanouilidou, E., Leandrou, E., Kartanou, C., Bougea, A., Panas, M., Stefanis, L., Karadima, G., Vekrellis, K., & Koutsis, G. (2020). Elevated Serum α-Synuclein Levels in Huntington's Disease Patients. *Neuroscience*, *431*(February), 34–39. https://doi.org/10.1016/j.neuroscience.2020.01.037

Burgess, S., Davey Smith, G., Davies, N. M., Dudbridge, F., Gill, D., Glymour, M. M., Hartwig, F. P., Holmes, M. V., Minelli, C., Relton, C. L., & Theodoratou, E. (2020). Guidelines for performing Mendelian randomization investigations. *Wellcome Open Research*, *4*. https://doi.org/10.12688/wellcomeopenres.15555.2

Byrne, L. M., & Wild, E. J. (2016). Cerebrospinal Fluid Biomarkers for Huntington's Disease. *Journal of Huntington's Disease*, *5*(1), 1–13. https://doi.org/10.3233/JHD-160196

Chaganti, S. S., McCusker, E. A., & Loy, C. T. (2017). What do we know about late onset Huntington's disease? *Journal of Huntington's Disease*, *6*(2), 95–103. https://doi.org/10.3233/JHD-170247

Charles, V., Mezey, E., Reddy, P. H., Dehejia, A., Young, T. A., Polymeropoulos, M. H., Brownstein, M. J., & Tagle, D. A. (2000). Alpha-synuclein immunoreactivity of huntingtin polyglutamine aggregates in striatum and cortex of Huntington's disease patients and transgenic mouse models. *Neuroscience Letters*, *289*(1), 29–32. https://doi.org/10.1016/S0304-3940(00)01247-7

Chen, L., Hua, J., Ross, C. A., Cai, S., van Zijl, P. C. M., & Li, X. (2019). Altered brain iron

content and deposition rate in Huntington's disease as indicated by quantitative susceptibility MRI. *Journal of Neuroscience Research*, *97*(4), 467–479. https://doi.org/10.1002/jnr.24358

Ciammola, A., Sassone, J., Cannella, M., Calza, S., Poletti, B., Frati, L., Squitieri, F., & Silani, V. (2007). Low brain-derived neurotrophic factor (BDNF) levels in serum of Huntington's disease patients. *American Journal of Medical Genetics, Part B: Neuropsychiatric Genetics*, *144*(4), 574–577. https://doi.org/10.1002/ajmg.b.30501

Constantinescu, R., Romer, M., Oakes, D., Rosengren, L., & Kieburtz, K. (2009). Levels of the light subunit of neurofilament triplet protein in cerebrospinal fluid in Huntington's disease. *Parkinsonism and Related Disorders*, *15*(3), 245–248. https://doi.org/10.1016/j.parkreldis.2008.05.012

Corrochano, S., Renna, M., Carter, S., Chrobot, N., Kent, R., Stewart, M., Cooper, J., Brown, S. D. M., Rubinsztein, D. C., & Acevedo-Arozena, A. (2012). α-Synuclein levels modulate Huntington's disease in mice. *Human Molecular Genetics*, *21*(3), 485–494. https://doi.org/10.1093/hmg/ddr477

Currie, S., Hoggard, N., Craven, I. J., Hadjivassiliou, M., & Wilkinson, I. D. (2013). Understanding MRI: Basic MR physics for physicians. *Postgraduate Medical Journal*, *89*(1050), 209–223. https://doi.org/10.1136/postgradmedj-2012-131342

Dalla Bella, S., Farrugia, N., Benoit, C. E., Begel, V., Verga, L., Harding, E., & Kotz, S. A. (2017). BAASTA: Battery for the Assessment of Auditory Sensorimotor and Timing Abilities. *Behavior Research Methods*, *49*(3), 1128–1145. https://doi.org/10.3758/s13428-016-0773-6

Davies, S. W., Turmaine, M., Cozens, B. A., DiFiglia, M., Sharp, A. H., Ross, C. A.,

Scherzinger, E., Wanker, E. E., Mangiarini, L., & Bates, G. P. (1997). Formation of neuronal intranuclear inclusions underlies the neurological dysfunction in mice transgenic for the HD mutation. *Cell*, *90*(3), 537–548. https://doi.org/10.1016/S0092-8674(00)80513-9

Deng, Y. P., Albin, R. L., Penney, J. B., Young, A. B., Anderson, K. D., & Reiner, A. (2004). Differential loss of striatal projection systems in Huntington's disease: A quantitative immunohistochemical study. *Journal of Chemical Neuroanatomy*, *27*(3), 143–164. https://doi.org/10.1016/j.jchemneu.2004.02.005

DiFiglia, M., Sapp, E., Chase, K. O., Davies, S. W., Bates, G. P., Vonsattel, J. P., & Aronin, N. (1997). Aggregation of huntingtin in neuronal intranuclear inclusions and dystrophic neurites in brain. *Science*, *277*(5334), 1990–1993. https://doi.org/10.1126/science.277.5334.1990

Duff, K. (2016). Demographically corrected normative data for the Hopkins Verbal Learning Test-Revised and Brief Visuospatial Memory Test-Revised in an elderly sample. *Applied Neuropsychology:Adult*, *23*(3), 179–185. https://doi.org/10.1080/23279095.2015.1030019

Emmanouilidou, E., Elenis, D., Papasilekas, T., Stranjalis, G., Gerozissis, K., Ioannou, P. C., & Vekrellis, K. (2011). Assessment of α-synuclein secretion in mouse and human brain parenchyma. *PLoS ONE*, *6*(7), 1–9. https://doi.org/10.1371/journal.pone.0022225

Estevez-Fraga, C., Scahill, R. I., Durr, A., Leavitt, B. R., Roos, R. A. C., Langbehn, D. R., Rees, G., Gregory, S., & Tabrizi, S. J. (2021). Composite UHDRS Correlates With Progression of Imaging Biomarkers in Huntington's Disease. *Movement Disorders*, 1–7. https://doi.org/10.1002/mds.28489

Fischl, B., & Dale, A. M. (2000). Measuring the thickness of the human cerebral cortex from magnetic resonance images. *Proceedings of the National Academy of Sciences of the United States of America*, *97*(20), 11050–11055. https://doi.org/10.1073/pnas.200033797

Fountoulakis, K. N., Tsolaki, M., Chantzi, H., & Kazis, A. (2000). Mini Mental State Examination (MMSE): A validation study in Greece. *American Journal of Alzheimer's Disease and Other Dementias*, *15*(6), 342–345. https://doi.org/10.1177/153331750001500604

Fusilli, C., Migliore, S., Mazza, T., Consoli, F., De Luca, A., Barbagallo, G., Ciammola, A., Gatto, E. M., Cesarini, M., Etcheverry, J. L., Parisi, V., Al-Oraimi, M., Al-Harrasi, S., Al-Salmi, Q., Marano, M., Vonsattel, J. P. G., Sabatini, U., Landwehrmeyer, G. B., & Squitieri, F. (2018). Biological and clinical manifestations of juvenile Huntington's disease: a retrospective analysis. *The Lancet Neurology*, *17*(11), 986–993. https://doi.org/10.1016/S1474-4422(18)30294-1

G. M. Halliday, D. A. McRitchie, V. Macdonald, K. L. Double, R. J. Trent, and E. M. (1998). *Regional Specificity of Brain Atrophy in Huntington's Disease*. *672*(154), 986919.

Garret, M., Du, Z., Chazalon, M., Cho, Y. H., & Baufreton, J. (2018). Alteration of GABAergic neurotransmission in Huntington's disease. *CNS Neuroscience and Therapeutics*, *24*(4), 292–300. https://doi.org/10.1111/cns.12826

Genetic Modifiers of Huntington's Disease (GeM-HD) Consortium*. (2015). Identification of Genetic Factors that Modify Clinical Onset of Huntington's Disease. *Cell*, *162*(3), 516–526. https://doi.org/10.1016/j.cell.2015.07.003

Georgiou-Karistianis, N., Gray, M. A., Domínguez D, J. F., Dymowski, A. R., Bohanna, I., Johnston, L. A., Churchyard, A., Chua, P., Stout, J. C., & Egan, G. F. (2013). Automated differentiation of pre-diagnosis Huntington's disease from healthy control individuals based on quadratic discriminant analysis of the basal ganglia: The IMAGE-HD study. *Neurobiology of Disease*, *51*, 82–92. https://doi.org/10.1016/j.nbd.2012.10.001

Guo, Z., Rudow, G., Pletnikova, O., Codispoti, K. E., Orr, B. A., Crain, B. J., Duan, W., Margolis, R. L., Rosenblatt, A., Ross, C. A., & Troncoso, J. C. (2012). Striatal neuronal loss correlates with clinical motor impairment in Huntington's disease. *Movement Disorders*, *27*(11), 1379–1386. https://doi.org/10.1002/mds.25159

Gusella, J. F., & MacDonald, M. E. (2009). Huntington's disease: the case for genetic modifiers. *Genome Medicine*, *1*(8), 80. https://doi.org/10.1186/gm80

Harrington, D. L., Smith, M., Zhang, Y., Carlozzi, N., Paulsen, J., Wassink, T., Cross, S., Kimble, M., Ryan, P., Wood, J., Epping, E. A., Beglinger, L. J., Chiu, E., Yastrubetskaya, O., Preston, J., Goh, A., Fonseka, C., Antonopoulos, S., Loi, S., … Danzer, P. (2012). Cognitive domains that predict time to diagnosis in prodromal Huntington disease. *Journal of Neurology, Neurosurgery and Psychiatry*, *83*(6), 612–619. https://doi.org/10.1136/jnnp-2011-301732

Harris, G. J., Aylward, E. H., Peyser, C. E., Pearlson, G. D., Brandt, J., Roberts-twillie, J. V, Barta, P. E., & Folstein, S. E. (2015). *Huntington ' s*. *Im*.

Hart, E. P., Dumas, E. M., Giltay, E. J., Middelkoop, H. A. M., & Roos, R. A. C. (2013). Cognition in Huntington's Disease in Manifest, Premanifest and Converting Gene Carriers over Ten Years. *Journal of Huntington's Disease*, *2*(2), 137–147.

https://doi.org/10.3233/JHD-130059

Hendricks, A. E., Latourelle, J. C., Lunetta, K. L., Cupples, L. A., Wheeler, V., MacDonald, M. E., Gusella, J. F., & Myers, R. H. (2009). Estimating the probability of de novo HD cases from transmissions of expanded penetrant CAG alleles in the Huntington disease gene from male carriers of high normal alleles (27-35 CAG). *American Journal of Medical Genetics, Part A*, *149*(7), 1375–1381. https://doi.org/10.1002/ajmg.a.32901

Hensman Moss, D. J., Flower, M. D., Lo, K. K., Miller, J. R. C., Van Ommen, G. J. B., Hoen, P. A. C. T., Stone, T. C., Guinee, A., Langbehn, D. R., Jones, L., Plagnol, V., Van Roon-Mom, W. M. C., Holmans, P., & Tabrizi, S. J. (2017). Huntington's disease blood and brain show a common gene expression pattern and share an immune signature with Alzheimer's disease. *Scientific Reports*, *7*(September 2016), 1–12. https://doi.org/10.1038/srep44849

Ho, V. B., Chuang, H. S., Rovira, M. J., & Koo, B. (1995). Juvenile Huntington disease: CT and MR features. *American Journal of Neuroradiology*, *16*(7), 1405–1412.

Hobbs, N. Z., Cole, J. H., Farmer, R. E., Rees, E. M., Crawford, H. E., Malone, I. B., Roos, R. A. C., Sprengelmeyer, R., Durr, A., Landwehrmeyer, B., Scahill, R. I., Tabrizi, S. J., & Frost, C. (2013). Evaluation of multi-modal, multi-site neuroimaging measures in Huntington's disease: Baseline results from the PADDINGTON study. *NeuroImage: Clinical*, *2*(1), 204–211. https://doi.org/10.1016/j.nicl.2012.12.001

Hoogeveen, A. T., Willemsen, R., Meyer, N., Roolj, K. E. d., Roos, R. A. C., Ommen, G. J. B. va., & Galjaard, H. (1993). Characterization and localization of the huntington disease gene product. *Human Molecular Genetics*, *2*(12), 2069–2073. https://doi.org/10.1093/hmg/2.12.2069

Huntington Study Group. (1996). Unified Huntington's Disease Rating Scale: Reliability - and-Consis tenc. *Movement Disorders*, *11*(2), 136–142. https://doi.org/10.1002/mds.870110204

J.C. Hedreen, S. . F. (1995). Early loss of neostriatal striosome neurons in Huntington's Disease. *Journal of Neuropathology and Experimental Neurology*, 105–120.

Jahanshahi, M., Obeso, I., Rothwell, J. C., & Obeso, J. A. (2015). A fronto-striato-subthalamic-pallidal network for goal-directed and habitual inhibition. *Nature Reviews Neuroscience*, *16*(12), 719–732. https://doi.org/10.1038/nrn4038

Johnson, E. B., & Gregory, S. (2019). Huntington's disease: Brain imaging in Huntington's disease. In *Progress in Molecular Biology and Translational Science* (1st ed., Vol. 165). Elsevier Inc. https://doi.org/10.1016/bs.pmbts.2019.04.004

Kegel, K. B., Schewkunow, V., Sapp, E., Masso, N., Wanker, E. E., DiFiglia, M., & Goldmann, W. H. (2009). Polyglutamine expansion in huntingtin increases its insertion into lipid bilayers. *Biochemical and Biophysical Research Communications*, *387*(3), 472–475. https://doi.org/10.1016/j.bbrc.2009.07.039

Khalil, M., Teunissen, C. E., Otto, M., Piehl, F., Sormani, M. P., Gattringer, T., Barro, C., Kappos, L., Comabella, M., Fazekas, F., Petzold, A., Blennow, K., Zetterberg, H., & Kuhle, J. (2018). Neurofilaments as biomarkers in neurological disorders. *Nature Reviews Neurology*, *14*(10), 577–589. https://doi.org/10.1038/s41582-018-0058-z

Klingelhoefer, L., & Reichmann, H. (2015). Pathogenesis of Parkinson disease - The gut-brain axis and environmental factors. *Nature Reviews Neurology*, *11*(11), 625–636. https://doi.org/10.1038/nrneurol.2015.197

Koutsis, G., Karadima, G., Kladi, A., & Panas, M. (2014). Late-onset Huntington's disease:

diagnostic and prognostic considerations. *Parkinsonism & Related Disorders*, *20*(7), 726–730. https://doi.org/10.1016/j.parkreldis.2014.03.017

Kuhle J, Barro C, Andreasson U, Derfuss T, Lindberg R, Sandelius Å, Liman V, Norgren N, Blennow K, Zetterberg H. (2016) Comparison of three analytical platforms for quantification of the neurofilament light chain in blood samples: ELISA, electrochemiluminescence immunoassay and Simoa. Clin Chem Lab Med. 2016 Oct 1;54(10):1655-61. doi: 10.1515/cclm-2015-1195.

Labadorf, A., Hoss, A. G., Lagomarsino, V., Latourelle, J. C., Hadzi, T. C., Bregu, J., MacDonald, M. E., Gusella, J. F., Chen, J. F., Akbarian, S., Weng, Z., & Myers, R. H. (2015). RNA sequence analysis of human huntington disease brain reveals an extensive increase in inflammatory and developmental gene expression. *PLoS ONE*, *10*(12), 1–21. https://doi.org/10.1371/journal.pone.0143563

Langbehn, D. R., Brinkman, R. R., Falush, D., Paulsen, J. S., & Hayden, M. R. (2004). A new model for prediction of the age of onset and penetrance for Huntington's disease based on CAG length. *Clinical Genetics*, *65*(4), 267–277. https://doi.org/10.1111/j.1399-0004.2004.00241.x

Larsen, I. U., Vinther-Jensen, T., Gade, A., Nielsen, J. E., & Vogel, A. (2015). Assessing impairment of executive function and psychomotor speed in premanifest and manifest huntington's disease gene-expansion carriers. *Journal of the International Neuropsychological Society*, *21*(3), 193–202. https://doi.org/10.1017/S1355617715000090

Lee, J. M., Ramos, E. M., Lee, J. H., Gillis, T., Mysore, J. S., Hayden, M. R., Warby, S. C., Morrison, P., Nance, M., Ross, C. A., Margolis, R. L., Squitieri, F., Orobello, S., Di

Donato, S., Gomez-Tortosa, E., Ayuso, C., Suchowersky, O., Trent, R. J. A., McCusker, E., … Gusella, J. F. (2012). CAG repeat expansion in Huntington disease determines age at onset in a fully dominant fashion. *Neurology*, *78*(10), 690–695. https://doi.org/10.1212/WNL.0b013e318249f683

Leitão, R., Guerreiro, C., Nunes, R. G., Gonçalves, N., Galati, G., Rosário, M., Guedes, L. C.,

Ferreira, J. J., & Reimão, S. (2020). Neuromelanin Magnetic Resonance Imaging of the Substantia Nigra in Huntington's Disease. *Journal of Huntington's Disease*, *9*(2), 143–148. https://doi.org/10.3233/JHD-190388

Lin, C.-H., Yang, S.-Y., Horng, H.-E., Yang, C.-C., Chieh, J.-J., Chen, H.-H., Liu, B.-H., & Chiu, M.-J. (2017). Plasma α-synuclein predicts cognitive decline in Parkinson's disease. *Journal of Neurology, Neurosurgery & Psychiatry*, jnnp-2016-314857. https://doi.org/10.1136/jnnp-2016-314857

Lovestone, S., Hodgson, S., Sham, P., Differ, A. M., & Levy, R. (1996). Familial psychiatric presentation of Huntington's disease. *Journal of Medical Genetics*, *33*(2), 128–131. https://doi.org/10.1136/jmg.33.2.128

Macerollo, A., Perry, R., Stamelou, M., Batla, A., Mazumder, A. A., Adams, M. E., & Bhatia, K. P. (2014). Susceptibility-weighted imaging changes suggesting brain iron accumulation in Huntington's disease: An epiphenomenon which causes diagnostic difficulty. *European Journal of Neurology*, *21*(2), 16–17. https://doi.org/10.1111/ene.12298

Marin, R. S., Biedrzycki, R. C., & Firinciogullari, S. (1991). Reliability and validity of the apathy evaluation scale. *Psychiatry Research*, *38*(2), 143–162. https://doi.org/10.1016/0165-1781(91)90040-V

Martin, D. D. O., Ladha, S., Ehrnhoefer, D. E., & Hayden, M. R. (2015). Autophagy in Huntington disease and huntingtin in autophagy. *Trends in Neurosciences*, *38*(1), 26–35. https://doi.org/10.1016/j.tins.2014.09.003

Masnata, M., & Cicchetti, F. (2017). The evidence for the spread and seeding capacities of the mutant huntingtin protein in in vitro systems and their therapeutic implications.

Frontiers in Neuroscience, *11*(NOV), 1–12. https://doi.org/10.3389/fnins.2017.00647

McColgan, P., Gregory, S., Seunarine, K. K., Razi, A., Papoutsi, M., Johnson, E., Durr, A., Roos, R. A. C., Leavitt, B. R., Holmans, P., Scahill, R. I., Clark, C. A., Rees, G., Tabrizi, S. J., Coleman, A., Decolongon, J., Fan, M., Petkau, T., Jauffret, C., … Crawfurd, D. (2018). Brain Regions Showing White Matter Loss in Huntington's Disease Are Enriched for Synaptic and Metabolic Genes. *Biological Psychiatry*, *83*(5), 456–465. https://doi.org/10.1016/j.biopsych.2017.10.019

McDonnell, E. I., Wang, Y., Goldman, J., & Marder, K. (2021). Age of Onset of Huntington's Disease in Carriers of Reduced Penetrance Alleles. *Movement Disorders*, 1–5. https://doi.org/10.1002/mds.28789

McNally, G., Rickards, H., Horton, M., & Craufurd, D. (2015). Exploring the validity of the short version of the Problem Behaviours Assessment (PBA-s) for Huntington's disease: A Rasch analysis. *Journal of Huntington's Disease*, *4*(4), 347–369. https://doi.org/10.3233/JHD-150164

Mestre, T. A., Forjaz, M. J., Mahlknecht, P., Cardoso, F., Ferreira, J. J., Reilmann, R., Sampaio, C., Goetz, C. G., Cubo, E., Martinez-Martin, P., & Stebbins, G. T. (2018). Rating Scales for Motor Symptoms and Signs in Huntington's Disease: Critique and Recommendations. *Movement Disorders Clinical Practice*, *5*(2), 111–117. https://doi.org/10.1002/mdc3.12571

Miller, E., Morel, A., Saso, L., & Saluk, J. (2014). Isoprostanes and neuroprostanes as biomarkers of oxidative stress in neurodegenerative diseases. *Oxidative Medicine and Cellular Longevity*, *2014*. https://doi.org/10.1155/2014/572491

Monckton, D. G. (2021). The Contribution of Somatic Expansion of the CAG Repeat to

Symptomatic Development in Huntington's Disease: A Historical Perspective. *Journal of Huntington's Disease*, *10*(1), 7–33. https://doi.org/10.3233/JHD-200429

Niccolini, F., Haider, S., Reis Marques, T., Muhlert, N., Tziortzi, A. C., Searle, G. E., Natesan, S., Piccini, P., Kapur, S., Rabiner, E. A., Gunn, R. N., Tabrizi, S. J., & Politis, M. (2015). Altered PDE10A expression detectable early before symptomatic onset in Huntington's disease. *Brain*, *138*(10), 3016–3029. https://doi.org/10.1093/brain/awv214

Niemelä, V., Landtblom, A. M., Blennow, K., & Sundblom, J. (2017). Tau or neurofilament light-Which is the more suitable biomarker for Huntington's disease? *PLoS ONE*, *12*(2), 1–11. https://doi.org/10.1371/journal.pone.0172762

Osório, F. L., Loureiro, S. R., Hallak, J. E. C., Machado-de-Sousa, J. P., Ushirohira, J. M., Baes, C. V. W., Apolinario, T. D., Donadon, M. F., Bolsoni, L. M., Guimarães, T., Fracon, V. S., Silva-Rodrigues, A. P. C., Pizeta, F. A., Souza, R. M., Sanches, R. F., dos Santos, R. G., Martin-Santos, R., & Crippa, J. A. S. (2019). Clinical validity and intrarater and test–retest reliability of the Structured Clinical Interview for DSM-5 – Clinician Version (SCID-5-CV). *Psychiatry and Clinical Neurosciences*, *73*(12), 754–760. https://doi.org/10.1111/pcn.12931

Pan, L., & Feigin, A. (2021). Huntington's Disease: New Frontiers in Therapeutics. *Current Neurology and Neuroscience Reports*, *21*(3). https://doi.org/10.1007/s11910-021-01093-3

Panas, M., Karadima, G., Vassos, E., Kalfakis, N., Kladi, a., Christodoulou, K., & Vassilopoulos, D. (2011). Huntington's disease in Greece: The experience of 14 years. *Clinical Genetics*, *80*(6), 586–590. https://doi.org/10.1111/j.1399-0004.2010.01603.x

Papoutsi, M., Labuschagne, I., Tabrizi, S. J., & Stout, J. C. (2014). The cognitive burden in

Huntington's disease: Pathology, phenotype, and mechanisms of compensation. *Movement Disorders*, *29*(5), 673–683. https://doi.org/10.1002/mds.25864

Paulsen, J. S., Long, J. D., Ross, C. a, Harrington, D. L., Erwin, C. J., Williams, J. K., Westervelt, H. J., Johnson, H. J., Aylward, E. H., Zhang, Y., Bockholt, H. J., & Barker, R. a. (2014). Prediction of manifest Huntington's disease with clinical and imaging measures: a prospective observational study. *The Lancet Neurology*, *13*(12), 1193–1201. https://doi.org/10.1016/S1474-4422(14)70238-8

Paulsen, J. S., Smith, M. M., Long, J. D., & Predict HD investigators and coordinators of the Huntington Study Group. (2013). Cognitive decline in prodromal Huntington Disease: Implications for Clinical Trials. *J Neurol Neurosurg Psychiatry*, *84*(11), 1233–1239. https://doi.org/10.1136/jnnp-2013-305114

Pecho-Vrieseling, E., Rieker, C., Fuchs, S., Bleckmann, D., Esposito, M. S., Botta, P., Goldstein, C., Bernhard, M., Galimberti, I., Müller, M., Lüthi, A., Arber, S., Bouwmeester, T., Van Der Putten, H., & Di Giorgio, F. P. (2014). Transneuronal propagation of mutant huntingtin contributes to non-cell autonomous pathology in neurons. *Nature Neuroscience*, *17*(8), 1064–1072. https://doi.org/10.1038/nn.3761

Penney, J. B., Vonsattel, J. P., MacDonald, M. E., Gusella, J. F., & Myers, R. H. (1997). CAG repeat number governs the development rate of pathology in huntington's disease. *Annals of Neurology*, *41*(5), 689–692. https://doi.org/10.1002/ana.410410521

Pennuto, M., Palazzolo, I., & Poletti, A. (2009). Post-translational modifications of expanded polyglutamine proteins: Impact on neurotoxicity. *Human Molecular Genetics*, *18*(R1), 40–47. https://doi.org/10.1093/hmg/ddn412

Pringsheim, T., Wiltshire, K., Day, L., Dykeman, J., Steeves, T., & Jette, N. (2012). The

incidence and prevalence of Huntington's disease: A systematic review and meta-analysis. *Movement Disorders*, *27*(9), 1083–1091. https://doi.org/10.1002/mds.25075

Raquel Duran, PhD, 1 Francisco J. Barrero, MD, 2 Blas Morales, MD, 2 Juan D. Luna, PhD, 3, & Manuel Ramirez, MD, 4 and Francisco Vives, PhD, M. (2010). Plasma a-Synuclein in Patients with Parkinson's Disease With and Without Treatment. *Movement Disorders*, *25*(4), 481–485. https://doi.org/10.1002/mds.22920

Reedeker, N., Bouwens, J. A., van Duijn, E., Giltay, E. J., Roos, R. A. C., & van der Mast, R. C. (2011). Incidence, course, and predictors of apathy in Huntington's disease: A two-year prospective study. *Journal of Neuropsychiatry and Clinical Neurosciences*, *23*(4), 434–441. https://doi.org/10.1176/jnp.23.4.jnp434

Roos, R. A. C. (2010). Huntington's disease: A clinical review. *Orphanet Journal of Rare Diseases*, *5*(1), 40. https://doi.org/10.1186/1750-1172-5-40

Ross, C. a, Aylward, E. H., Wild, E. J., Langbehn, D. R., Long, J. D., Warner, J. H., Scahill, R. I., Leavitt, B. R., Stout, J. C., Paulsen, J. S., Reilmann, R., Unschuld, P. G., Wexler, A., Margolis, R. L., & Tabrizi, S. J. (2014). Huntington disease: natural history, biomarkers and prospects for therapeutics. *Nature Reviews. Neurology*, *10*(4), 204–216. https://doi.org/10.1038/nrneurol.2014.24

Ruchinskas, R. (2019). Wechsler adult intelligence scale-4th edition digit span performance

in subjective cognitive complaints, amnestic mild cognitive impairment, and probable dementia of the Alzheimer type. *Clinical Neuropsychologist*, *33*(8), 1436–1444. https://doi.org/10.1080/13854046.2019.1585574

Runne, H., Kuhn, A., Wild, E. J., Pratyaksha, W., Kristiansen, M., Isaacs, J. D., Régulier, E., Delorenzi, M., Tabrizi, S. J., & Luthi-Carter, R. (2007). Analysis of potential transcriptomic biomarkers for Huntington's disease in peripheral blood. *Proceedings of the National Academy of Sciences of the United States of America*, *104*(36), 14424–14429. https://doi.org/10.1073/pnas.0703652104

Schapiro, M., Cecil, K. M., Doescher, J., Kiefer, A. M., & Jones, B. V. (2004). MR imaging and spectroscopy in juvenile Huntington disease. *Pediatric Radiology*, *34*(8), 640–643. https://doi.org/10.1007/s00247-004-1159-y

Shannon, K. M. (2016). Pridopidine for the treatment of Huntingtons disease. *Expert Opinion on Investigational Drugs*, *25*(4), 485–492. https://doi.org/10.1517/13543784.2016.1153627

Shapiro, A. M., Benedict, R. H. B., Schretlen, D., & Brandt, J. (1999). Construct and concurrent validity of the Hopkins Verbal Learning Test - Revised. *Clinical Neuropsychologist*, *13*(3), 348–358. https://doi.org/10.1076/clin.13.3.348.1749

Silajdžić, E., Rezeli, M., Végvári, Á., Lahiri, N., Andre, R., Magnusson-Lind, A., Nambron, R., Kalliolia, E., Marko-Varga, G., Warner, T. T., Laurell, T., Tabrizi, S. J., & Björkqvist, M. (2013). A critical evaluation of inflammatory markers in huntingtons disease plasma. *Journal of Huntington's Disease*, *2*(1), 125–134. https://doi.org/10.3233/JHD-130049

Siller, N., Kuhle, J., Muthuraman, M., Barro, C., Uphaus, T., Groppa, S., Kappos, L., Zipp,

F., & Bittner, S. (2019). Serum neurofilament light chain is a biomarker of acute and chronic neuronal damage in early multiple sclerosis. *Multiple Sclerosis Journal*, *25*(5), 678–686. https://doi.org/10.1177/1352458518765666

Simmons, D. A., Casale, M., Alcon, B., Pham, N., Narayan, N., & Lynch, G. (2007). Altering DNA base excision repair: Use of nuclear and mitochondrial-targetedN-methylpurine DNA glycosylase to sensitize astroglia to chemotherapeutic agents. *Glia*, *55*(14), 1074–1084. https://doi.org/10.1002/glia

Singhrao, S. K., Neal, J. W., Morgan, B. P., & Gasque, P. (1999). Increased complement biosynthesis by microglia and complement activation on neurons in Huntington's disease. *Experimental Neurology*, *159*(2), 362–376. https://doi.org/10.1006/exnr.1999.7170

Snowden, J. S., Craufurd, D., Thompson, J., & Neary, D. (2002). Psychomotor, executive, and memory function in preclinical Huntington's disease. *Journal of Clinical and Experimental Neuropsychology*, *24*(2), 133–145. https://doi.org/10.1076/jcen.24.2.133.998

Srinageshwar, B., Petersen, R. B., Dunbar, G. L., & Rossignol, J. (2020). Prion-like mechanisms in neurodegenerative disease: Implications for Huntington's disease therapy. *Stem Cells Translational Medicine*, *9*(5), 559–566. https://doi.org/10.1002/sctm.19-0248

St-Amour, I., Turgeon, A., Goupil, C., Planel, E., & Hébert, S. S. (2018). Co-occurrence of mixed proteinopathies in late-stage Huntington's disease. *Acta Neuropathologica*, *135*(2), 249–265. https://doi.org/10.1007/s00401-017-1786-7

Stefanis L. α-Synuclein in Parkinson's disease. Cold Spring Harb Perspect Med. 2012 Feb;2(2):a009399. doi: 10.1101/cshperspect.a009399

.

Stern, H. (2014). Preimplantation Genetic Diagnosis: Prenatal Testing for Embryos Finally

Achieving Its Potential. *Journal of Clinical Medicine*, *3*(1), 280–309. https://doi.org/10.3390/jcm3010280

Stout, J. C., Queller, S., Baker, K. N., Cowlishaw, S., Sampaio, C., Fitzer-Attas, C., & Borowsky, B. (2014). HD-CAB: a cognitive assessment battery for clinical trials in Huntington's disease 1,2,3. *Movement Disorders : Official Journal of the Movement Disorder Society*, *29*(10), 1281–1288. https://doi.org/10.1002/mds.25964

Stoy, N., Mackay, G. M., Forrest, C. M., Christofides, J., Egerton, M., Stone, T. W., & Darlington, L. G. (2005). Tryptophan metabolism and oxidative stress in patients with Huntington's disease. *Journal of Neurochemistry*, *93*(3), 611–623. https://doi.org/10.1111/j.1471-4159.2005.03070.x

Sun, Y.-M., Zhang, Y.-B., & Wu, Z.-Y. (2016). Huntington's Disease: Relationship Between Phenotype and Genotype. *Molecular Neurobiology*. https://doi.org/10.1007/s12035-015-9662-8

Tabrizi, S. J., Flower, M. D., Ross, C. A., & Wild, E. J. (2020). Huntington disease: new insights into molecular pathogenesis and therapeutic opportunities. *Nature Reviews Neurology*, *16*(10), 529–546. https://doi.org/10.1038/s41582-020-0389-4

Tabrizi, S. J., Langbehn, D. R., Leavitt, B. R., Roos, R. A., Durr, A., Craufurd, D., Kennard, C., Hicks, S. L., Fox, N. C., Scahill, R. I., Borowsky, B., Tobin, A. J., Rosas, H. D., Johnson, H., Reilmann, R., Landwehrmeyer, B., & Stout, J. C. (2009). Biological and clinical manifestations of Huntington's disease in the longitudinal TRACK-HD study: cross-sectional analysis of baseline data. *The Lancet Neurology*, *8*(9), 791–801. https://doi.org/10.1016/S1474-4422(09)70170-X

Tabrizi, S. J., Reilmann, R., Roos, R. A. C., Durr, A., Leavitt, B., Owen, G., Jones, R.,

Johnson, H., Craufurd, D., Hicks, S. L., Kennard, C., Landwehrmeyer, B., Stout, J. C., Borowsky, B., Scahill, R. I., Frost, C., & Langbehn, D. R. (2012). Potential endpoints for clinical trials in premanifest and early Huntington ' s disease in the TRACK-HD study : analysis of 24 month observational data. *The Lancet Neurology*, *11*(1), 42–53. https://doi.org/10.1016/S1474-4422(11)70263-0

Tabrizi, S. J., Scahill, R. I., Owen, G., Durr, A., Leavitt, B. R., Roos, R. A., Borowsky, B., Landwehrmeyer, B., Frost, C., Johnson, H., Craufurd, D., Reilmann, R., Stout, J. C., & Langbehn, D. R. (2013). Predictors of phenotypic progression and disease onset in premanifest and early-stage Huntington's disease in the TRACK-HD study: Analysis of 36-month observational data. *The Lancet Neurology*, *12*(7), 637–649. https://doi.org/10.1016/S1474-4422(13)70088-7

Tan, B., Shishegar, R., Poudel, G. R., Fornito, A., & Georgiou-Karistianis, N. (2021). Cortical morphometry and neural dysfunction in Huntington's disease: a review. *European Journal of Neurology*, *28*(4), 1406–1419. https://doi.org/10.1111/ene.14648

The U.S.–Venezuela Collaborative Research Project* and Nancy S. Wexler. (2004). *Venezuelan kindreds reveal that genetic and environmental factors modulate Huntington ' s*. *101*(10).

Thu, D. C. V., Oorschot, D. E., Tippett, L. J., Nana, A. L., Hogg, V. M., Synek, B. J., Luthi-Carter, R., Waldvogel, H. J., & Faull, R. L. M. (2010). Cell loss in the motor and cingulate cortex correlates with symptomatology in Huntington's disease. *Brain*, *133*(4), 1094–1110. https://doi.org/10.1093/brain/awq047

Tomé, S., Manley, K., Simard, J. P., Clark, G. W., Slean, M. M., Swami, M., Shelbourne, P. F., Tillier, E. R. M., Monckton, D. G., Messer, A., & Pearson, C. E. (2013). MSH3

Polymorphisms and Protein Levels Affect CAG Repeat Instability in Huntington's Disease Mice. *PLoS Genetics*, *9*(2). https://doi.org/10.1371/journal.pgen.1003280

Vaportzis, E., Georgiou-Karistianis, N., Churchyard, A., & Stout, J. C. (2015). Effects of task difficulty during dual-task circle tracing in Huntington's disease. *Journal of Neurology*, *262*(2), 268–276. https://doi.org/10.1007/s00415-014-7563-9

Wahlin, T. B. R., Luszcz, M. A., Wahlin, Å., & Byrne, G. J. (2015). Non-Verbal and Verbal Fluency in Prodromal Huntington's Disease. *Dementia and Geriatric Cognitive Disorders Extra*, *5*(3), 517–529. https://doi.org/10.1159/000441942

Wang, R., Ross, C. A., Cai, H., Cong, W. N., Daimon, C. M., Carlson, O. D., Egan, J. M., Siddiqui, S., Maudsley, S., & Martin, B. (2014). Metabolic and hormonal signatures in pre-manifest and manifest Huntington's disease patients. *Frontiers in Physiology*, *5 JUN*(June), 1–10. https://doi.org/10.3389/fphys.2014.00231

Wiggins, R., & Feigin, A. (2021). Emerging therapeutics in Huntington's disease. *Expert Opinion on Emerging Drugs*, *26*(3), 295–302. https://doi.org/10.1080/14728214.2021.1962285

Wild, E. J., & Tabrizi, S. J. (2017). Therapies targeting DNA and RNA in Huntington's disease. *The Lancet Neurology*, *16*(10), 837–847. https://doi.org/10.1016/S1474-4422(17)30280-6

Wilson, H., Dervenoulas, G., & Politis, M. (2018). Structural Magnetic Resonance Imaging in Huntington's Disease. In *International Review of Neurobiology* (1st ed., Vol. 142). Elsevier Inc. https://doi.org/10.1016/bs.irn.2018.09.006

Winder, J. Y., Roos, R. A. C., Burgunder, J. M., Marinus, J., & Reilmann, R. (2018). Interrater Reliability of the Unified Huntington's Disease Rating Scale-Total Motor

Score Certification. *Movement Disorders Clinical Practice*, *5*(3), 290–295. https://doi.org/10.1002/mdc3.12618

Zeun, P., Scahill, R. I., Tabrizi, S. J., & Wild, E. J. (2019a). Fluid and imaging biomarkers for Huntington's disease. *Molecular and Cellular Neuroscience*, *97*, 67–80. https://doi.org/10.1016/j.mcn.2019.02.004

Zeun, P., Scahill, R. I., Tabrizi, S. J., & Wild, E. J. (2019b). Fluid and imaging biomarkers for Huntington's disease. *Molecular and Cellular Neuroscience*, *97*(October 2018), 67–80. https://doi.org/10.1016/j.mcn.2019.02.004

APPENDIX

Computational analysis of genetic HD modifiers & RNA-seq datasets

Transcriptional dysregulation in the human HD brain has been well-established. However, the exact underlying mechanisms remain unknown. The study of differential gene expression in diseases is an approach to understand the biological differences between affected individuals and healthy controls. Recent genome-wide analysis of mRNA expression in human HD prefrontal cortex revealed a differential expression (predominantly up-regulation) and for 19% (5.480) of the 28.087 confidently detected genes (FDR<0.05) (Labadorf et al., 2015).

Labadorf et al. applied a novel hypothesis-free gene set enrichment method which categorizes large gene lists into functionally and transcriptionally related groups. The differentially expressed genes identified were enriched mainly for immune response, neuroinflammation and developmental genes. A systemic response in the brain area was observed as markers for all major brain cell types were found. Of note, the most strongly differentially expressed genes were a homeotic gene set (Hox and other homeobox genes). This homeotic gene set was almost exclusively expressed in HD (Labadorf et al. 2016).

Furthermore, in another study, comparative transcriptomics of HD and PD in post-mortem human brains showed highly enriched gene sets related to immune processes and inflammatory pathways common in both diseases. The strong positive enrichment of immune and inflammatory pathways has been described in both HD and PD separately but also in a

comparative study showing a great similarity of these inflammatory signatures between HD and PD (Labadorf et al. 2017).

In addition, in this comparative transcriptomics study of HD and PD DNA damage and repair and tRNA related processes were uniquely perturbed and negatively enriched in PD. DNA damage and repair gene set enrichment is thought to reflect mitochondrial DNA damage. It is known that in PD, dopaminergic neurons of the substantia nigra but not cortical neurons are vulnerable to mitochondrial DNA damage (Labadorf et al. 2017).

Moreover, a large global GWAS of 6000-9000 HD patients with broad genetic diversity identified genes involved in DNA damage repair as significant age of onset and disease severity modifiers with some pathways related to redox signaling and mitochondrial function. A lack of involvement of protein homeostasis regulators led to the conclusion that concluded HD modifiers are mainly involved in DNA repair mechanisms. Furthermore, a study of an independent cohort of 1.462 subjects with HD and polyglutamine SCAs selecting from the previous HD GWAS the most significant hits in the HD study showed that DNA repair genes significantly modify age at onset in HD and SCAs, suggesting a common pathogenic mechanism that can be modulated by genetic manipulation of DNA repair (Tabrizi et al.2020, Bettencourt et al. 2016).

We sought to investigate differential gene expression signatures in HD, their comprehensive functional characterization, and connectivity analysis. Using RNA-seq datasets from prefrontal HD cortices and HD peripheral blood, we performed comparative transcriptomics between significantly perturbed pathways in blood and CNS transcriptomes to explore underlying signatures and a potential overlap or difference in the peripheral pathways. Genetic data from

previous HD GWAS were also used and a focus was given on *SNCA* pathway, as well as DNA repair genes implicated in recent GWAS in HD such as *FAN1*, *PMS2P1*.

Analysis of datasets

RNA-seq data on HD gene expression data were obtained via the Gene Expression Omnibus (GEO) repository either via direct inquiry or via the RNA-seq Experiments Interactive Navigator (GREIN) back-end pipeline. GREIN uses its back-end computational pipeline to extract knowledge from Sequence Read Archive (SRA) runs and generate gene signatures that may be subsequently used in gene set enrichment analyses (GSEA).

GREIN (GEO RNA-seq Experiments Interactive Navigator) provides a user-friendly interface to analyze GEO RNA-seq data deposited in Gene Expression Omnibus (GEO) and Sequence Read Archive (SRA). Using GREIN, a large number of more than 6.500 datasets are processed. GREIN provides interactive visualization. statistical power analyses. construction of differential gene expression signatures and their comprehensive functional characterization. and connectivity analysis with LINCS L1000 data. GREIN is accessible at: https://shiny.ilincs.org/grein. the source code at: https://github.com/uc-bd2k/grein. and the Docker container at: https://hub.docker.com/r/ucbd2k/grein (Mahi et al. 2019).

Pathway analyses, head-to-head comparisons and visualization of GREIN-extracted gene signatures were subsequently analyzed via GeneTrail 3.0 and GeneMania. GeneTrail applies a modified Kolmogorov-Smirnov on previously extracted data, Independent Samples Shrinkage T-test scores, and the Benjamini Yekutieli procedure were performed to adjust p-values for multiple comparisons. For all tests, false discovery rates (FDRs) and q-values<0.05 were

considered statistically significant (Gerstner et al. 2020). Genetrail 3 interrogates curated pathway databases such as GO BP, GO MF, KEGG, Reactome to retrieve significantly enriched pathways.

GWAS HD data provided by Bettencourt et al 2016 study (UCL) were re-analyzed with advanced techniques in combination with RNA datasets to discover interactions and potential pathways (Bettencourt et al 2016).

Search results

GREIN was accessed on 01/04/2021. A search using the terms «Huntington's Disease». restricting the samples to «homo sapiens» and sorting the retrieved studies by sample size lead to the selection of study GSE64810 (20 HD prefrontal cortex samples versus 49 healthy controls). Labadorf et al. 2018 provides a detailed description of the cohort.

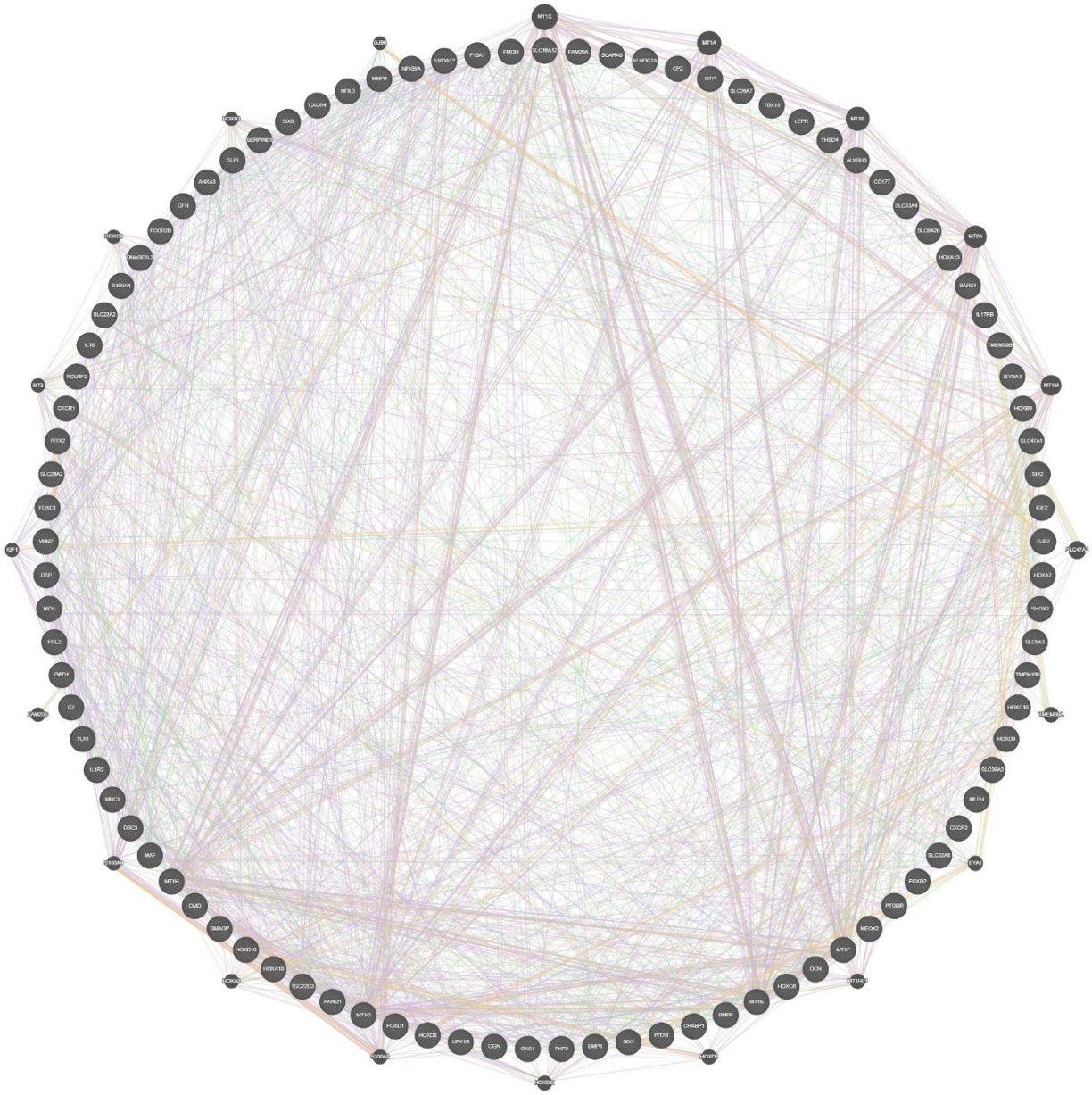

Appendix. Figure 1. *A schematic representation of the GREIN-derived gene signature. with edges representing genes belonging to the same pathways. The width and intensity of the line represent the strength and overlap of the evidence.*

Differentially expressed genes detected at this stage (Figure 1 and Supplementary Materials 1) were subsequently supplied to GeneTrail 3.0 for GSEA – gene set enrichment analysis. The results of these analyses revealed a statistically significant enrichment of immune system – associated pathways. corroborated by multiple databases (Tables 1-3) as well as the depletion of pathways associated with neuronal survival, synaptogenesis and metal ion homeostasis (Figure 2 and Supplementary Materials 2).

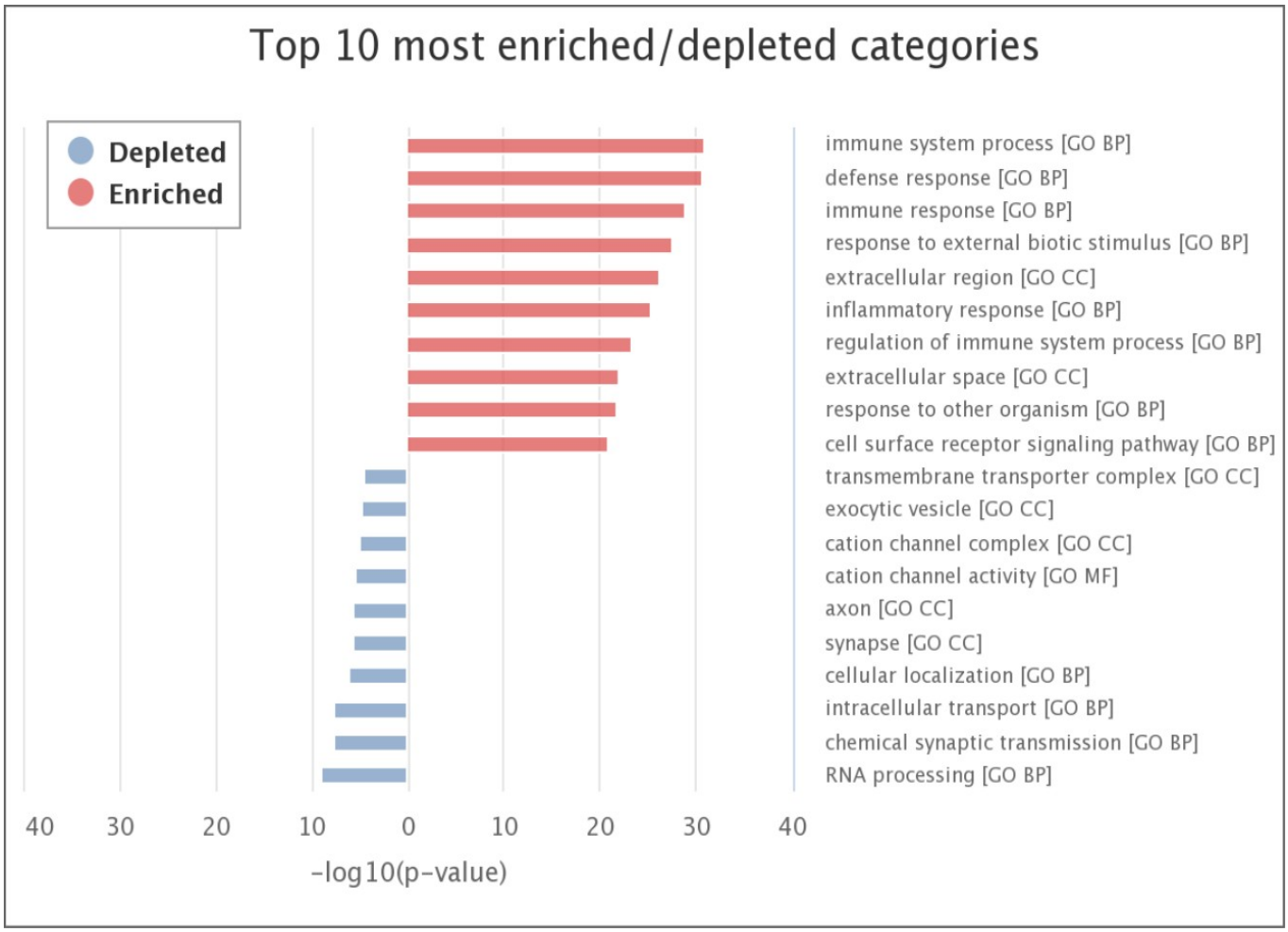

Appendix. Figure 2. *A schematic representation of the GREIN-derived gene signature. with edges representing genes belonging to the same pathways. The width and intensity of the line represent the strength and overlap of the evidence (CNS).*

A GEO Datasets inquiry using the terms «Huntington's Disease», «blood» and sorting the retrieved studies by sample size, lead to the selection of study GSE1751 (Peripheral blood trascriptomes- affymetrix. 12 HD patients vs. 14 healthy controls. GSE1751 was analyzed via Genetrail 3 (FDR<0.05).

Comparative transcriptomics

We performed head-to-head comparisons (blood vs CNS) with results from both datasets after GSEA using Genetrail 3 to assess significantly overlapping perturbed pathways in blood and CNS transcriptomes. Comparisons revealed significant overlap between mRNA surveillance, DNA repair, protein trafficking, regulation of exocytosis and natural immunity pathways (FDR<0.05; Figure 3 and Supplementary Materials 3).

Appendix. Figure 3. *A schematic representation of the ten most salient, significantly enriched / depleted pathways as detected by GeneTrail 3.0. Databases included are Gene Ontology Biological Pathways (GO BP). Gene Ontology Cellular Compartment (GO CC). Gene Ontology Molecular Function (GO MF), (blood).*

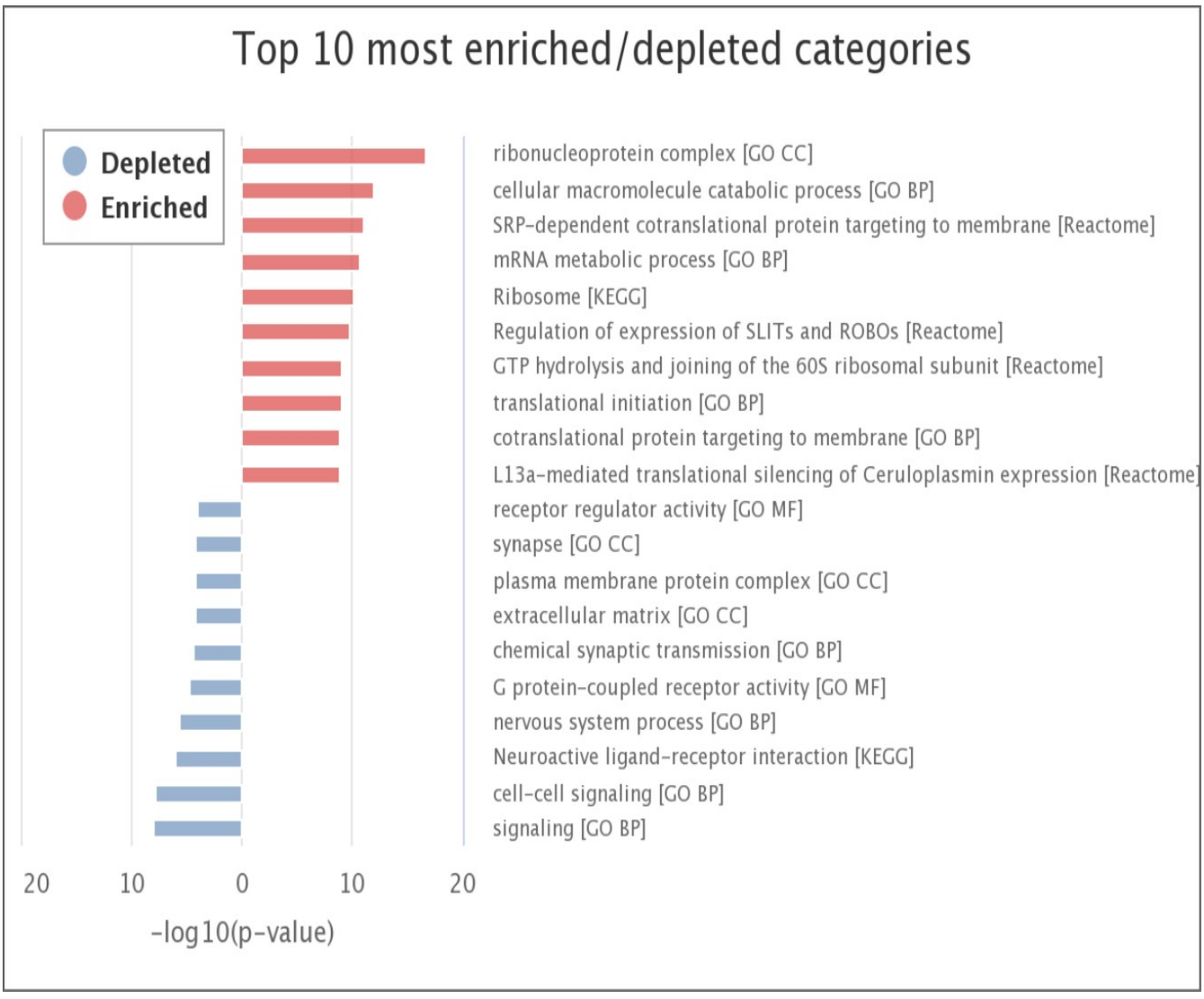

The *SNCA* gene was significantly enriched only in the peripheral blood dataset GSE1751 and involved in pathways associated with mitochondrial bioenergetics, transport and the regulation of exocytosis. (FDR<0.05; Supplementary Materials 4).

The *FAN1* gene was significantly enriched only in peripheral blood dataset GSE1751. and was associated with pathways involved in the pathway «cellular response to DNA damage stimulus» (FDR= 2.800e-2; Supplementary Materials 5).

Appendix. Table: DNA repair signature. significantly enriched genes as detected by GOBP

Databases included are Gene Ontology Biological Pathways (GO BP)

Rank	Name	Score	Contained in	
2373	FAN1	1.31	cellular response to DNA damage stimulus - 2.800e-2	gobp
10822	PMS2P1	-2.23	cellular response to DNA damage stimulus - 2.800e-2	gobp
5329	PMS2P2	-0.52	cellular response to DNA damage stimulus - 2.800e-2	gobp
6618	PMS2P3	-0.91	cellular response to DNA damage stimulus - 2.800e-2	gobp

Table 1. Significantly enriched gene ontologies (GOs) via Genetrail 3 for the GREIN derived signature GSE64810 (HD-CNS) – Gene ontologies

Type	Rank	Name	Number of hits	q-value <0.05
enriched	1	immune system process	491	1.45e-31

enriched	2	defense response	247	2.05e-31
enriched	3	immune response	239	1.57e-29
enriched	4	response to external biotic stimulus	248	2.48e-28
enriched	5	inflammatory response	119	6.51e-26
enriched	6	regulation of immune system process	353	4.80e-24
enriched	7	response to other organism	196	1.94e-22
enriched	8	cell surface receptor signaling pathway	470	1.38e-21
enriched	9	positive regulation of immune system process	243	1.65e-21
enriched	10	cell activation	262	7.53e-18

Table 2. Significantly enriched signatures via KEGG database analyzed with Genetrail 3 for the GREIN derived signature GSE64810 (HD-CNS) – Pathway analysis

Type	Rank	Name	Number of hits	Score	q-value
enriched	1	Viral protein interaction with cytokine and cytokine receptor	36	83280	1.07e-11
enriched	2	Cytokine-cytokine receptor interaction	73	118682	2.73e-11
enriched	3	Ribosome	50	76350	3.75e-6
enriched	3	Staphylococcus aureus infection	25	53272	3.75e-6
enriched	5	Transcriptional misregulation in cancer	50	74392	8.03e-6

enriched	6	Complement and coagulation cascades	27	51849	2.59e-5
enriched	7	IL-17 signaling pathway	24	47142	6.59e-5
enriched	8	Pathways in cancer	99	96111	9.67e-5
enriched	9	Legionellosis	24	44730	2.59e-4
enriched	10	Malaria	14	32637	4.32e-4
Type	Rank	Name	Number of hits	Score	q-value

Table 3. Significantly enriched signatures via REACTOME database analyzed with Genetrail 3 for the GREIN derived signature GSE64810 (HD-CNS) – Pathway analysis

Type	Rank	Name	Number of hits	Score	q-value
enriched	1	Chemokine receptors bind chemokines	23	58869	2.36e-8
enriched	2	Interleukin-10 signaling	21	54123	5.25e-8
enriched	2	Neutrophil degranulation	137	145263	5.25e-8
enriched	4	Formation of a pool of free 40S subunits	47	71769	2.89e-5
enriched	4	Immunoregulatory interactions between a Lymphoid and a non-Lymphoid cell	32	58702	2.89e-5
enriched	4	Metallothioneins bind metals	8	25896	2.89e-5
enriched	4	Nonsense Mediated Decay (NMD) independent of the Exon Junction Complex (EJC)	46	70242	2.89e-5
enriched	4	Peptide chain elongation	46	70242	2.89e-5

enriched	4	Regulation of expression of SLITs and ROBOs	48	72192	2.89e-5
enriched	10	SRP-dependent cotranslational protein targeting to membrane	51	73257	3.22e-5

We performed a data driven transcriptomic analysis in peripheral blood and CNS in the setting of Huntington's disease. For this purpose, CNS and peripheral blood HD gene expression data were retrieved from the Gene Expression Omnibus (GEO) database. Using a pre-constructed query, a total of 2 studies were initially retrieved. Gene set enrichment analyses (GSEA) revealed significantly enriched pathways (FDR<0.05) were detected in both peripheral blood and CNS datasets. These included DNA repair pathways, immune related pathways, regulatory systems and autophagy dysfunction. We combined findings from previous GWAS data and focused on DNA repair mechanisms as well as a-synuclein that we found elevated in HD patients in this thesis.

Our results confirm previous results from HD GWAS data implicating immune pathways in the pathophysiology of HD. To date, several studies connect neurodegeneration with immune response and surveillance dysregulations. mHTT is known to cause transcriptional dysregulation both in CNS and in the peripheral tissues, resulting in immune response upregulation and mRNA processing upregulation, followed by downregulation of synaptic function and metabolic processes. In addition, immune activation has been reported in peripheral blood of HD patients, with higher levels of pro-inflammatory cytokines, other molecules related to microglia. Over-activation of microglia, and abnormalities of the innate immune system have been described in HD patients. mHTT is present in leukocytes and microglia, and it has the potential of deranging immune system. However, understanding of

such changes is limited by infections and other immune derangements unrelated to HD. Furthermore, it is unclear whether the neuroinflammatory response is protective or deleterious and if immune activation and inflammation is a secondary event or not. (Björkqvist et al., 2008, Dalrymple et al., 2007).

Neuroinflammation in HD has been also confirmed neuropathologically as a unique pattern of reactive gliosis around striatum. In addition, a small proteomic study identified elevated levels of prothrombin and haptoglobin, that are both proteins involved in inflammatory response (Wertz et al. 2020, Zeun et al. 2019a , Huang et al. 2011, Björkqvist et al. 2008).

The involvement of DNA repair pathways in neurodegenerative diseases and in HD is well-established and presents numerous opportunities for therapeutic intervention. However, the exact mechanism that they contribute to the pathophysiology remains to be explored. *FAN1* variants are the strongest modifiers but how any of the *FAN1* variants modify disease is unknown. We replicated here *FAN1* gene enrichment but only in the peripheral blood dataset.

We have shown elevated a-synuclein levels in peripheral blood of HD patients in this thesis. Of note, the *SNCA* gene was significantly enriched only in the peripheral blood and not in CNS. This is compatible with the elevated protein expression we have detected in HD serum, and suggests that the source of this increased a-synuclein is excessive mRNA production from peripheral sources, likely erythrocytes, where a-synuclein is most abundantly expressed (Breza et al., 2020).

This study is not without caveats. Although the genes identified and the pathways implicated in this analysis have been reported to play a crucial role, these findings are computational and remain to be confirmed. Only two studies exist to date, and experimental validation of the

results are needed. However, pathways are complex to study, particularly in human brain tissues. Numerous genes are implicated in these pathways and their interplay remains unknown, making it difficult to analyze. Furthermore, the exact pathophysiology of the disease is still unknown. The results here are thus proposed as potentially fruitful avenues of future study and replicate previous findings, to aid understanding HD mechanism. Further studies are needed in different tissues and with more advanced techniques such as single-cell RNA technologies.